

An Investigation of Non-destructive Testing Techniques for Concrete Structures



by

Mehmet Emin Uyanik

A thesis submitted to the University of Birmingham for the degree of

Master of Science by Research

School of Metallurgy and Materials

College of Engineering and Physical Sciences

The University of Birmingham

April 2019

UNIVERSITY OF
BIRMINGHAM

University of Birmingham Research Archive

e-theses repository

This unpublished thesis/dissertation is copyright of the author and/or third parties. The intellectual property rights of the author or third parties in respect of this work are as defined by The Copyright Designs and Patents Act 1988 or as modified by any successor legislation.

Any use made of information contained in this thesis/dissertation must be in accordance with that legislation and must be properly acknowledged. Further distribution or reproduction in any format is prohibited without the permission of the copyright holder.

Synopsis

Concrete is the most commonly preferred material for the construction of a wide range of different types of civil structures. Concrete is a composite material produced by mixing aggregate, cement, water and chemical admixtures. It is an adaptable material, which can be conveniently mixed to meet various design and structural requirements whilst it can practically be formed in almost any useful shape. However, the in-service lifetime of concrete structures is drastically reduced when cracking, dynamic displacement or distortion are not immediately detected so as appropriate repairs can be carried out in time. Several important existing structures are inching closer to their end of their serviceable lifetime. Therefore, the application of quantitative non-destructive testing and conditioning monitoring techniques is becoming more important and a necessity in order to accurately and reliably evaluate the overall structural integrity of existing and future concrete structures.

This research study is concerned with the investigation of advanced quantitative condition monitoring techniques for concrete structures. More specifically, the combination of Ultrasonic Pulse Velocity (UPV), Acoustic Emission (AE) testing and Visual Inspection (VI) have been selected in order to perform quantitative quality control of concrete beam specimens with different strength levels specifically manufactured for the present research study. The UPV method operational principles are based on the transmission of ultrasonic waves through the thickness of the concrete components. Any differences in the ultrasonic wave velocity measured can be used to effectively evaluate the actual strength of the concrete in a quantitative manner. On the other hand, AE testing is a passive technique, which can be employed to quantitatively monitor damage propagation in concrete structures as well as other materials in order to determine the actual level of structural degradation with time.

Experiments were conducted using a range of different concrete specimen types including both cube and beam-shaped ones with intentionally varying quality. AE data were acquired during compressive and flexural tests performed on the concrete samples manufactured. Various statistical analysis methodologies such as cumulative energy have been considered in trying to effectively quantify damage evolution. This thesis summarises the key findings of this research effort.

Acknowledgements

I would first like to thank Dr. Mayorkinos Papaelias, without whom this research study could never have come into existence. I am grateful for the opportunity he provided to me to carry out this research study under his supervision. He helped me to study at the University of Birmingham and spent precious time throughout my Master of Science program to discuss experiments and results obtained as well as their analysis with me.

I would also like to express my eternal gratitude to the National Education Ministry of the Republic of Turkey (MEB) and the General Directorate of State Hydraulic Works (DSI) for supporting me morally and financially.

Finally, I want to express my gratitude to my family members and fiancé Deniz Uyanik who has been giving me support and encouragement throughout my study in the United Kingdom.

TABLE OF CONTENTS

| | |
|---|-----------|
| Synopsis | 1 |
| Acknowledgements | 3 |
| | |
| CHAPTER 1 - Introduction | 11 |
| 1.1 Background | 11 |
| 1.2 A brief history of modern NDT for concrete structures | 15 |
| 1.3 Aim and scope | 18 |
| | |
| CHAPTER 2 - Literature Review | 20 |
| 2.1 Concrete | 20 |
| 2.1.1 Concrete constituents..... | 20 |
| 2.1.1.1 Pozzolan..... | 21 |
| 2.1.1.2 Portland cement | 22 |
| 2.1.1.2.1 Chemical composition of the portland cement..... | 22 |
| 2.1.1.2.2 Main types of the portland cement | 23 |
| 2.1.1.3 Concrete aggregates | 24 |
| 2.1.1.3.1 Classification of aggregates | 25 |
| 2.1.2 Fresh mass concrete..... | 27 |
| 2.1.3 Hardened concrete | 27 |
| 2.1.3.1 Main properties of the hardened concrete | 28 |
| 2.1.3.2 Factors affecting durability of hardened concrete | 28 |
| 2.1.3.3 Factors affecting strength of the hardened concrete | 30 |
| 2.2 Discontinuities and defects in concrete structure | 32 |
| 2.2.1 Cracks before the hardening process | 32 |
| 2.2.2 Cracks after hardening process..... | 34 |
| | |
| CHAPTER 3 - Experimental Methods Considered | 37 |
| 3.1 Summary of the chapter..... | 37 |
| 3.2 Destructive testing methods | 37 |
| 3.2.1 Flexural strength testing | 38 |
| 3.2.2 Compressive strength test..... | 39 |
| 3.3 Non-Destructive Testing Methods | 40 |
| 3.3.1 Visual inspection test | 41 |

| | |
|--|-----------|
| 3.3.2 Ultrasonic pulse velocity testing (UPVT) | 43 |
| 3.3.2.1 General procedure of the UPVT | 43 |
| 3.3.2.2 Application methods of UPV testing for concrete components | 45 |
| 3.3.2.3 Measurement of the crack depth by using surface transmission | 48 |
| 3.3.2.4 Strength estimation for the concrete by using UPVT | 50 |
| 3.3.2.5 Factors affecting the pulse velocity in concrete | 51 |
| 3.3.2.6 Measurement of the concrete quality by using UPVT | 58 |
| 3.3.3 Acoustic Emission (AE) Testing | 60 |
| 3.3.3.1 General procedure of the AE testing for concrete material | 60 |
| 3.3.3.2 AE signal characteristics | 62 |
| 3.3.3.3 Kaiser and Felicity effect in AE testing | 65 |
| 3.3.3.4 Determination of the concrete quality and durability using AE testing..... | 67 |
| | |
| CHAPTER 4 - Experimental Results and Discussion..... | 68 |
| 4.1 Summary of the chapter. | 68 |
| 4.2 Experimental group 1 concrete samples..... | 68 |
| 4.2.1 Preparation of the group 1 samples | 70 |
| 4.2.2 Destructive testing for the group 1 | 73 |
| 4.2.2.1 Compressive strength testing results for group 1 samples | 73 |
| 4.2.2.2 Flexural strength testing results for the group 1 | 74 |
| 4.2.3 Non-destructive testing of group 1 | 76 |
| 4.2.3.1 Ultrasonic pulse velocity testing for the group 1..... | 76 |
| 4.2.3.2 UPV testing results and discussions for the group 1 | 77 |
| 4.2.3.3 Acoustic emission tests for the group 1 | 82 |
| 4.2.3.3.1 AE energy results and discussion for the group 1 | 85 |
| 4.2.3.3.2 Quantifications of the progressive structural integrity losses for the group 1 . | 90 |
| 4.2.3.3.3 AE RMS results and discussions for the group 1 | 99 |
| 4.2.3.3.4 AE Amplitude results and discussions for the group 1 | 103 |
| 4.2.3.3.5 AE Average frequency results and discussions for the group 1 | 106 |
| 4.3 Experimental group 2 | 109 |
| 4.3.1 Preparation of the group 2 specimens | 110 |
| 4.3.2 Destructive tests for the group 2..... | 110 |
| 4.3.2.1 Compressive and flexural strength test results for the group 2 | 111 |
| 4.3.3 Non-destructive testing for the group 2..... | 112 |
| 4.3.3.1 UPV test results and discussion for the group 2..... | 112 |

| | |
|---|------------|
| 4.3.3.2 Acoustic emission test for the group 2 | 117 |
| 4.3.3.2.1 AE energy results and discussion for the group 2 | 118 |
| 4.3.3.2.2 Quantification of the progressive structural integrity losses for the group 2 | 120 |
| 4.3.3.2.3 AE RMS results and discussions for the group 2 | 121 |
| 4.3.3.2.4 AE Amplitude results and discussions for the group 2 | 123 |
| 4.3.3.2.5 AE Average frequency results and discussions for the group 2 | 125 |
| 4.2.3.4 Visual inspection test for the group 2 samples..... | 126 |
| | |
| CHAPTER 5 - Conclusions | 128 |
| 5.1 Conclusions from the acoustic emission testing | 129 |
| 5.2 Conclusions from the ultrasonic pulse velocity and visual inspection testing..... | 130 |
| | |
| CHAPTER 6 - Future Work | 131 |
| CHAPTER 7 - References | 132 |

LIST OF FIGURES

| | |
|---|----|
| Figure 1: Reduction of cross-sectional area after taken a core sample. | 12 |
| Figure 2: Common aggregate shapes. | 25 |
| Figure 3: Three different types of aggregate gradations or size distributions..... | 31 |
| Figure 4: The difference between uniform and non-uniform concrete..... | 31 |
| Figure 5: Plastic shrinkage cracks because of rapid evaporation on the surface [70]..... | 33 |
| Figure 6: Formwork movement cracks [71]..... | 33 |
| Figure 7: Agitators used to prevent cracks and segregation [72]..... | 34 |
| Figure 8: Bleeding on concrete surface..... | 35 |
| Figure 9: First and final stage of the spalling cracks [75]..... | 35 |
| Figure 10: Honeycombing distortions in hardened concrete [76]..... | 36 |
| Figure 11: Effects of dusting, rain damage and crazing on concrete surface [77]..... | 36 |
| Figure 12: 4-point bend setup of the flexure strength test. | 38 |
| Figure 13: Compression test and standard cubic specimen dimensions. | 39 |
| Figure 14: Types of hardened concrete cracks depending on some factors..... | 41 |
| Figure 15: Types of hardened concrete surface cracks depending on the causes. | 42 |
| Figure 16: Working principle of UPVT. | 44 |
| Figure 17: Display unit and an application of the UPV test. | 44 |
| Figure 18: Direct and semi direct transmission techniques. | 46 |
| Figure 19: Effects of surface discontinuities on transition time and path length..... | 47 |
| Figure 20: Measurement of crack depth perpendicular to the surface. | 48 |
| Figure 21: Crack depth measurement for the oblique or inclined cracks (BS 1881 part 203).49 | |
| Figure 22: Pulse movements under certain conditions [112]..... | 51 |
| Figure 23: Comparison of the concrete samples having light and heavyweight agg. [116]. .. | 53 |
| Figure 24: Comparison of the specimens having gravel, granite and limestone [116]..... | 54 |
| Figure 25: Effect of the different mix-proportions for cement and aggregate [118]. | 55 |
| Figure 26: Effects of the water to cement ratio and ageing factors [121]..... | 56 |
| Figure 27: Effect of the distance between transducers [122]..... | 57 |
| Figure 28: Effect of moisture content [125]..... | 58 |
| Figure 29: AE test measuring system used in the research study. | 61 |
| Figure 30: AE system architecture. | 61 |
| Figure 31: R50A resonant AE sensors and PAC pre-amp. employed in the research study. . | 62 |
| Figure 32: Main terms of an AE signal [132]. | 63 |
| Figure 33: AE waves originating from a propagating crack as a flexural load is applied. | 63 |

| | |
|---|-----|
| Figure 34: General behaviour exhibited by a hardened concrete specimen under comp[134] | 64 |
| Figure 35: Example of the continuous AE waveform [135]. | 64 |
| Figure 36: Example of a burst AE waveform. | 65 |
| Figure 37: Kaiser and Felicity effect on AE activity. | 66 |
| Figure 38: Mixture designs 1 and 2 in the experimental group 1. | 70 |
| Figure 39: Casting of the fresh concrete mixture 1 and 2. | 71 |
| Figure 40: Specimen types and numbers of specimens produced in group 1. | 72 |
| Figure 41: The compressive testing device showing the results of S4 | 73 |
| Figure 42: 4-point bending setup and AE testing from research studies. | 75 |
| Figure 43: Calibration of the test device and application of direct, semi-direct transmission. | 77 |
| Figure 44: Correlation between UPV and the strength values from the mixture 1 samples. | 80 |
| Figure 45: Correlation between UPV and the strength values for the mixture 2 samples. | 81 |
| Figure 46: Connections of the sensor, amplifier, display and digitization components. | 82 |
| Figure 47: Placing of the sensors on the concrete surface by using a glue. | 83 |
| Figure 48: AE hits during the pencil lead test. | 83 |
| Figure 49: 4 point bending setup and AE application. | 84 |
| Figure 50: Plot of the AE signal energy versus time for the sample 1, 2 and 3. | 85 |
| Figure 51: Plot of the AE cumulative energy versus time for S1,2,3. | 86 |
| Figure 52: Plot of the AE signal energy versus time for the sample 5 and 6. | 87 |
| Figure 53: Plot of the AE cumulative energy versus time for S5 and 6. | 88 |
| Figure 54: Cumulative energy comparison of S2,3,6. | 89 |
| Figure 55: Paris-Erdogan crack growth model and cumulative energy plot of the S3 | 91 |
| Figure 56: The fatigue crack growth model presented by J. R. Rice and D. M. Tracey | 91 |
| Figure 57: An example of the quantification of the progressive structural integrity loss. | 92 |
| Figure 58: Quantification of the progressive structural integrity loss for the sample 1. | 93 |
| Figure 59: Quantification of the progressive structural integrity loss for the sample 2. | 94 |
| Figure 60: Quantification of the progressive structural integrity loss for the sample 3. | 95 |
| Figure 61: Quantification of the progressive structural integrity loss for the specimen 5. | 96 |
| Figure 62: Quantification of the progressive structural integrity loss for the specimen 6. | 97 |
| Figure 63: Comparison of the progressive structural integrity losses for the group 1. | 98 |
| Figure 64: An example plot of RMS voltage (yellow) and raw signal (blue). | 100 |
| Figure 65: RMS Voltage plot of the sample 1 | 100 |
| Figure 66: RMS Voltage plot of the specimen 2. | 101 |
| Figure 67: RMS voltage plot of the sample 3. | 101 |
| Figure 68: RMS voltage plot of the sample 5. | 102 |
| Figure 69: RMS voltage plot of the specimen 6. | 102 |
| Figure 70: AE amplitude plot of the specimen 1. | 103 |

| | |
|--|-----|
| Figure 71: AE amplitude plot of the sample2. | 104 |
| Figure 72: AE amplitude plot of the sample3. | 104 |
| Figure 73: AE amplitude plot of the sample 5. | 104 |
| Figure 74: AE amplitude plots of the specimen 6. | 105 |
| Figure 75: Rise time and duration for a typical waveform [157]. | 106 |
| Figure 76: Average frequency values of the AE signals detected from the sample S1. | 106 |
| Figure 77: Average frequency values of the AE signals detected from the specimen S2. .. | 107 |
| Figure 78: Average frequency values of the AE signals detected from the sample S3. | 107 |
| Figure 79: Average frequency values of the AE signals detected from the sample S5. | 108 |
| Figure 80: Average frequencies of the AE signals detected from the specimen S6. | 108 |
| Figure 81: 4 point bending setup, flexural strength and failure load for the specimen M3. . | 112 |
| Figure 82: UPV tests for 2 cubes from group 2 samples. | 113 |
| Figure 83: Linear interpolations of the UPV and w/c values for the group 2 samples. | 114 |
| Figure 84: Linear interpolations of the UPV and strength values for the group 2. | 116 |
| Figure 85: 4 points bending setup and AE test for the beam sample M3. | 118 |
| Figure 86: AE signal energy plots for the M3 and S3. | 118 |
| Figure 87: AE signal cumulative energy graphs for M3 and S3. | 119 |
| Figure 88: Quanification of the progressive structural integrity loss for the sample M3. | 120 |
| Figure 89: RMS voltage plot for the specimen M3 from group 2. | 122 |
| Figure 90: RMS voltage plot for the specimen S3 from group 1. | 122 |
| Figure 91: AE amplitude plot of the sample M3 from the group 2. | 123 |
| Figure 92: AE amplitude plot of the specimen 3 from the group 1. | 124 |
| Figure 93: Average frequency plot of the AE signals detected from the specimen M3. | 125 |
| Figure 94: Average frequency plot of the AE signals detected from the sample S3. | 125 |
| Figure 95: Bleeding cracks on the concrete surface. | 126 |
| Figure 96: Bleeding cracks on surface of the sample M6. | 127 |

LIST OF TABLES

| | |
|--|-----|
| Table 1: Concrete quality classification based on BS 1881, 1983. | 59 |
| Table 2: Pulse velocity limits according to ASTM. | 59 |
| Table 3: Suggestion of J.R. Leslie and W.J. Cheesman for concrete quality estimation..... | 59 |
| Table 4: Mixture content of number 1 and 2..... | 71 |
| Table 5: The names of cubic and beam specimens. | 72 |
| Table 6: Copressive strength testing results of the group 1 cubic specimens. | 74 |
| Table 7: Bending test results of beam samples in group 1..... | 75 |
| Table 8: Direct and semi-direct trasmission time and velocities for the group 1 specimens.. | 77 |
| Table 9: Mixture contents of the group 2 specimens | 110 |
| Table 10: Copressive strength test results of the group 2 cubic specimens. | 111 |
| Table 11: Comressive strength and UPV test results of the group 2 cubes..... | 113 |

CHAPTER 1

Introduction

1.1 Background

Concrete is a cheap multi-purpose composite material which has been used in almost any type of civil structure including buildings, bridges, dams, regulators, canals, roads and many others.

Concrete structures can be directly affected by dynamic events such as earthquakes, storms, flooding, ground movement, etc. with possible catastrophic sequences.

Concrete structures are designed with a finite useful service lifetime. Therefore, they can gradually lose strength, whilst quality and durability of such structures can deteriorate year after year. Numerous concrete structures are nearing their end of their serviceable life. Most importantly, the service lifetime of concrete will exponentially decrease when damage has not been detected and properly treated in time [1]. For this reason, trained engineers are required to control and evaluate the quality and durability of hardened concrete elements by using appropriately selected destructive and non-destructive test (NDT) methods.

For several years, the quality and durability of existing concrete and reinforced concrete structures have been tested by extracting cylindrical core samples using trepanning techniques. The cores retrieved with the trepanning process are subsequently set to undergo compressive loading up to the point of failure under laboratory conditions in order to evaluate their mechanical strength. However, this particular testing approach involving the removal of cylindrical cores using trepanning results in voids and possibly cracking in the structural elements tested (e.g a column, beam or slab) [2]. Figure 1 shows the reduction in the cross-sectional area of a simplified concrete component after trepanning has been carried out and a cylindrical core has been removed for compressive testing.

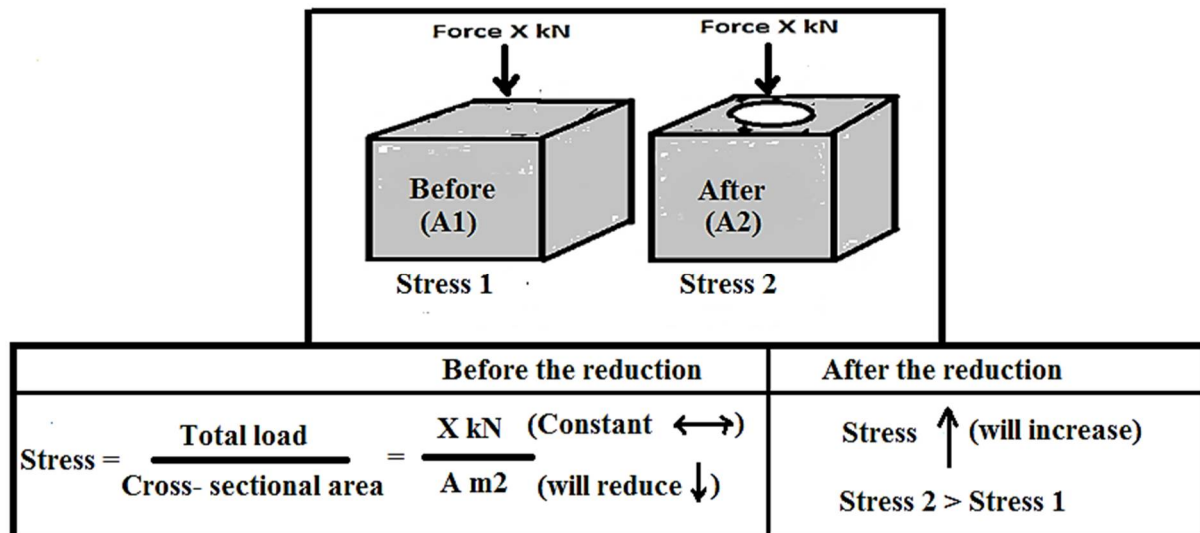


Figure 1: Reduction of cross-sectional area after taken a core sample.

As it is shown in figure 1, the sum of the dead and live loads to which the structural component is exposed will have a total finite value equal to X kN. Before taking a core sample, the cross-sectional area of the component is equal to A1 m². After the extraction of the cylindrical core with the trepanning method, there is a reduction of the cross-sectional area from A1 to A2 m² (hence A1>A2). However, the load remains constant and hence equal to X kN. Therefore, the stress, affecting the component, will increase further each time a core is extracted from the structure [3].

Therefore, stress increments are highly undesirable in ageing concrete structures as they may have a devastating effect on their structural integrity and causing damage to accelerate or even result in final failure (e.g. the Ponte Morandi bridge whose failure has been attributed partially to further loads added on the structure). In addition to these, distortion and damage will arise in practically any type of destructive tests, resulting generally to an adverse effect on the durability, quality and strength of a concrete structure.

Effective evaluation of concrete structures based on non-destructive methods has been a research topic of significant interest in modern engineering. This is due to the fact that NDT techniques provide engineers with the opportunity of monitoring the structural health of a

concrete structure or component without causing any form of damage to it and hence without causing any reduction to the current structural integrity level [4].

More specifically, crack detection in concrete elements is particularly important. This is due to the fact that cracks adversely influence concrete strength and long-term durability. There are various types of concrete cracking including, shrinkage, settlement, structural, spalling, honeycombing and bleeding. For the purpose of assessing the quality, durability and detecting the presence of minor and major cracks, homogeneity, density, discontinuities, displacement, rebar location and corrosion, bonding between concrete and rebar, NDT testing has been frequently used in the construction industry [5-7].

As it was mentioned earlier, an increasing number of civil structures have been nearing end of their useful service lifetime. Thus, catastrophic events such as earthquakes coupled with ageing effects, improper design and the possibility of flawed construction have necessitated the widespread application of appropriate NDT methods in order to evaluate the actual structural health of concrete structures. For instance, the Republic of Turkey is located in earthquake-prone region of the planet with frequent strong earthquakes well above 6 in the Richter scale [8]. This is due to the fact that there are various fault line East, West, North and South of the Minor Asian plate. Moreover, due to poor construction standards in the past, Turkey still has a significant number of structures which carry a significant risk of collapse in the event of a powerful earthquake. For this reason, construction engineers have been trying to quantitatively examine the durability, strength and actual structural health of concrete structures.

Due to the undesirable effects of destructive testing methods, it has gradually become obsolete with focus remaining on the further improvement of appropriate NDT methods as means of phasing out completely the need for trepanning. Using exclusively NDT techniques for the examination of concrete structures has significantly risen in Turkey and the rest of the world in recent years [9]. This trend is expected to continue at an even stronger pace.

Various types of equipment and accordingly NDT techniques can be employed to examine the quality and durability of existing and future concrete structures without any undesirable damage resulting [10]. Visual inspection has been traditionally used to detect surface cracks in concrete structures. Furthermore, the half-cell electrical potential method has become the preferred approach for the detection of rebar corrosion-related damage in reinforced concrete [11].

Rebound hammer test is necessary for the evaluation of the surface hardness of concrete. Carbonation depth measurement test is helpful in determining the moisture content reaching the depth at which reinforcement rebars are placed [12].

Moreover, permeability tests are performed so as to measure water flow through concrete elements. Penetration resistance and Windsor probe testing have been preferred alternative to the rebound hammer for testing the surface hardness of concrete elements [13].

Cover metre testing has been frequently used to detect the distance between rebars and surface of the reinforced concrete structures. Also, it has been used to measure the diameter of the reinforced concrete rebars [14]. Radiographic testing has been preferred for the detection of voids and discontinuities that may be present inside the concrete structure and may evolve with time in service. Either Gamma or X-ray testing can be used to readily detect voids, discontinuities, rebar location and rebar diameter placed inside the reinforced concrete structures [15].

UPVT has been widely recognised as one of the key NDT methods that can be employed in order to evaluate the quality, durability and actual strength of concrete components and structures. However, UPV is more effectively and reliably used to estimate concrete strength in components with no other form of damage also present. The UPVT method is based on the transmission of ultrasonic waves through the concrete component. The changes occurring in the ultrasonic wave velocity can be reliably related to the actual strength of the concrete structure under consideration [16].

On the other hand, AE is a highly capable and appropriate NDT and condition monitoring technique which can be used effectively for accurate quantitative assessments. AE is a passive NDT or condition monitoring technique which can be employed to quantitatively monitor damage propagation in concrete structures in order to determine the severity of structural degradation with time. It has been frequently used in various condition monitoring (CM) applications and in Structural Health Monitoring (SHM) systems [17]. Fundamentally, during AE testing, acoustic waves generated inside or on the surface of a component are detected by the piezoelectric sensors. The data are subsequently logged and analysed using appropriate statistical tools.

1.2 A brief history of modern NDT for concrete structures

Visual testing is the oldest and most common NDT method for various materials including concrete; though, it is difficult to pinpoint the exact where NDT techniques became to be a requirement for quality control and structural health evaluation.

Apart from visual testing, modern NDT begun in the second half of the 19th century. In 1868, the British scientist S.M. Saxby used the magnetic characteristics of a compass to detect cracks in a gun barrel [18]. Magnetic particle testing has been frequently used in the industry for the presence of surface-breaking or very near to the surface defects. In 1876, A. Hering took a U.S. patent for finding discontinuities in railway steel rails by using the technique developed by S. M. Saxby [19]. Later on, the method was applied for the assessment of various components. Magnetic particle testing has become an important NDT method for steel and iron-based materials [20]. Magnetic particle, X-ray and radiographic testing have been frequently used in reinforced concrete components comprising steel rebars.

Another technique commonly employed is based on the use of Liquid or Dye Penetrant Inspection (LPI or DPI). It is preferred due to the very high sensitivity of this technique in

finding small surface discontinuities. Currently, LPI is widely used in the various industries, including oil and gas, power generation, aerospace, maritime and so on. LPI is hence a quite significant NDT method for concrete structures and for discovering the indication and inspecting a surface crack [21].

Ultrasonic testing (UT) is a versatile NDT method, which has been used in a great range of industrial inspection applications for many years. UT was invented by the British physicist and mathematician James Prescott Joule in 1847 [22]. His methods were further improved by the French physicist Pierre Curie and his brother Paul Jacques Curie in 1880 [23]. After the tragic sinking of the Titanic in 1912, the use of ultrasonic testing was recommended. In 1929, it was introduced as a means for testing metal castings in the United Kingdom [24].

In concrete technology, scientists have focused on different testing methods. At the beginning of the 1930s, they began looking into vibration-based testing methods. In 1938, 1939 and 1940, Powers, Obert, Hornibrook and British Physicist J.J. Thomson carried out the first vibration or pulse studies by using resonance frequency methods [25]. During World War 2, research relating to NDT intensified rapidly. One of the key areas investigated was on elastic stress wave propagation and interactions in solid materials such as metals. From 1950s to present, NDT techniques have been directly related to safety, reliability and improvement in the design of the new materials, quality control and identification and quantification of damage in engineering components. NDT methods are in constant use in practically every industry including construction and manufacturing.

The UPV method was also invented in the United Kingdom. In 1948, the first ultrasonic tester was manufactured by R. Jones [26]. Since then many different UPV test devices have been invented and used in the construction industry for the evaluation of the quality of concrete structures.

AE is one of the oldest NDT methods known to us. Fundamentally, AE is based on “listening” for sounds propagating inside a material which is exposed to tensile, compressive or other loads, in the form of elastic stress waves. Back in 6500 BC, potters used this approach by carefully listening for any acoustic sounds during cooling of their ceramic products whilst trying to identify any structural defects [27]. The first written observations related to AE were the work of Arab philosopher Jabir ibn Hayyan back in the 8th century AD. In his books, ibn Hayyan mentioned that during forging, tin or Jupiter and iron or Mars materials generated “harsh sound” and “sounds much” respectively [28].

In the 19th century, many studies focused on audible or acoustic sounds generated in materials such as cadmium, zinc and tin [29]. ascertain researchers, e.g. Albert Portevin, observed and tried to classify materials depending on the audible sounds generated under load [30]. Through the next 20 years, many important experiments were carried out. For instance, R. Anderson carried out tensile testing on aluminum alloy samples whilst E. Scheil combined tensile testing of steel specimens with the recording of audible noise generated during the test [31].

In 1950, Joseph Kaiser investigated AE measurements in metallic materials under tension which led to the discovery of the Kaiser effect [32]. The Kaiser effect relates the AE activity generated in a material during initial loading, unloading and subsequent reloading. Unless the previous maximum has been exceeded during the reloading stage AE activity remains negligible and only resumes once the previous maximum has been exceeded. This holds true depending on the level of damage already sustained by the material. Hence, for a material damaged to a level close to final failure, significant AE activity will be generated even if the previous maximum has not been exceeded. Therefore, this approach can be used to identify the severity of damage already accumulated in the material at least in a qualitative manner. The Kaiser effect has been found to be applicable in concrete structures also. After Kaiser’s discovery, Bradford Schofield established the first research programme in order to investigate

the engineering applications of AE. Generally, the research conducted by Kaiser is considered to be the starting point of modern AE testing. Today, many advanced devices have been designed and built in order to measure AE activity in steel and concrete exposed to different loading scenarios, including in-service loading conditions. AE, has been proven as a reliable test method for obtaining information regarding the material quality and durability under loading conditions.

The NDT Society of Great Britain (NDTS) and Society of Non-Destructive Examination (SONDE) were founded in 1954 [33]. In 1976, The British Institute of Non-Destructive Testing or BINDT was established for engineers and professionals related to NDT and condition monitoring in the United Kingdom. Similarly, many other countries have introduced their own institutes, training centres and standards relating to NDT and CM operations [34-39].

1.3 Aim and scope

The main aim of this research study is to investigate the reliability of NDT in evaluating quantitatively rather than qualitatively the overall strength and durability of concrete structures produced using a variety of mixture content. AE and UPV tests combined with visual inspection have been selected for this study due to their versatility and potential in evaluating the condition of concrete structures during loading.

To reach the main objective appropriate experiments had to be designed and carried out along with the production of the necessary reference concrete samples.

To investigate the capability and reliability of the NDT methods chosen for this study, two different specimen groups were designed. Each specimen group consists of cubic and beam specimens with different mixture content and material types resulting in different compressive strengths.

The prepared samples were visually inspected prior to carrying out UPV and AE testing. UPV testing was carried out under no loading conditions whilst AE activity was studied under compressive and flexural loading conditions. From the compressive and flexural strength tests, it was also possible to obtain the exact strength values of all samples and compare them with the results obtained with the NDT methods employed. The results arising from the destructive and non-destructive tests were analysed in depth in order to evaluate the reliability of the chosen approach in the present study. More specifically, UPV results obtained for each of the samples tested were evaluated against the compressive strength values experimentally recorded.

The effect of water content in concrete on the UPV test results was also investigated in order to evaluate the changes in ultrasonic wave velocity, water-cement ratio and hence compressive strength of concrete samples. For this purpose, water-cement ratio versus ultrasonic wave velocity, and ultrasonic wave velocity with respect to compressive strength graphs have been plotted and analysed. The linear functions and correction factors have been calculated in order to evaluate the applicability and reliability of this testing approach in the field.

The evaluation of damage propagation and the quantification of the damage sustained in concrete structures while in service has been investigated with the help of AE testing. The present investigation looked into correlating all parameters of interest (including AE activity recorded, the nature of the AE activity, damage severity and concrete strength) during the evaluation of the suitability of concrete structures for remaining in-service or not. Various AE parameters have been considered including AE signal amplitude, cumulative AE energy, signal duration, RMS, counts, etc.

The characteristics of AE results have been analysed to evaluate the relationship between concrete mixture content, strength, damage propagation and damage accumulation. It has been clearly observed that the slope of the cumulative AE energy plot with increasing load and hence damage sustained by the samples increases with increasing compressive and flexural strength.

CHAPTER 2

Literature Review

2.1 Concrete

Concrete is one of the most commonly and widely used construction materials due to its excellent properties, long service lifetime, simple production methods and relatively low cost.

Concrete is a composite material made from several readily available constituents such as aggregate and water.

It is a very versatile material that can be mixed easily with the content needed in order to meet a variety of special requirements and can be formed to almost any shape. Concrete has several advantages as a construction material since it is economical, sustainable, durable, fire resistant, energy efficient and easily transportable. However, it also has certain disadvantages, including low tensile strength, low ductility and volume instability [40].

The concrete constituents including, aggregate, water, cement and chemical admixtures have a strong influence on the quality and mechanical properties exhibited. Moreover, the concrete content has direct influence on the results obtained using NDT methods as shown later on. For instance, the aggregate shape, size, cement type, water content all directly influence the test results enabling a relationship to be established with quality and mechanical properties of concrete structures.

2.1.1 Concrete constituents

Concrete is produced by mixing cement, pozzolanic materials, water and fine and coarse aggregate. Chemical admixtures can also be added, if there is the need for special concrete design. In such cases special chemicals such as hardening accelerators, super fluids, etc. can be employed [41-42].

Cement is generally known also as portland cement. Its raw materials are 67% limestone (CaO), silica (SiO₂), ferric oxide (Fe₂O₃), alumina (Al₂O₃) and gypsum (SO₃). Once portland cement is mixed with water, a hydration process occurs. This hydration process involves the following chemical reaction:



C-S-H is a Calcium sulfate hydrate gel resulting in higher concrete strength. Ca(OH)₂ does not affect the strength. However, it does influence concrete durability. After the hydration process, hardened concrete is obtained. Strength and durability of the concrete structures have been specified with mixture designs containing mixture proportions such as gradation, size and amount of aggregates, water to cement ratio, chemical admixtures and cement types [43].

2.1.1.1 Pozzolan

The name of pozzolan comes from the town Pozzuoli in Italy. Ancient Romans back in 120 BC, produced a hydraulic binder by mixing hydrate lime with soil which was mainly based on volcanic ash. It was used to provide binding to fresh concrete. Old or ancient structures stay in-service with natural stones and pozzolanic mortars. For instance, Horosan mortar based on mixing lime with fine burned clay, was extensively used by the Ottomans and other ancient civilisations [44].

Nowadays, direct use of pozzolan by mixing it with calcium hydroxide is no longer common practice thanks to the improvements in cement technology. Pozzolan is generally used in production of blended cements by grinding clinker + pozzolan + gypsum. It is used in admixture of cement, water, and aggregate. It is a siliceous or aluminous material and it has in itself low amount or no cementitious material.

Furthermore, its chemical structure consists of high amounts of silica and alumina and less iron oxide, calcium oxide, silica and magnesium oxide alkaline [45]. Most importantly the total

amount of SiO_2 , Al_2O_3 and Fe_2O_3 increases the binding level of pozzolans. The binding level or pozzolanic activity increases as particle fineness is increased. Fundamentally, pozzolan is reacted to lime with moisture and being converted to cementitious material at the end of this reaction [46]. When it is used in portland cement, it contributes to the mechanical properties exhibited by the hardened concrete through hydraulic or pozzolanic activity or both. Natural pozzolans are resulting from volcanic ash, volcanic tuff and pumice stone. Artificial pozzolans are produced from fly ash, silica-fume and granulated blast furnace slag.

2.1.1.2 Portland cement

Portland cement is produced by mixing CaCO_3 with pozzolanic material consisting in SiO_2 , Al_2O_3 , Fe_2O_3 , clinker and gypsum [47].

If portland cement is mixed with water, paste results. If it is mixed with water and sand, mortar is obtained instead. Finally, if it is mixed with water, sand and aggregates, concrete is produced.

2.1.1.2.1 Chemical composition of the portland cement

Raw materials of portland cement are mainly calcareous rocks consisting of more than 75 % CaCO_3 . They are generally composed of limestone, chalk, marl and marine shell deposits. The other raw material may be Argillo calcareous rocks containing between 40% and 75% CaCO_3 in their chemical composition [48]. They are clayey limestone, marl and chalk. Furthermore, argillaceous rocks are good examples of raw materials. They consist of lower than 40% CaCO_3 in their composition. Clay, shale and slate are good examples of constituents found in argillaceous rock. Many of the oxides in Portland cement are produced at the end of the heating process or clinker. CaO is obtained from limestone, SiO_2 , Fe_2O_3 and Al_2O_3 are obtained from clay, and SO_3 from gypsum. CaO is the main constituent of portland cement accounting for approximately 67% of its total mass [49].

2.1.1.2.2 Main types of the portland cement

There are five main types of cement (CEM) which are given below [50].

CEM I: Portland Cement

CEM II: Portland Composite Cement

CEM III: Portland Blast Furnace Slag Cement

CEM IV: Pozzolanic Cement

CEM V: Composite Cement

CEM I and CEM II cement types are the most commonly used concrete materials worldwide.

In this research study, CEM I has been used for the production of concrete beam and cubic samples employed in the experiments.

Fundamentally, during the production of a cement, raw materials are crushed and stockpiled. Afterwards, they are mixed using calculated proportions to obtain raw-mix. Then, the mixture is put into a rotary kiln having a temperature between 1300 and 1600 C°. This process is commonly known as “burning”. The output is known as clinker containing four main oxides C₂S, C₃S, C₃H and C₄AF.

Afterwards, it is cooled and stored before being mixed with gypsum to adjust the hardening time of concrete. Gypsum extends the setting time in order to increase the workability of concrete. However, too much gypsum causes a high level of volume expansion of the hardened paste or concrete which has adverse effects. Importantly, if excess amount of gypsum is added, minor and major cracking can occur. After the granulation process of clinker, portland cement is obtained [51].

The cement types given above can result in different ultrasonic wave velocities due to the difference in their mechanical properties.

2.1.1.3 Concrete aggregates

Aggregates is one of the most important concrete constituents. In general, sand, crushed stone and gravel have been widely used as concrete aggregates.

There are some important advantages arising by using aggregates in concrete. For instance, workability of the fresh mass concrete can be controlled by changing the aggregate size, shape and amount. Furthermore, strength and durability of hardened concrete can be positively influenced by the presence of aggregates. In addition, the cost of the final product may be significantly lower by using aggregate since it is a proper filler material for concrete [52].

Fundamentally, aggregates have three main functions when used in concrete. Firstly, aggregates provide a mass of particles which is important for resisting the effects of an applied load and giving better durability than cement paste alone. Secondly, it is a relatively cheap filler in the cement. Therefore, it reduces the overall cost of concrete. Finally, it decreases the volume changes resulting from the setting and hardening processes and any moisture changes that occur during drying [53].

Significantly, the mechanical properties of the concrete are directly influenced by mechanical properties of the aggregates. Hence the mineral characteristics of aggregates influence the strength, durability and elasticity of concrete.

Furthermore, the surface characteristics of aggregates impact on the workability of fresh mass and bond between the aggregate and cement paste in hardened concrete. If the aggregate has a rough surface, the workability of the fresh mass concrete decreases and binding increases.

Moreover, grading of the aggregate affects the workability, density and cost of the concrete. High amounts of aggregate decrease volume changes in concrete during setting, hardening and moisture content changes. The amount of the aggregate used increases strength and durability positively.

2.1.1.3.1 Classification of aggregates

The aggregate occupies approximately 70% of a fresh concrete volume. Therefore, this is why aggregate quality, durability, type, shape are all so important in cement production. Moreover, concrete aggregate has to be an inert material which should not react with other substances like cement. Reactive materials which exhibit low inertness cause physical, chemical and thermal-related effects such as swelling, shrinkage, alkali reaction and expansion [54-55].

Similar to the other substances, the aggregate has to be chosen with certain care to obtain a satisfactory concrete quality with the desired mechanical properties. The source of the aggregate is a particularly important criterion during the selection process. Aggregate types can be divided into two categories; namely natural and artificial aggregates. Natural aggregates are generally sand, gravel and crushed stone which are the cheapest and most preferred types of aggregates. Artificial aggregates are obtained after special manufacturing processes such as heating. The most preferred artificial aggregates are blast furnace slag and expanded perlite.

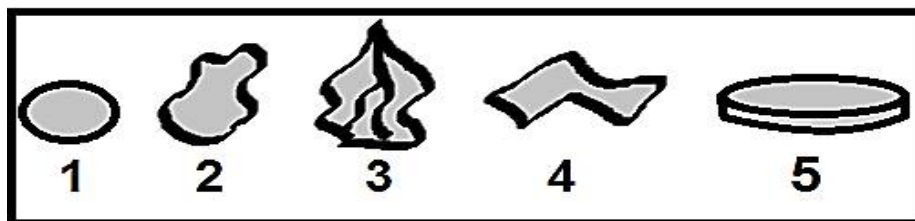


Figure 2: Common aggregate shapes.

As shown in figure 2, the shape of the aggregate is a significant criterion in the production of high-quality concrete. The aggregate shape influences several important concrete properties such as workability, strength and durability. In figure 2, number 1 case shows rounded shape aggregates. They are commonly based on river gravel. Rounded shape is the most suitable to use in fresh mass concrete because flaky, elongated and angular shapes reduce workability and increase water demand. Therefore, strength of the concrete will decrease due to water content increase.

Case number 2 shows an irregular shaped aggregate. It is partly shaped by attrition, so it contains some rounded edges. Such aggregate is generally land gravel. Angular ones have sharp corners which shows little evidence of wear as shown in case number 3 in figure 2. Angular aggregate tends to be crushed stone. Angular particles have stronger bond between cement paste than other shapes, but they also increase water demand in order to increase workability, so they generally result in decreased concrete strength. However, they may result in an increase in the tensile strength of the hardened concrete. Flaky aggregates have the smallest thickness, when compared with the other shapes. They can be circular and angular as shown in case number 4 of figure 2. Finally, elongated aggregates have the largest surface area and their shapes are generally like that of a coin as shown in drawing number 5.

Apart from this, the aggregate size is another significant factor in the production of concrete affecting the resulting properties. Aggregates can be categorized based on the particle size into coarse aggregate having a diameter which exceeds 5 mm or fine aggregates having diameter no larger or equal to 5 mm. Sand is generally used as fine aggregate. It constitutes usually between 35% and 40% of the total amount of aggregate which consists of a mixture of both coarse and fine particles. Concrete aggregate size should be between 0.25 mm and 31.5 mm to enable calculation of the proper concrete mixture design. The particle size distribution in an aggregate sample is known as gradation. It is necessary to mix aggregates because the use of coarse aggregates alone leads to lower workability whilst the use of fine aggregate alone results in higher production and hence construction cost [56]. Therefore, gradation is very important with each country employing different gradation limits depending on local requirements. Aggregate grade and quality parameters are specified in the relevant standards, e.g. EN13139 and BS8204. All aggregate properties mentioned above can influence NDT data obtained during measurements. For instance, the ultrasonic wave velocity and the rebound hammer test results are all influenced by aggregate shape, type and size used in concrete.

2.1.2 Fresh mass concrete

Fresh concrete is produced by mixing of cement (C3S, C2S), water, aggregate and chemical admixtures as discussed earlier. Mixing of C3S with H₂O results in the fresh concrete part. As water reacts with cement concrete hydration takes place. This is an exothermic process causing temperature to increase as the reaction continues. C3S is the constituent that dictates the strength level of the final concrete product [57].

The increase of the fresh concrete temperature causes fast hydration and rapid evaporation of water. Moreover, it causes surface and deep cracks to initiate and propagate due to the sudden evaporation of water molecules resulting in gas pressure to build up. Rapid hydration causes surface cracks and pores to form in the interior of the concrete. Therefore, it necessary to apply curing to decrease the concrete temperature during the hardening process. The hydration process continues throughout the entire lifetime of concrete with concrete pore density increasing with time as water is lost through evaporation. Therefore, the overall durability and strength of concrete remarkably decreases during its lifetime as water content is reduced [58].

2.1.3 Hardened concrete

The chemical formula C-S-H + Ca (OH)₂ represents hardened concrete. C-S-H gel results in the overall concrete strength. It forms after the hydration process of portland cement. Ca(OH)₂ (calcium hydroxide) does not affect the strength of the concrete but it does influence the durability of the hardened concrete [59].

As mentioned earlier, the hydration process continues throughout the lifetime of hardened concrete causing gradual reduction in the total water content present in the composition. As water content reduces concrete porosity will increase with time reducing strength.

2.1.3.1 Main properties of the hardened concrete

The two key properties of concrete are durability and strength. They are measured to evaluate concrete quality. Durability is the ability of concrete to resist external and internal conditions such as weathering action, chemical attack, and abrasion while preserving its designed structure [60]. The strength of a material can be explained as the resistance to failure under a load which can be either compressive, tensile, flexural or a combination of those. Especially for concrete, compressive strength is a significant key parameter indicator of the quality of hardened concrete which directly influences behavior under in-service conditions. Generally, there is a balance to be stricken between durability and strength. Concrete durability increases when strength rises. However, high strength does not always suggest good durability performance since strength and durability are two different properties which are both related to concrete quality. Similarly, concrete exhibiting excellent durability performance may not exhibit high strength because strength is not a durability performance indicator, which can be related to water absorption and permeability [61].

2.1.3.2 Factors affecting durability of hardened concrete

Durable concrete can retain its quality, structural form and serviceability. However, it may be affected by physical, chemical and biological factors [62].

Physical factors are generally abrasion, cavitation, erosion, freezing thawing, thermal effect, overloading, wetting, drying and volume changes. Abrasion starts on concrete surface because of dynamic loads and in case of marine environments tide effects. It can be prevented by using high amount of cement on the concrete surface. Additionally, cavitation is a significant physical factor affecting concrete durability. It has been frequently observed on dam structures due to hydraulic problems. For instance, excessive water velocity and air bubble formation may reduce concrete mass in the dam structure. Furthermore, erosion is a good example of issues associated with concrete durability. It may occur after certain events such as canal lining or spillway

activity in dams. Freezing thawing and thermal effects can negatively affect concrete durability because of the sudden volume changes and potential for cracking initiation and propagation. For instance, water freezing may increase the volume of hardened concrete by 9% resulting in significant tensile stresses to arise internally. Therefore, temperature can strongly influence the durability and strength adversely [63].

Chemical factors are very important for concrete durability, quality and strength. Firstly, alkali aggregate reaction between aggregate and cement may cause minor and major cracking to form in concrete. Because of the reactions taking place, alkali silicate gel expands and damages the hardened concrete structure. Secondly, concrete water and solid components consisting of clayey soils may result in sulfate attacks inside the concrete. Sodium sulfate may react with concrete. Such reactions can cause huge volume changes and expansions in the concrete structure causing tensile stresses to arise and leading to cracking to initiate and propagate. Cracks always cause major reduction in the durability and strength of the concrete although the effect is directly linked to the size of the cracks. Macro cracks pose far more important concern in comparison with micro-cracks. Also, internal cracking has a far more serious effect in comparison with surface cracking that does not propagate through the thickness of the concrete structure. Moreover, acid attack is an important chemical activity affecting concrete durability. For instance, acidic substances such as sulfuric acid can produce air bubbles inside the concrete. Finally, rebar corrosion may occur if chlorine, oxygen, and water affect the concrete chemically. Therefore, they may be principle factors affecting the durability [64].

Finally, biological factors can adversely influence concrete durability significantly. As a good example of biological factors influencing concrete durability, it is possible to consider the effect of tree roots that are located near a concrete structure. Certain types of fungus and bacteria can consume the calcium in the concrete causing the material to lose its fracture toughness and increase brittleness profoundly.

2.1.3.3 Factors affecting strength of the hardened concrete

Compressive and flexural strength of concrete depends on various factors such as water cement ratio, cementitious and binder material content, curing process, degree of compaction, uniformity of concrete, size, gradation, moisture levels, aggregate quality, production method, mixture content and void ratio [65].

First of all, water to cement ratio may affect the strength and durability of hardened concrete. If the water to cement ratio increases, the pore density inside hardened concrete will increase. After the hardening process, amount of the water is reduced. Therefore, porosity in the concrete will significantly increase. Afterwards, harmful chemical substances can easily permeate in the concrete structure because of the numerous pore zones. Furthermore, discontinuities may rise inside the concrete. At the end, strength and durability of the hardened concrete will decrease. Secondly, cementitious and binder materials such as fly ash and cement directly influence compressive and flexural strength of the concrete positively.

Aggregate size also influences the strength. Generally, there is a balance between aggregate diameter and concrete strength. When the aggregate particle size increases, the friction surface of the aggregate increases. This will decrease the concrete workability and increase porosity. Hence, aggregate gradation or size distribution is an important factor affecting concrete strength. Moisture content of the aggregate can influence the concrete strength if water to cement ratio changes in a fresh concrete mixture.

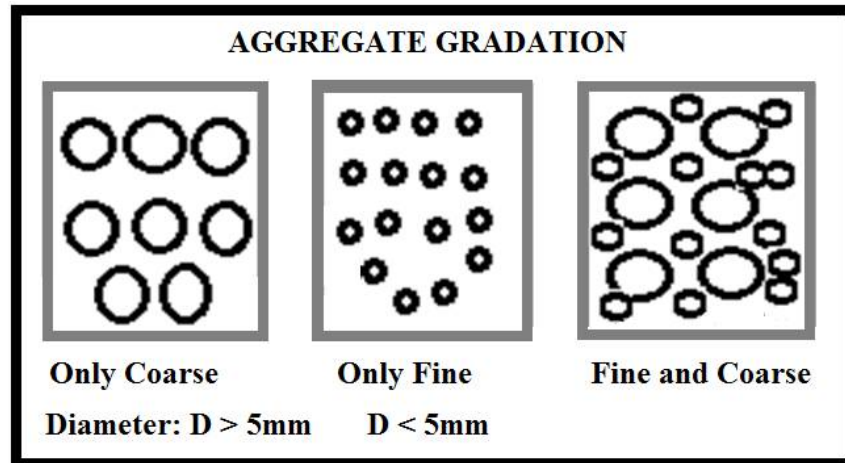


Figure 3: Three different types of aggregate gradations or size distributions.

As it is shown in the schematic diagram in figure 3, coarse aggregate has higher than 5 mm diameter while fine aggregate has a diameter lower than or equal to 5 mm. Most importantly, aggregates have to be selected combining coarse and fine particles as a correctly balanced mixture generally results in less porosity inside the concrete and hence higher strength and durability [66].

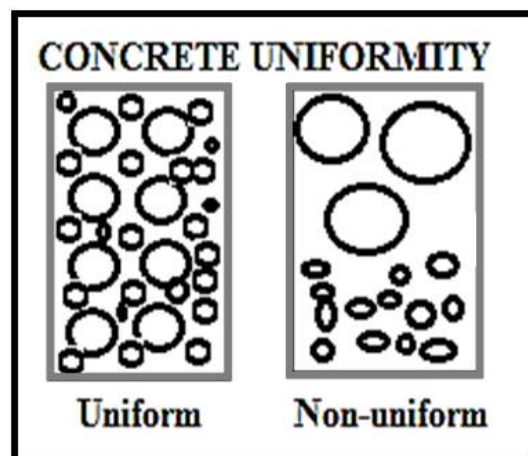


Figure 4: The difference between uniform and non-uniform concrete.

In addition to the aggregate gradation, concrete uniformity may affect concrete strength. Concrete has to be mixed properly to obtain a uniform concrete structure. As it is shown in the

schematic diagram in figure 4, coarse and fine aggregates have to be distributed uniformly to reduce voids and discontinuities inside hardened concrete [67].

Furthermore, curing is an important process influencing both concrete durability and strength, especially under hot weather conditions. Under hot weather conditions, hydration and evaporation process occurs more rapidly. Hence, concrete will require additional water for hydration, especially during the first week. If there is not enough water, major and minor cracks can form inside the concrete [68].

Finally, the degree of compaction and production method of the concrete are significant factors affecting strength and durability. For instance, proper use of a concrete agitator may eliminate the voids that may be present inside fresh concrete.

2.2 Discontinuities and defects in concrete structure

Concrete structures produced by using portland cement commonly achieve exceptional durability [69]. Therefore, it is the most widely used construction material in the world. However, severe external and internal factors may cause deteriorations of the concrete structure. For this reason, aesthetic, functional and structural problems can be observed. As it is mentioned previously, concrete may deteriorate due to various chemical, physical, environmental and biological factors. The following sections of the present thesis discuss common causes of concrete defects.

2.2.1 Cracks before the hardening process

Fundamentally, concrete cracks may be divided into three main groups, which are: plastic shrinkage, plastic settlement and formwork movement cracks. They are frequently observed before the hardening process takes place.

Significantly, plastic shrinkage cracks occur under hot and windy weather conditions. Due to bleeding and shrinkage combined with fast hydration, water inside the concrete moves upwards and evaporates suddenly resulting in cracks such as those shown in figure 5 to form [70].

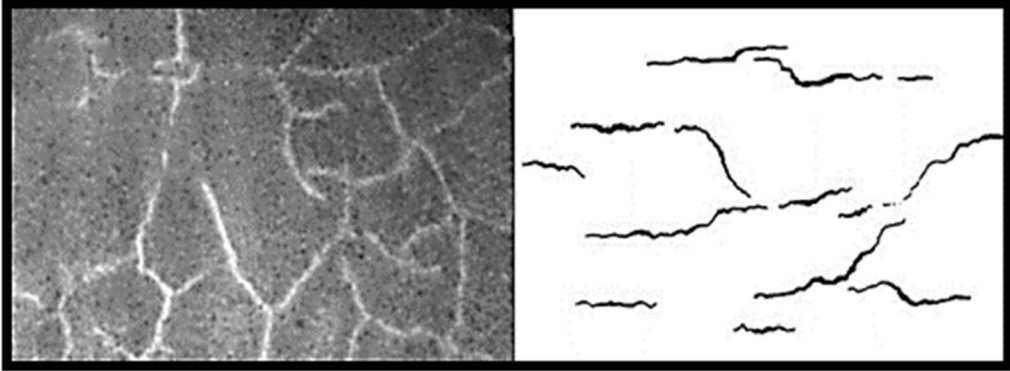


Figure 5: Plastic shrinkage cracks because of rapid evaporation on the surface [70].

Also, inadequate curing may cause this type of cracks to form on the concrete surface. To take preventive measures against the occurrence of this phenomenon, proper curing and wet covers can be applied on the concrete surface, especially during hot weather conditions.

Furthermore, minor and major cracks as shown in figure 6, can form if concrete formworks are moved during the hardening process [71].

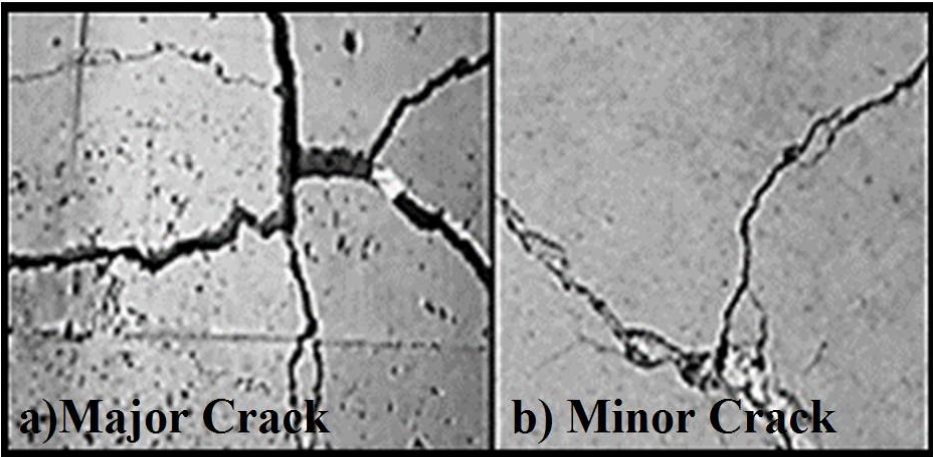


Figure 6: Formwork movement cracks [71].

Apart from this, plastic settlement cracks may also form when fresh mass concrete suddenly moves to fill the large voids inside the structure. To prevent the cracks from forming, agitators can be used in fresh concrete during pouring process as shown in figure 7 [72].



Figure 7: Agitators used to prevent cracks and segregation [72].

Moreover, the use of agitators can prevent segregation, void and discontinuity formation which are frequently observed after hardening [73].

2.2.2 Cracks after hardening process

Bleeding crack is one of the main problems after the hardening process. Sudden movement of water in concrete towards the top surface causes settlement of the heavier particles such as coarse aggregate towards the bottom side of the structure. This results in high amount of water with low amount of cement and aggregate to accumulate on the surface as shown in figure 8. This can result in bleeding cracks to be observed on the concrete surface [74].

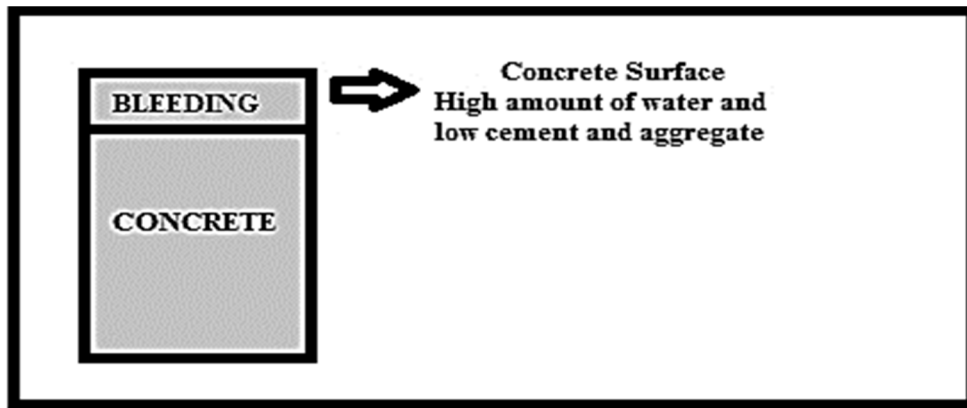


Figure 8: Bleeding on concrete surface.

Spalling is a common problem especially in older reinforced concrete structures [75]. It is frequently observed after bleeding cracks form. Firstly, the water to cement ratio increases while concrete strength decreases on the concrete surface. After evaporation of the water, bleeding cracks are observed. Afterwards, external water and chlorine can easily pass into the reinforced concrete from its surface and cause corrosion of the rebars. Finally, the volume of the rebars increases and spalling cracks similar to those shown in figure 9.

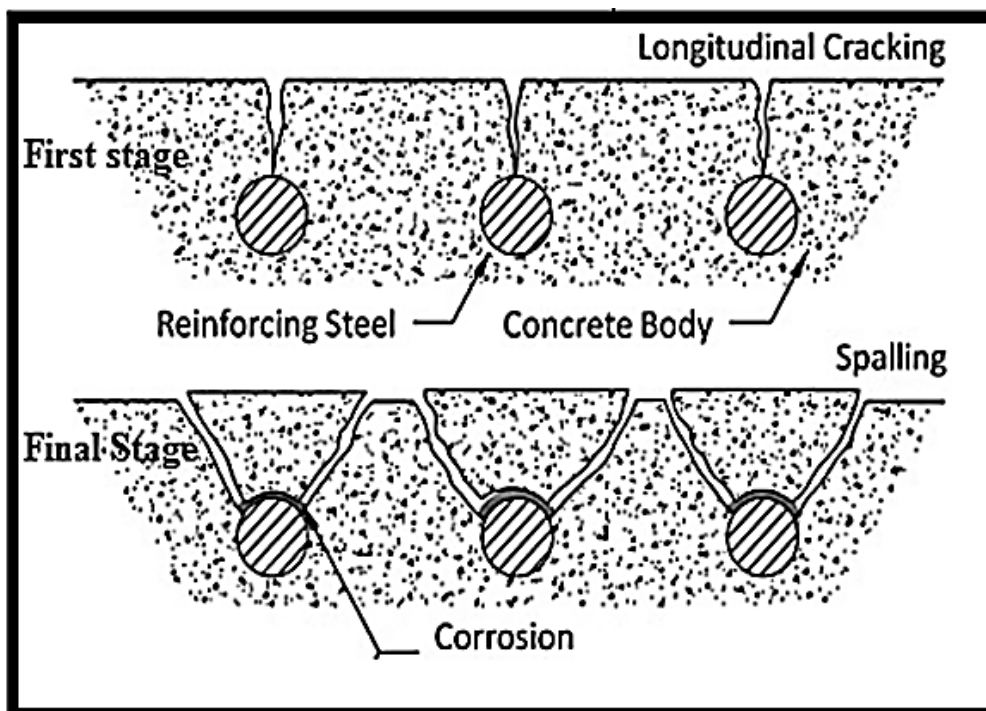


Figure 9: First and final stage of the spalling cracks [75].

Honeycombing is another common concrete degradation mechanism. It occurs on the concrete surface when the amount of coarse aggregate particles is too high [76]. Furthermore, inadequate agitation can cause rough hardened concrete surface and discontinuities to form as shown in figure 10.

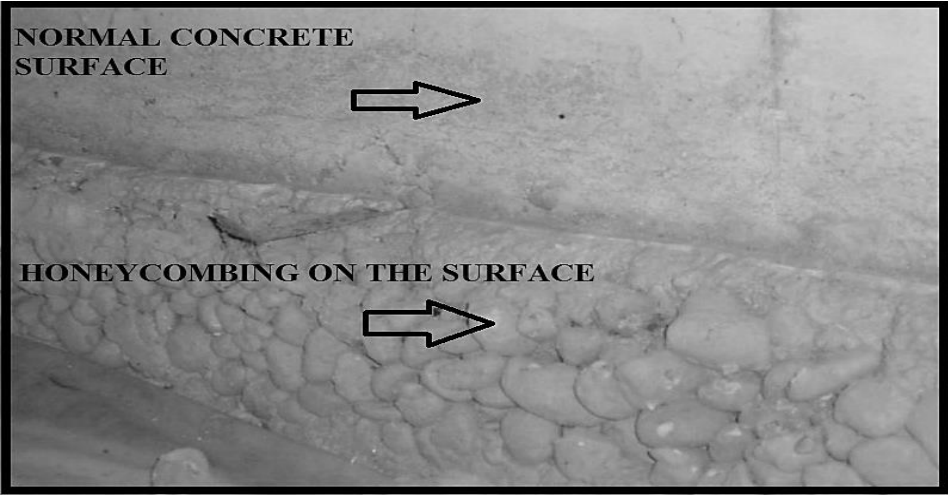


Figure 10: Honeycombing distortions in hardened concrete [76].

Dusting, crazing and rain damage, as shown in figure 12 all adversely affect quality, durability and strength of concrete.



Figure 11: Effects of dusting, rain damage and crazing on concrete surface [77].

Crazing forms an equiaxed pattern on the concrete surface because of inadequate curing and water shortage. Additionally, dusting occurs as a result of bleeding effects on the surface. Finally, rain droplets can damage concrete if a protector such as cover is not used on the concrete surface during hardening process [77].

CHAPTER 3

Experimental Methods Considered

3.1 Summary of the chapter

As mentioned in chapter 1, there are various types of different techniques which can be used to evaluate quality, durability and strength of a concrete structure. Concrete structural defects can be examined and evaluated using appropriate NDT without causing further degradation to the structure.

This chapter is presented to explain which destructive and non-destructive testing techniques have been employed in this research study. Visual inspection, UPV and AE testing have been selected as the NDT techniques in order to perform accurate and reliable quantitative quality control of concrete beam and cubic specimens specifically produced for this study. To obtain the actual flexural and compressive strength values of the samples, compressive and flexural testing has been employed as destructive techniques in conjunction with the NDT techniques considered herewith.

3.2 Destructive testing methods

Destructive tests have been commonly used to directly assess concrete strength. There are different destructive testing techniques which can be used, such as pull out, pull off, core, bending, compression and splitting testing. Flexural and compressive strength tests are the most frequently used methods to obtain the exact strength values of concrete components of interest [78]. Core testing has been used often for the quantitative assessment of existing structural components. Destructive tests are also employed in order to validate the findings of NDT methods and increase confidence in the results obtained [79]. The data obtained can also be used to predict the future durability exhibited by a particular concrete structure.

Destructive testing can be the preferred approach for obtaining information about the actual structural condition of concrete, such as uniformity of a hardened concrete component.

The destructive testing techniques used in this research study are discussed in the following sections.

3.2.1 Flexural strength testing

Flexural strength or bending testing has been used to classify materials according to the flexure strength or modulus of rupture recorded for the different sample used [80]. There are different standard formulations depending on specimen dimensions, loading points (P), inner distance between loading points (Li) and outer distance (L). The schematic diagram in figure 12 shows the test setup used for 4-point bending of concrete beam structures. The standard formula employed is also provided where $P=F/2$.

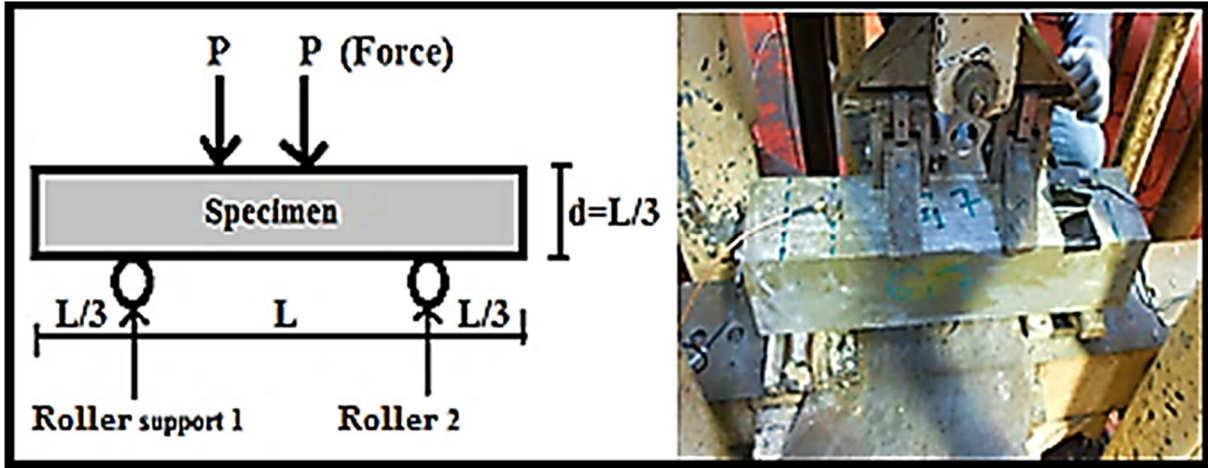


Figure 12: 4-point bend setup of the flexure strength test.

The flexural strength can be calculated using the formula below.

Flexural Strength = Modulus of rupture = Bending strength;

$$\frac{N}{m^2} = \sigma = \frac{F L}{b d^2} = \frac{2P L}{b d^2}$$

where,

F is the load (force) and it is equal to $2P$.

L is the length of the support span.

b is width.

d is thickness.

The flexural test is used to also evaluate the tensile strength of the concrete. The method gives the failure load capacity of a reinforced or unreinforced concrete beam or slab undergoing bending. From the test results the modulus of rupture in MPa can be obtained quantitatively. Test specimens can be classified depending on their flexural strength capacity up to failure [81].

3.2.2 Compressive strength test

Compressive tests are used to determine the compressive strength of cubic and/or cylindrical samples [82]. After the production of fresh concrete, cubic and cylindrical moulds are filled with fresh concrete to test their strengths in a laboratory. These moulds have specific dimensions as specified by the standard employed. General standard dimensions of cubic samples are shown in figure 13. After one day of setting, hardened concrete specimens can be moved from the construction site to the laboratory and placed in the curing pool. After twenty-eight days in the pool, specimens can then be tested in compression.

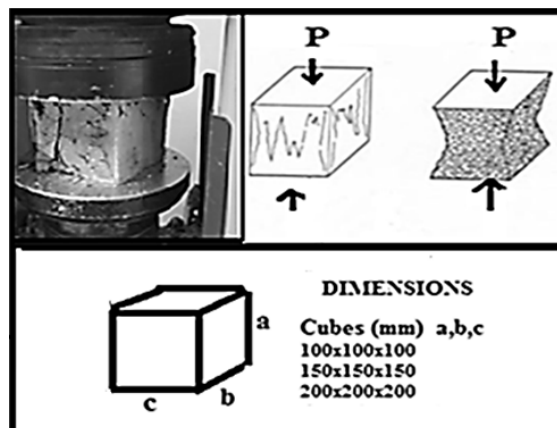


Figure 13: Compression test and standard cubic specimen dimensions.

Compressive strength is obtained from the failure load divided by the cross-sectional area of the specimen. In modern tests, the dimensions of the specimens are entered as parametric information of the test and once the device applies the load the stress levels are calculated automatically. The exact same method can be applied on cylindrical core sample trepanned from an existing structure.

For instance, the designed compressive strength of an existing structure may be equal to 30 MPa. However, the strength may decrease as the structure ages, due to improper production or other factors discussed in chapter 2. Therefore, cylindrical specimens may need to be extracted from different components of a structure in order to perform compressive strength testing and evaluate the actual current compressive strength. By evaluating the compressive strength of the components of the structure durability and quality can be confirmed [83].

However, as explained earlier, destructive testing causes undesired damage on existing structural components. Therefore, NDT methods are strongly preferred for estimating the quality, durability and strength of an existing structure.

3.3 Non-Destructive Testing Methods

There are many reasons to use NDT such as visual inspection, UPV or AE testing. First of all, voids, cracks, honeycombing and other types of defects, discussed already in chapter 2, can be determined. The quality and durability of an existing structure can hence be accurately quantified. Moreover, the location of reinforcing rebars, their diameter and level of corrosion damage affecting them can also be assessed. Also, the bonds between hardened concrete and rebars can be examined by using appropriate NDT methods, radiography or ultrasonic phased array testing [84-86].

In addition, the approximate lifetime of an in-service concrete structure (e.g. column, beam or slab) may be determined by investigating the porosity level, the presence of discontinuities, cracking and various other types of defects [87].

3.3.1 Visual inspection test

Visual inspection is the oldest and most common NDT method for almost any type of concrete structure. Surface cracks can be readily detected and classified depending on their shapes and locations on the surface of concrete elements. Figures 14 and 15 illustrate the various crack types and their main causes [87-88].

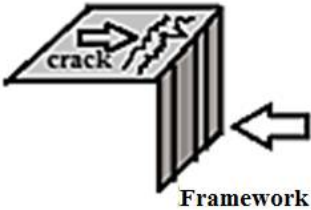
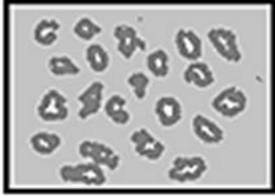
| | | |
|--|---|---|
|  |  |  |
| <p>- Cracks due to inadequate distance between concrete surface and steel rebars</p> | <p>- Cracks due to framework movement during hardening process of fresh concrete.</p> | <p>-Rain damage -Excess water on concrete surface</p> |
|  |  |  |
| <p>-Cracks due to earthquake -Differential settlement</p> | <p>-Earthquake, excess load effects -Shear and bending stress -Shear and bending moment</p> | <p>-Bleeding cracks</p> |

Figure 14: Types of hardened concrete cracks depending on some factors.

The danger level arising from cracks can be determined depending on their shapes and depths. In figure 14, some critical crack types have been given in detail. For example, differential settlement earthquake and excess load cracks are extremely important because they may drastically affect strength and durability of the concrete components.

In addition, the depth, length and location of the crack are important in the estimation of the danger level arising. For instance, earthquake cracks, posing high danger level, generally occur in the joint between the column and beam. Therefore, they can increase the probability of structural collapse exponentially. Bending, moment and shear cracking, shown in figure 14, is critical. Such cracking can be detected by evaluating the angular shape of the cracks, frequently located at the bottom of a beam and top of a column [89].

Bleeding cracks and rain damage, shown in figure 14, also negatively affect hardened concrete surface durability and appearance. As explained in chapter 2, they can result in additional damage such as spalling as shown in figure 15 [90].

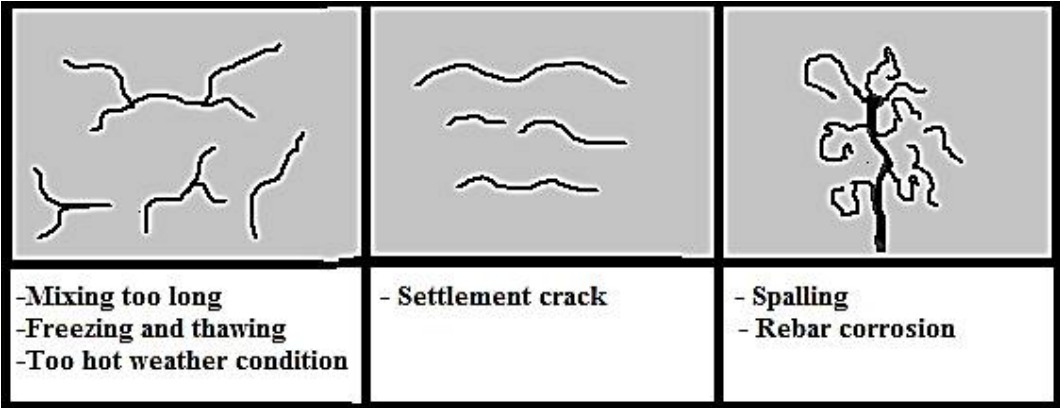


Figure 15: Types of hardened concrete surface cracks depending on the causes.

In the presence of surface cracks, chlorine may pass into reinforced concrete structures and cause rebar corrosion. Cracking due to inadequate distance between concrete surface and steel rebars and cracking due to framework movement may have important effect, due to the large crack depths.

Hence, visual inspection can quickly provide a general picture of the nature and severity of various crack types. Maintenance can then be decided depending on the visual inspection or further testing may be required to increase confidence in the findings and increase the reliability of the maintenance actions decided to be carried out [91].

3.3.2 Ultrasonic pulse velocity testing (UPVT)

As mentioned in chapter 1, ultrasonic testing is one of the most widely used NDT methods, in several industries. Portable UT devices are widely employed for the rapid evaluation of concrete elements in construction sites.

UT equipment consists of a piezoelectric transducer which operate at a given frequency. The piezoelectric element produces pulses of ultrasonic waves which are transmitted from the transducer to the test piece and propagate along its microstructure at a specific velocity which also depends on the type of wave (compressive, shear, Rayleigh, Lamb or creep).

3.3.2.1 General procedure of the UPVT

UT methods have been frequently used for the quality control of homogeneous materials such as metals and welds. UT has been increasingly employed for the quality and durability assessment of concrete materials [92]. UPV testing is a reliable and quick method for assessing the strength of concrete structures. Additionally, it provides a repetitive means of assessment. In other words, it can be performed as many times as required in order to maximise confidence. The test procedure for concrete materials has been specified in relevant standards, e.g. BS 4408 part 5 and BS1881 part 203.

Modern testing devices comprise of a transmitting and receiving transducer, ultrasonic pulse generator, time measuring circuit, time display unit and signal amplifier [93].

In UPV the ultrasonic pulse generator produces pulses which travel from the transmitting transducer to the receiving transducer through the concrete structure as shown in figure 16.

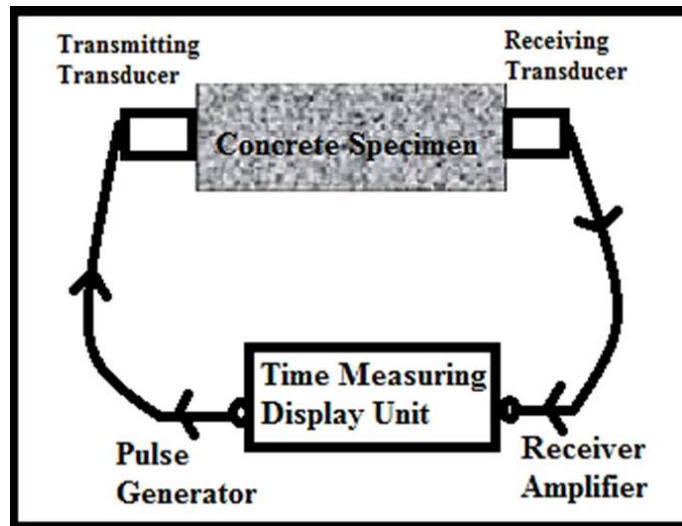


Figure 16: Working principle of UPVT.

The display on the test devices shows the average travel time of the ultrasonic wave between the transmitting and receiving transducers in μs as shown in figure 17.



Figure 17: Display unit and an application of the UPV test.

The average pulse velocity can then be calculated by using the formula given below provided that the distance between the two transducers has also been measured [94].

$$\text{Velocity}(V) = \frac{\text{Distance between transducers (X)}}{\text{Time (t)}}$$

The changes occurring in the ultrasonic pulse velocity can be directly related to the strength of the concrete.

Before applying the test, vaseline, liquid soap, grease or other similar gels can be used to couple the transducers on the surface of the testpiece, as shown in figure 17. Grease is suitable for rough surface as it removes the effect of air pockets and reduces acoustic impedance mismatch. Liquid soap on the other hand is good for coupling on relatively smooth surfaces. Gel eliminates air pocket between the surface of the transducer and concrete material and decreases the acoustic impedance mismatch enabling higher transmissibility of the ultrasonic wave energy into the concrete [95]. However, care needs to be taken to ensure the couplant path is not excessive as this will add to the distance travelled by the ultrasonic wave and will increase the error in the measurement. The couplant film needs to be maintained as consistent and as thin as possible in all measurements to avoid errors in the extrapolation of the strength.

3.3.2.2 Application methods of UPV testing for concrete components

In BS1881 and BS4408, three key application methods of UPV testing are discussed for concrete structures. They generally depend on the position of transmitting and receiving transducers.

The first approach is direct transmission. It provides the most reliable pulse velocity results because pulse waves can be easily transmitted from the transmitting to receiving transducer, thanks to the fact that the transducers face against each other as shown in figure 18. Moreover, the sound path length can be measured very accurately although care needs to be given not to include errors arising from the couplant film thickness through which the ultrasonic wave also needs to travel [96].

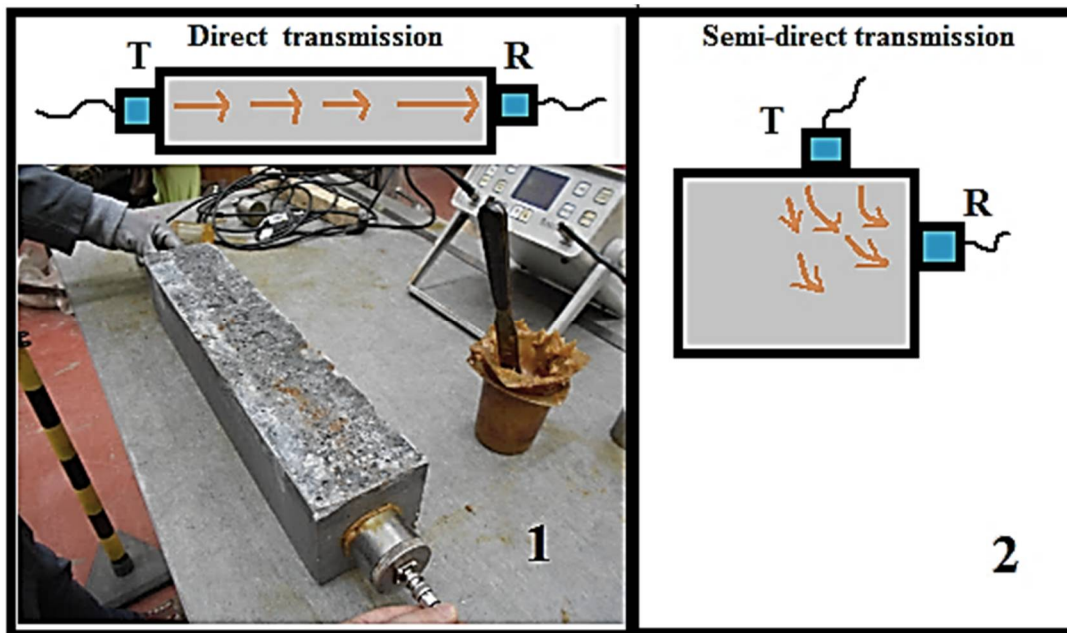


Figure 18: Direct and semi direct transmission techniques.

The second approach is based on the semi-direct transmission, which is applied with an angle between the two transducers of less or equal to 90° as shown in figure 18. This approach is generally employed when direct transmission is not possible. It is less reliable technique because a part of the ultrasonic waves does not reach the receiving transducer [97]. Furthermore, because of the angle between transducers, the sound path length may not be accurately determined. Therefore, the results produced with this approach are prone to a higher level of error which needs to be taken into account [98].

The last approach is indirect or same face transmission. It has the lowest reliability because the exact sound path length cannot be measured to obtain an accurate ultrasonic pulse velocity value [99]. Additionally, it may not provide sufficient information regarding the entire concrete structure since the transducers are applied on the same face [100]. According to BS1881 part 203, this method should be used when only one face of a concrete element is accessible.

This particular UPV testing approach has been generally used on concrete slabs for the evaluation of surface cracks.

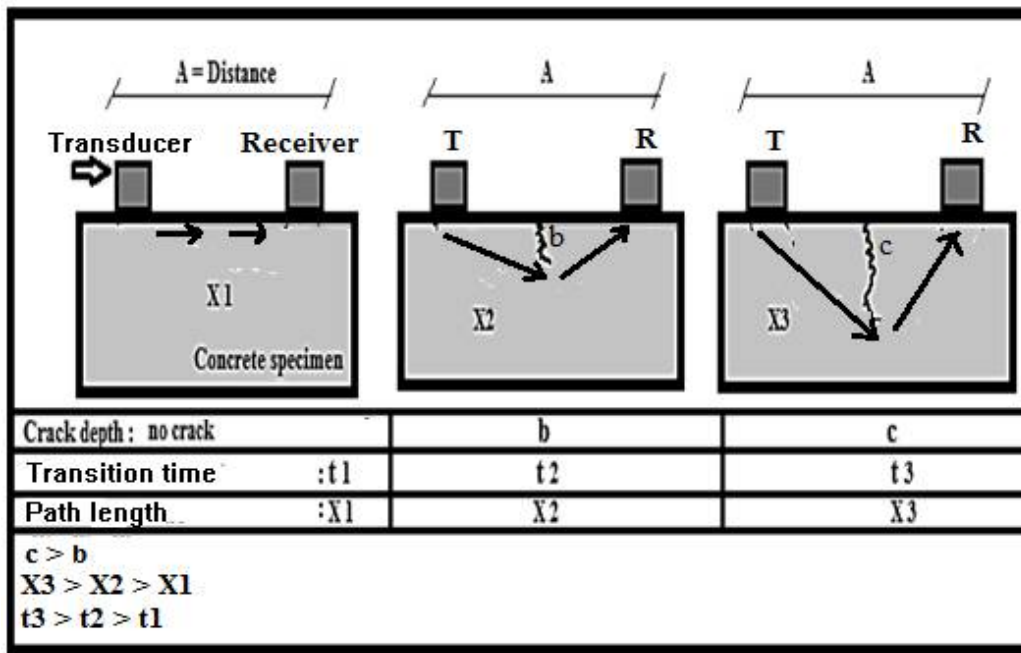


Figure 19: Effects of surface discontinuities on transition time and path length.

The schematic drawings in figure 19 show different concepts used for indirect transmission of the ultrasonic wave. The drawings show the transition time and sound path lengths depending on crack depth. If the crack depth increases, so does the transition time of the ultrasonic waves. Hence the, measured pulse velocity appears to increase although in reality this is due to the longer sound path that the ultrasound is forced to follow when travelling from the transmitting transducer to the receiving one. Hence, apparent, ultrasonic wave velocity changes can be used to indirectly estimate the crack depths. Water filled voids and pore zones cause lower ultrasonic wave velocity when compared with normal ultrasonic wave velocity for high-quality concrete [101-102].

3.3.2.3 Measurement of the crack depth by using surface transmission

As shown in figure 20, the first approach can be employed to measure the crack depth when the crack is propagating normal to the concrete surface [103].

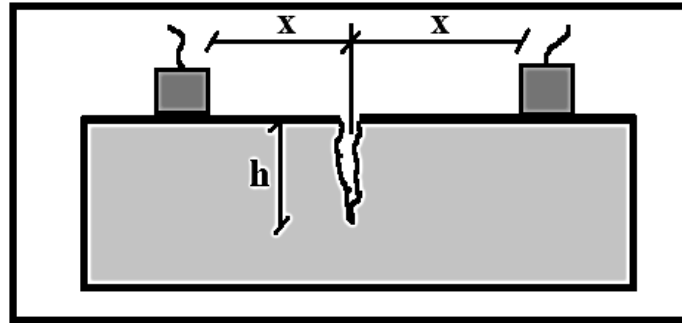


Figure 20: Measurement of crack depth perpendicular to the surface.

According to BS 1881 part 203, first formula to calculate the vertical crack depth ‘h’ is;

$$h = 150 \sqrt{\frac{4t_2^2 - t_1^2}{t_2^2 - t_1^2}}$$

Where,

t₁ is the transit time when x is 150mm;

t₂ is the transit time when x is 300mm.

According to C.Watanable [104] an alternative formula that can be employed is the following;

Path length without crack = 2x

Path length around crack = $2\sqrt{x^2 + h^2}$

Surface travel time without crack = $\frac{2x}{V} T_s$

Travel time around crack = $\frac{2\sqrt{x^2 + h^2}}{V} = T_c$

Crack depth = $h = x \sqrt{\left(\frac{T_c^2}{T_s^2} - 1\right)}$

In the formula proposed by Watanabe, T_s can be obtained from non-crack location of the same concrete element by keeping the distance between the transducers at $2x$. T_c is already obtained from the crack location. The reliability of this formula can normally be $\pm 15\%$ according to experimental evidence. However, it may decrease when crack width is too small.

In both cases, the distance, x , between the crack and each of the transducers has to be equal and the crack has to propagate normal to the surface as shown in figure 20. Many alternative approaches such as the T_c-T_0 , Delta and L-L method can be applied for the measurement of depth of cracks propagating perpendicular to the surface.

However, for the oblique or inclined crack types, different test methods should be selected to measure crack depth [105].

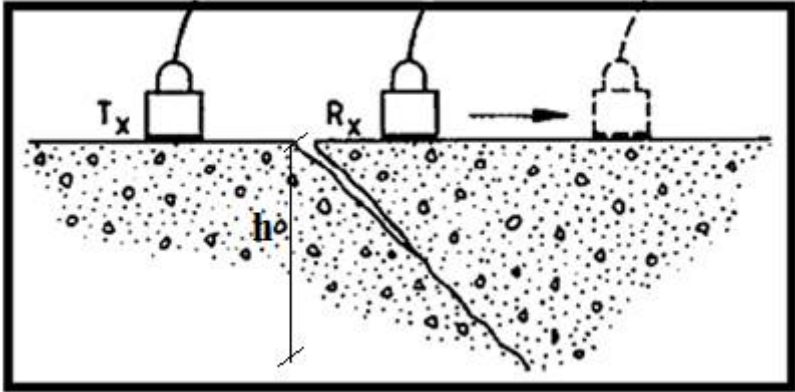


Figure 21: Crack depth measurement for the oblique or inclined cracks (BS 1881 part 203).

In figure 21, an oblique crack and transducer arrangement is shown. According to BS 1881, part 203, the formula to calculate the inclined crack depth, h , is:

$$h = \frac{x}{2} \sqrt{\left[\left(\frac{2Ta^2 + 3Tb^2}{Ta Tb} \right)^2 - 25 \right]}$$

Where,

T_a is the transit time for distance $2x$;

T_b is the transit time for distance $3x$.

To employ this formula correctly, T_x has to be placed at a distance of $2.5x$ from the centre of the crack and R_x should be placed $2x$ and $3x$ distances from the centre of the crack to obtain T_2 and T_3 respectively, where x is 150 mm. After these steps, the crack depth can be calculated..

3.3.2.4 Strength estimation for the concrete by using UPVT

Concrete quality can be extrapolated from the average transition time of the pulses between transmitting transducer and receiving transducer. Also, the ultrasonic wave velocity can provide information about the strength, durability and homogeneity of the concrete structure [106]. As mentioned in chapter 2, various types of defects such as cracking and segregation can also be detected.

Ultrasonic pulse velocity in a concrete sample increases when the compressive strength of the sample increases [107-108]. This is expected since the velocity of compression ultrasonic waves is a function of the Young's modulus of elasticity of the material (E) and its density (ρ), whilst the shear wave velocity is a function of the shear modulus (G) and density (ρ) [6]. Generally, the elastic modulus of a material is defined as the slope of its stress-strain curve in the elastic deformation region [109].

In accordance with the ACI 318, 363 and BS8110 the general equation of the modulus of elasticity for a hardened concrete is:

$$E_c = 33 w_c^{1.5} (f'_c)^{1/2} \text{ psi.}$$

Where,

w_c = Unit weight of the concrete, f'_c = Compressive strength of the concrete (after 28 days).

The modulus of elasticity of concrete depends on its density and compressive strength [110].

However, compressive strength of the concrete may be affected by the type, amount and mix-proportion of aggregate, cement, water and chemical admixtures.

3.3.2.5 Factors affecting the pulse velocity in concrete

Various experiments and reports have indicated that aggregate type, moisture content, concrete age, water to cement ratio, sound path length, discontinuities, defects, voids, porosities and cracks are the main factors affecting the ultrasound pulse velocity in concrete. Studies by R. Jones and I. Facaoaru have shown that the type, amount, shape, volume and mix-proportion of the aggregate remarkably affect the ultrasound pulse velocity [111].

Based on extensive experimental measurements plots associating ultrasound pulse velocity and compressive strength has been produced which are discussed later on.

According to J. H. Bungey, velocity, intensity and direction of the pulse wave in concrete changes under the presence of rebars, voids and micro-crack as shown in figure 22 [112].

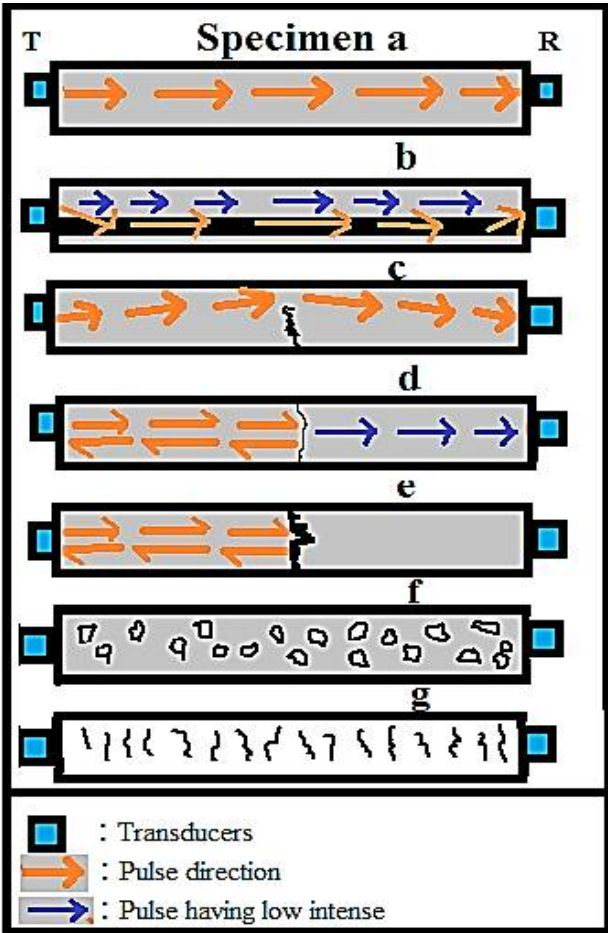


Figure 22: Pulse movements under certain conditions [112].

Figure 22 illustrates different experimental setups employed by Bungey [112]. In his experiments, specimen “a” indicates the concrete specimen without a rebar. Pulse waves transmitted through the specimen travel along the shortest path from transmitting to receiving transducer.

Specimen “b” is the reinforced concrete sample. An important part of the energy of the pulse waves travels along the steel rebars and a small amount of the pulses travels through the concrete itself. Rebars in this case serve effectively as wave guides.

Bungey reported that the steel rebars present in concrete affect UPV measurements because the ultrasonic wave velocity in steel rebar is almost 1.7 times higher than that in concrete. Bungey proposed certain relationships and formulas to quantify the effect of the presence of rebars in reinforced concrete UPV measurements. To achieve this correction factors were applied in order to obtain reliable ultrasound pulse velocity results [113].

Specimen “c” was employed to evaluate the effect of shallow cracks on pulse direction and velocity. The presence of cracks decreased ultrasound pulse velocity and increased transition time between transducers.

Sample “d” was used to evaluate the impact of narrow cracks on ultrasound pulse velocity and direction in concrete. Part of the ultrasound energy was reflected by the crack and other part of the waves was transmitted by losing their wave amplitudes and velocities.

Specimen “e” considered the effect of wide cracks causing total reflection of ultrasonic waves. Therefore, for this particular scenario ultrasound pulse velocity could not be measured.

Ultrasonic waves in specimens “f” and “g” travelled around voids and microcracks resulting in a reduction in wave energy and measured velocity. Also, the ultrasonic waves were capable of propagating through the water filled voids and microcracks but some energy was lost and the velocity decreased [114]. Significantly, scientists Popovic and Wu confirmed that the presence of micro-cracks in concretes led to a decrease in the measured ultrasonic pulse velocity [115].

Apart from this, as shown in the following figure, R. Jones and I. Facaoaru reported that concrete samples made with lightweight aggregates had lower pulse velocity than concrete samples made with heavier aggregates [116].

For instance, in concrete samples containing Leca, ultrasound pulse velocity was measured in the range of 3.3 km/s for 20 MPa compressive strength. However, for concrete samples containing gravel the measured ultrasonic wave velocity was found to be 4.5 km/s pulse velocity for the same compressive strength. The plots in figures 23 and 24 show the differences in ultrasonic pulse velocity for different aggregate types and different compressive strength measured. In all cases, the measured ultrasonic wave velocity clearly increases with increasing compressive strength.

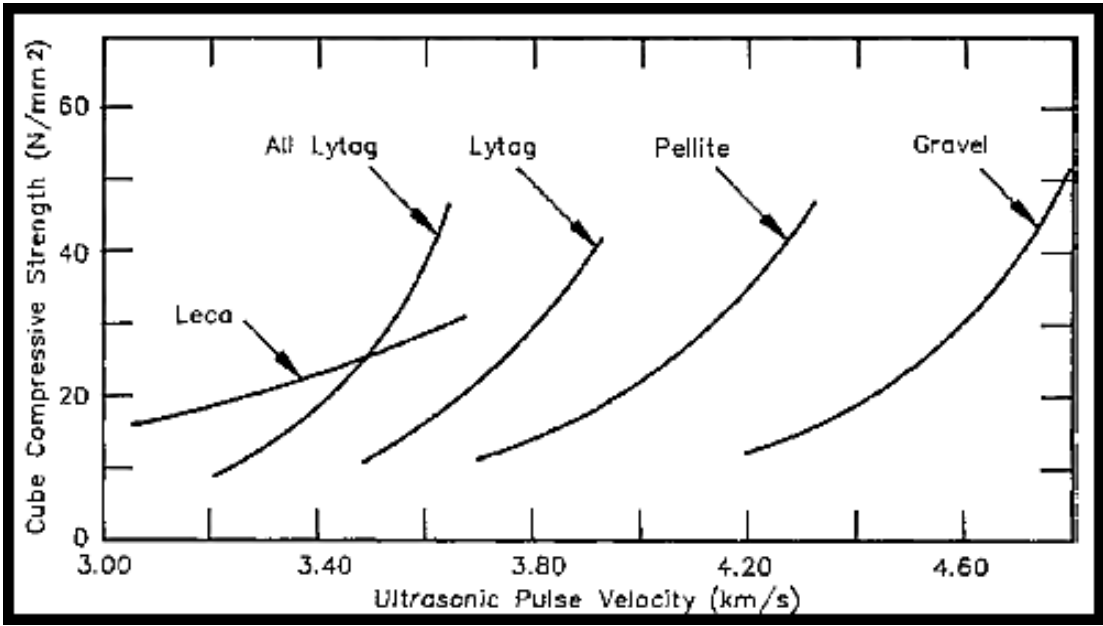


Figure 23: Comparison of the concrete samples having light and heavyweight aggregates [116].

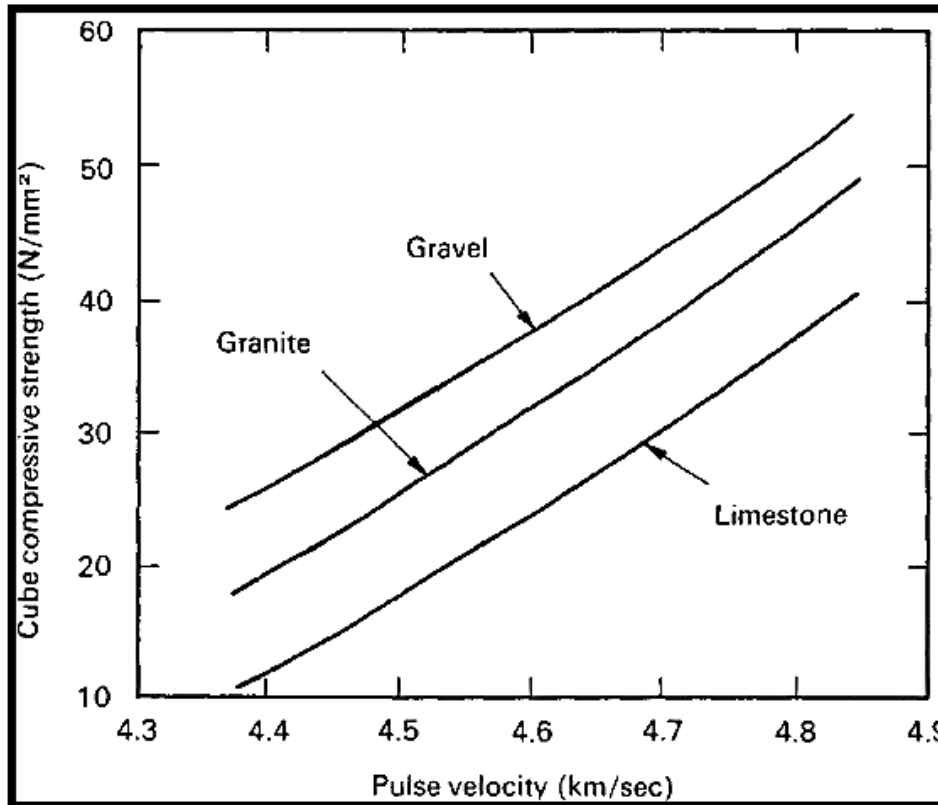


Figure 24: Comparison of the specimens having gravel, granite and limestone [116].

As it can be seen in figure 24, concrete made with gravel has lower pulse velocity than limestone and granite for the same compressive strengths. Additionally, for the same mixture design, i.e. for the same water to cement ratio, it was found that concrete sample having rounded stone aggregates had higher ultrasonic pulse velocity than the specimen containing crushed stone as its aggregate. However, their respective measured ultrasound pulse velocities were close to each other. Cement paste in hardened concrete has also been measured to have a lower pulse velocity than gravel aggregate [117].

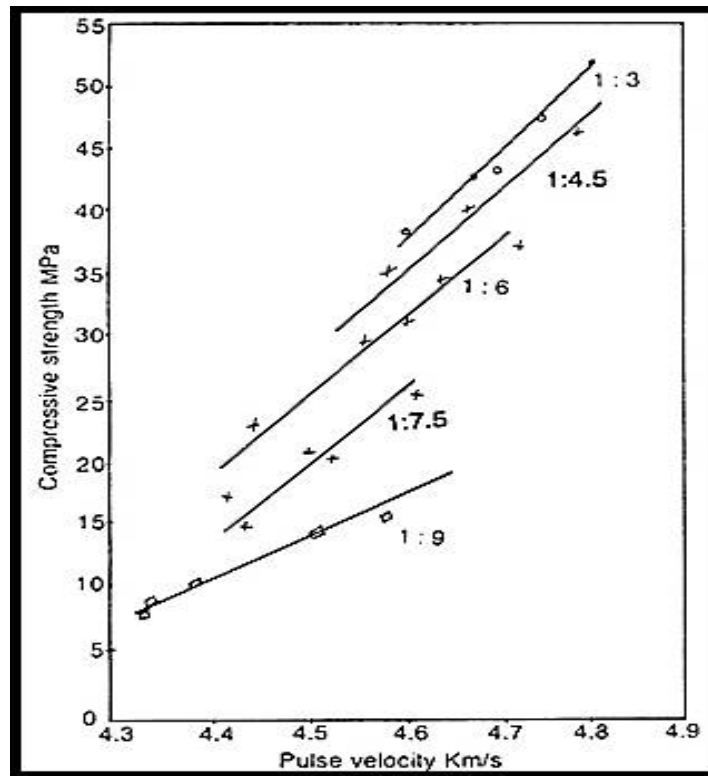


Figure 25: Effect of the different mix-proportions for cement and aggregate [118].

Jones produced concrete samples, having various aggregate mix-proportions, to investigate their pulse velocities. He observed that for a constant water to cement ratio, higher aggregate content resulted in higher ultrasonic pulse velocities being measured. Moreover, it was noticed that the ultrasound pulse velocity in aggregate was generally higher than that measured for cement paste [118].

The other factors affecting the ultrasonic pulse velocity in concrete are related to the cement type and chemical admixture employed. Although it was originally suggested that cement type and chemical admixtures did not affect the pulse velocity this was proven not to be the case after experiments reported in later studies carried out. Experiments involving different chemical admixtures decreasing hardening time of the concrete resulted in a slight increase of the measured ultrasonic pulse velocity in concrete [119].

Furthermore, water to cement ratio and concrete age have a significant effect on measured ultrasonic pulse velocity. According to several studies, increase of the water content in concrete decreases the compressive strength and corresponding ultrasonic pulse velocity [120].

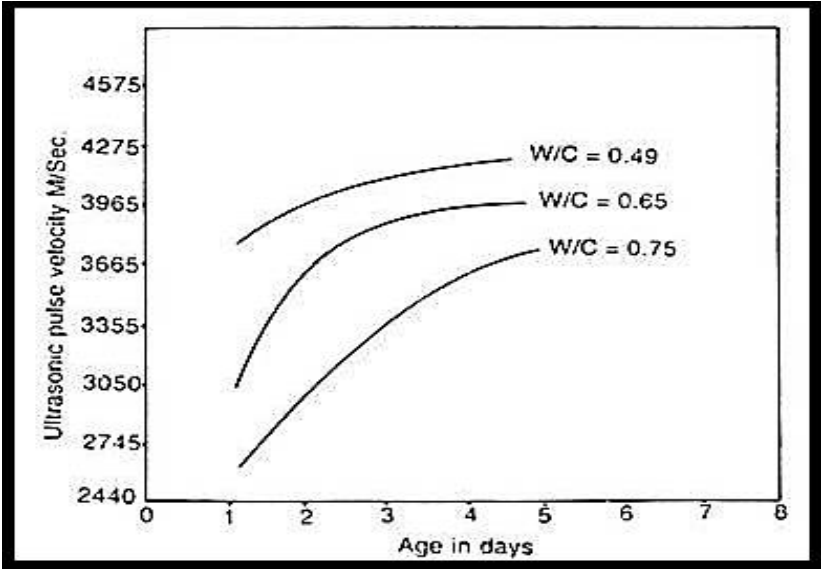


Figure 26: Effects of the water to cement ratio and ageing factors [121].

Figure 26 shows the increase in the measured pulse velocity with hardening for the ageing during the first 7. Approximately 7 days later, measured ultrasonic pulse velocities are almost constant. From the plots in figure 26, it can be concluded that the ultrasonic pulse velocity decreases while the water to cement ratio is higher. Water to cement ratio decreases the concrete strength and increases the void ratio in concrete. In the long term, concrete ageing adversely affects the ultrasonic pulse velocity because the hydration process goes on throughout its entire lifetime. Therefore, the amount of water decreases and void ratio increases with time. Hence, the increasing void to volume ratio results in a noteworthy reduction in the measured ultrasonic pulse velocity [121].

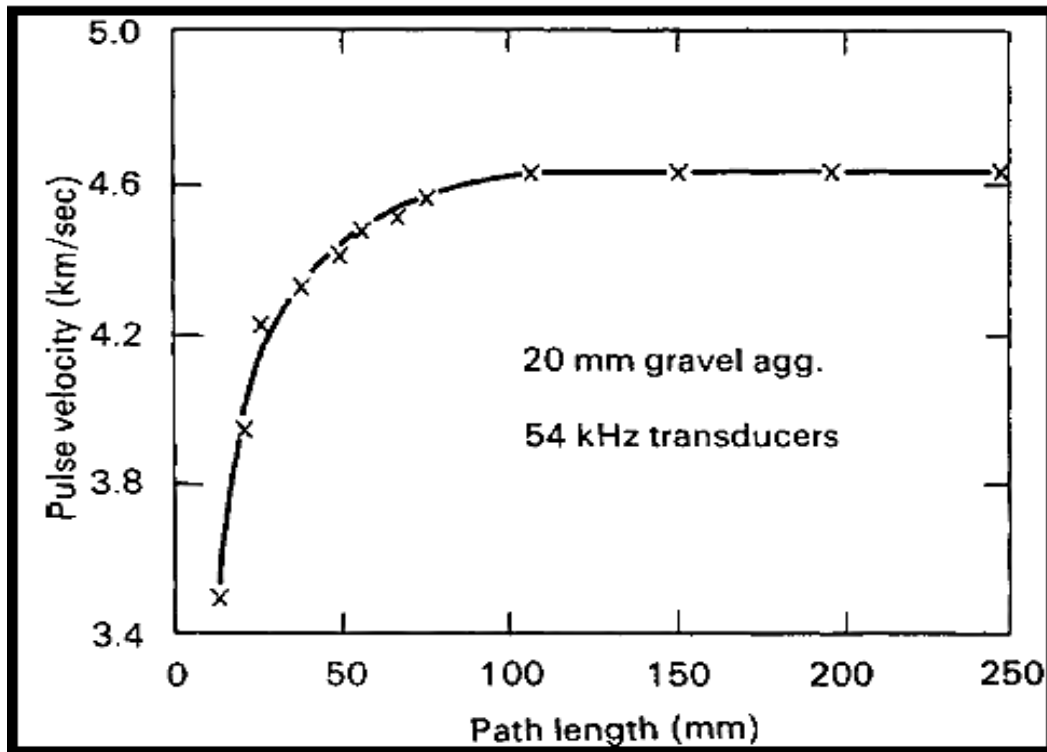


Figure 27: Effect of the distance between transducers [122].

Jones also identified that the distance between the transmitting transducer and receiver did not affect the measured ultrasonic pulse velocity above a certain length. However, for ultrasound path lengths lower than 100 mm strong variability is observed in the measured ultrasonic pulse velocity due to the heterogeneous nature of concrete at local level [122]. BS1881, part 203 recommends that the minimum path lengths set are 100 mm and 150 mm for 20 mm and 40 mm maximum aggregate size respectively.

A number of studies have suggested that for temperatures between 5 and 30°C no significant changes in ultrasonic pulse velocity occurred. However, during freezing and thawing conditions changes in the ultrasonic wave velocities were clearly observed [123-124].

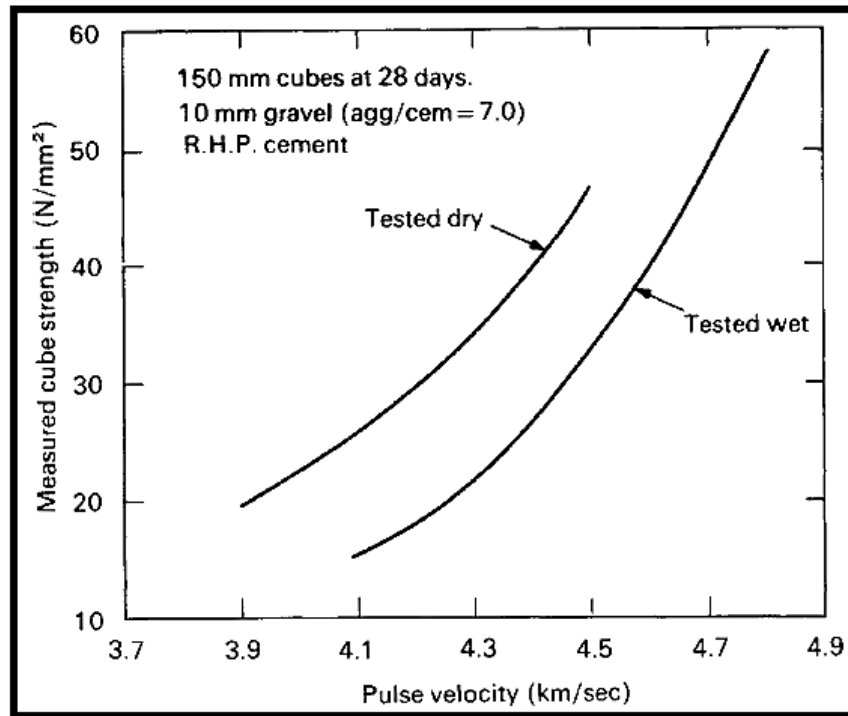


Figure 28: Effect of moisture content [125].

The ultrasonic wave pulse velocity, measured for a saturated concrete sample, was approximately 5% higher than a dry concrete specimen having the same mixture content. Also, this change depended on concrete porosity because it was estimated that the dry specimen had a higher void to volume ratio than the wet sample [125].

3.3.2.6 Measurement of the concrete quality by using UPVT

By using UPV testing, the exact strength value of a hardened concrete cannot be obtained. However according to many studies, concrete quality can be successfully estimated [126]. As it was discussed earlier, the concrete void to volume ratio increases year by year and hence the ultrasonic wave pulse velocity and compressive strength should decrease simultaneously [127]. Although concrete durability can also be estimated through UPV measurements, results may vary considerably depending on concrete age, as well as external and internal degradation factors mentioned in chapter 2, 3.

International standards have been used to classify concrete quality depending on ultrasonic pulse velocity [128]. These standards present generalised ultrasonic pulse velocity ranges according to which concrete condition can be classified as poor, good, very good and excellent as shown in table 1,2 and 3.

| UPV(m/s) | Concrete quality |
|--------------|------------------|
| Above 4500 | Excellent |
| 3500 to 4500 | Good |
| 3000 to 3500 | Medium |
| Below 3000 | Doubtful |

Table 1: Concrete quality classification based on BS 1881, 1983.

| <i>Pulse velocity in m/sec</i> | <i>General condition of concrete</i> |
|--------------------------------|--------------------------------------|
| > 4500 | Excellent |
| 3500-4500 | Good |
| 3000-3500 | Doubtful |
| 2000-3000 | Poor |
| <2000 | Very poor |

Table 2: Pulse velocity limits according to ASTM.

| <i>Pulse velocity in m/sec</i> | <i>General condition of concrete</i> |
|--------------------------------|--------------------------------------|
| 4575 | Excellent |
| 3660 — 4575 | Good |
| 3050 — 3660 | Questionable |
| 2135 — 3050 | Poor |
| 2135 | Very poor |

Table 3: Suggestion of J.R. Leslie and W.J. Cheesman for concrete quality estimation [129].

Table 1, from BS 1881 and 1983, shows the quality classification of concrete based on ultrasonic wave velocity. Table 2 shows the classification according to the ASTM international standard. Finally, table 3 shows the classification according Leslie and Cheesman [129].

3.3.3 Acoustic Emission (AE) Testing

AE testing operating principles are significantly different from those of UPV testing as discussed next. Firstly, AE sensors are passive, detecting or “listening” the acoustic or elastic stress waves generated inside a material while UPVT transducers produce interrogating ultrasonic pulse waves which are transmitted from the transducer through the specimen. Secondly, AE sensors can only detect active defects, i.e. a growing crack emitting elastic stress waves at each tip as it grows. Therefore, a load or a stimulating event causing damage evolution is required for AE sensors to detect damage. Hence, AE testing requires sufficient stress to be applied for damage to propagate, while UPV testing does not require any loading to be applied. Furthermore, each AE application has unique features, but UPV inspection is largely repeatable. AE is far more sensitive than UPV testing since even microcracks propagating are potentially detectable. AE is less geometry-sensitive, whilst UPV has high geometry-sensitivity. More importantly, by using a sufficient number of AE sensors the entire concrete structure can be tested at once. However, UPV can only interrogate the area immediately in front of the sound path.

3.3.3.1 General procedure of the AE testing for concrete material

The photograph in figure 29 shows the main components comprising a commercial AE testing system, including AE sensors, pre-amplification, data acquisition, display and storage. One of the concrete samples used in this study can also be seen on which the AE sensor is mounted.

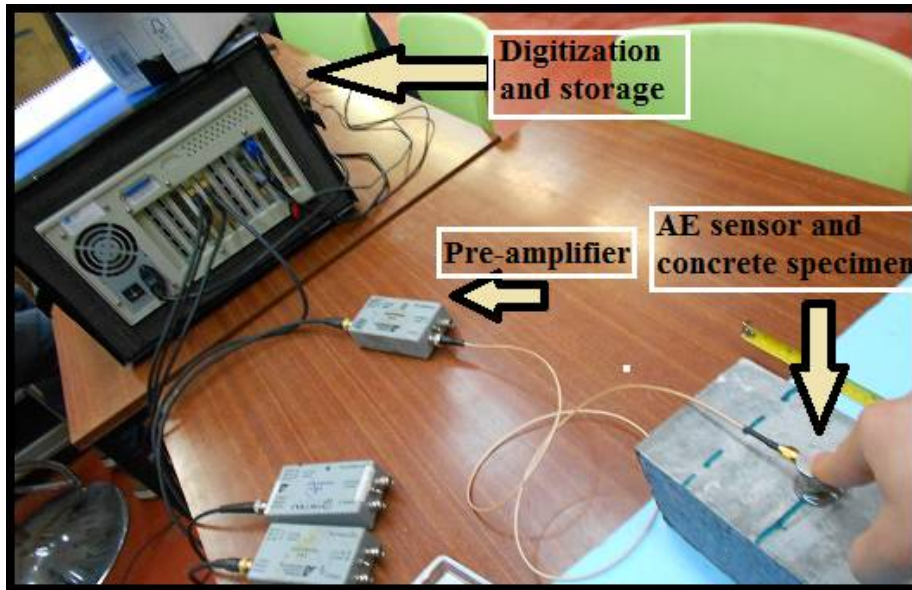


Figure 29: AE test measuring system used in the research study.

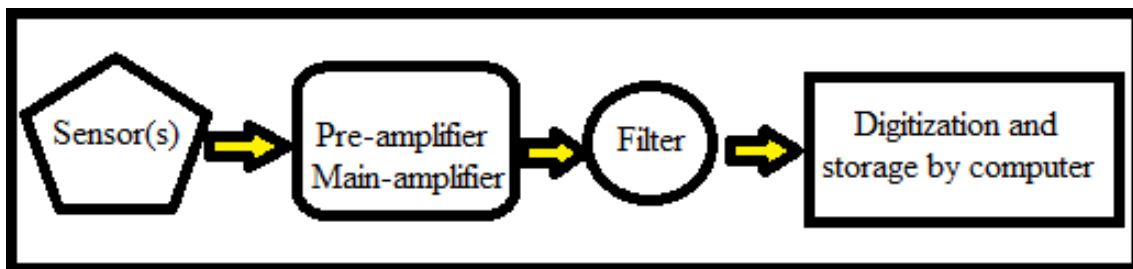


Figure 30: AE system architecture.

The simplified schematic diagram in figure 30 shows the typical AE system architecture. Crack propagation will result in elastic stress waves emitted towards the surface of the sample. These elastic stress waves as they propagate along the surface will cause local deformations which despite being minor are sufficient to cause the AE sensor to detect them through the direct piezoelectric effect [130]. A crack will only produce signals when a sufficiently high load is applied on the structure to cause the tip of the crack to propagate. If no propagation occurs then no AE activity will occur. The AE sensor electric signals have very low intensity and therefore need to be amplified using an appropriate preamplifier as shown in figure 31. In this study R50A resonant sensors were employed during testing.

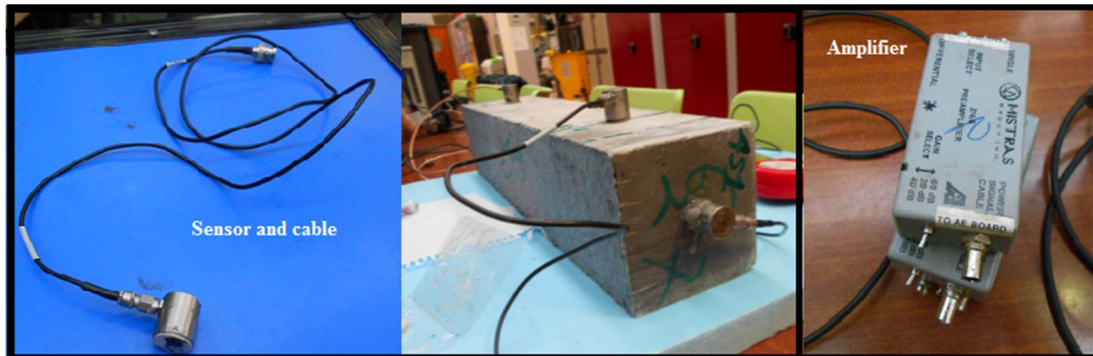


Figure 31: R50A resonant AE sensors and PAC pre-amplifiers employed in the research study.

Generally, the acoustic waves generated within the concrete specimen are very weak. Therefore, the pre-amplifier alone is not sufficient and a main amplification stage is also required in order to increase the gain of the captured signals.

AE signals are generally filtered using appropriate band filters in order to collect the signals of interest related to damage propagation and reject any unwanted background noise [131]. This increases the quality of the AE data and improves the interpretation reliability of the results obtained with the respect to the damage accumulated in the test piece being monitored. Finally, the electric signals are digitized by a high-speed data acquisition board with two or more channels and the data are stored in a computer file.

3.3.3.2 AE signal characteristics

The AE signals have typically burst-like characteristics as shown in the schematic diagram in figure 32. The main features of interest in an AE signal include the signal threshold, i.e. the amplitude above which a signal will be recorded, the signal duration, the count number, i.e. how many times the signal exceeds the threshold, the maximum amplitude, the rise-time, i.e. the time taken for the signal to reach its maximum amplitude and the energy which represents the envelope of the signal.

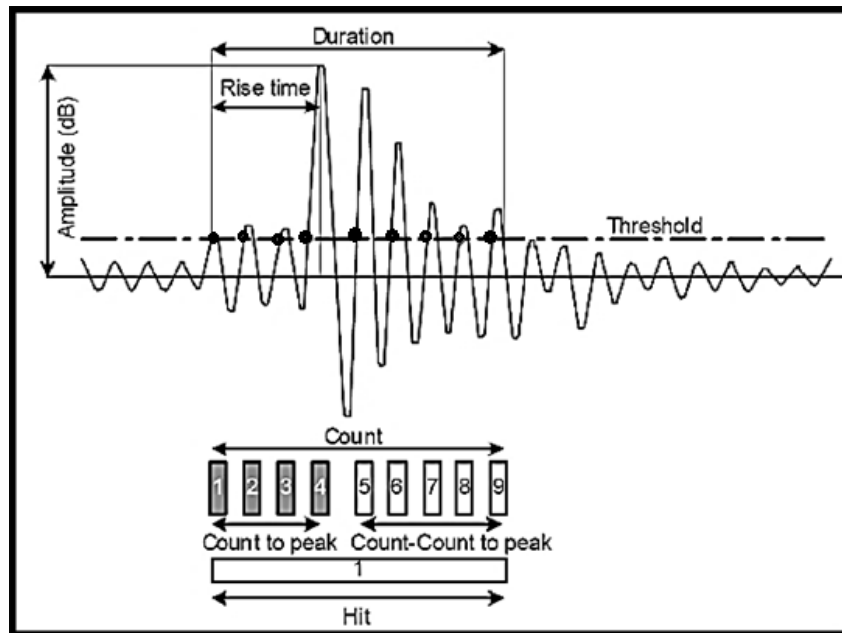


Figure 32: Main terms of an AE signal [132].

As shown in figure 32, duration indicates the time gap between the start and end of the AE signal. Duration is measured in μs . The AE signal energy is related to the magnitude of the event and its duration [132]. The schematic diagram in figure 33 shows the principle of AE testing.

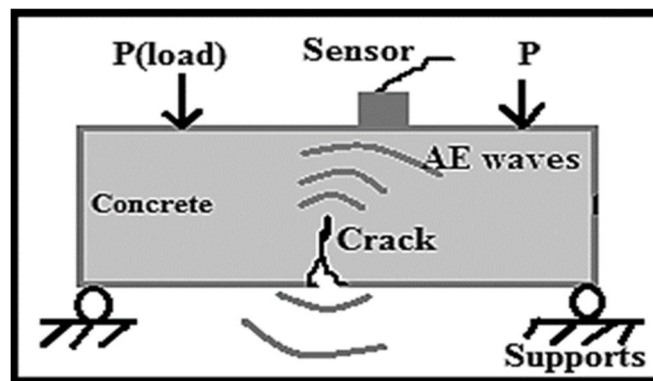


Figure 33: AE waves originating from a propagating crack as a flexural load is applied.

Figure 33 also illustrates the testing setup for a concrete beam specimen under four-point flexural loading. Due to the applied stress crack growth and dynamic displacements will occur inside a concrete structure resulting in AE waves to be emitted. The AE sensors will detect and convert the arriving acoustic waves to corresponding electric signals as mentioned earlier [133].

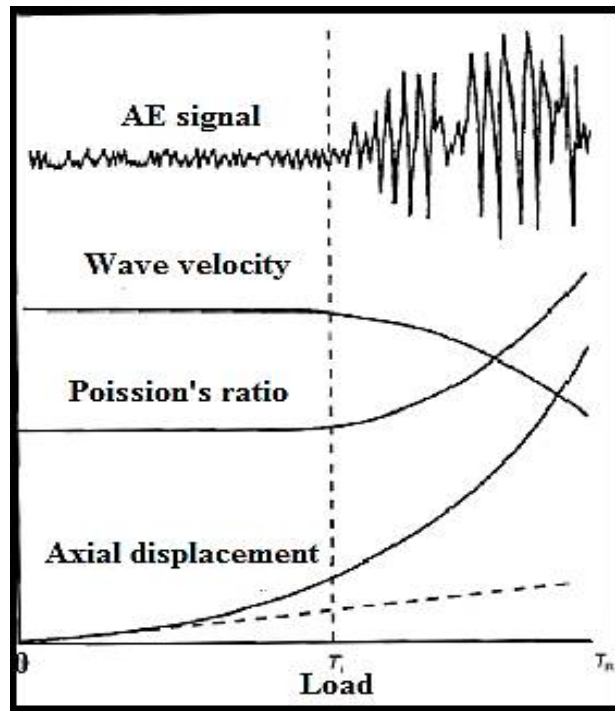


Figure 34: General behaviour exhibited by a hardened concrete specimen under compression [134].

The plot in figure 34 shows a typical AE signal generated in a hardened concrete element under flexural stress. AE activity increases as deformation increases. Ultrasonic wave velocity decreases as displacement increases and damage accumulates with increasing deformation [134]. There are two main AE waveforms; namely the continuous and burst type as shown in figures 35 and 36 respectively.

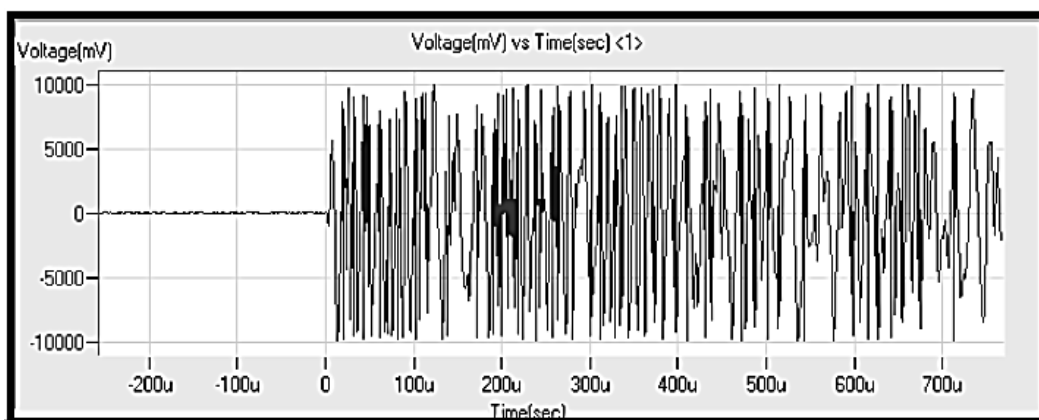


Figure 35: Example of the continuous AE waveform [135].

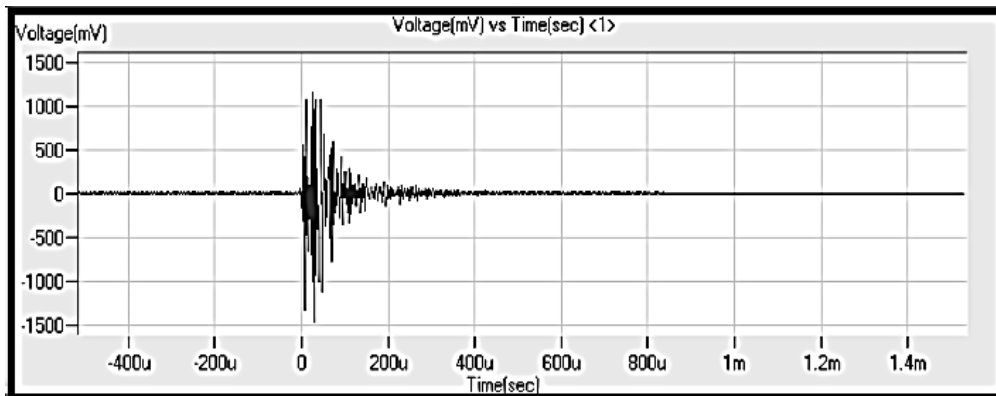


Figure 36: Example of a burst AE waveform.

Continuous AE signals are generally detected in ductile materials such as mild steel. Because of the ductility, AE signal duration is longer resulting in a continuous waveform with a much longer duration than burst-type waveforms.

Burst AE waveform is mainly detected in brittle materials or materials with lower ductility. Hardened concrete generally exhibits sudden failure under increasing flexural stress when a critical value has been reached. In concrete due to its brittle nature burst-type AE signals will generally be detected under flexural stress [135].

3.3.3.3 Kaiser and Felicity effect in AE testing

The Kaiser effect is an important consideration in all AE tests and should never be ignored as it could have catastrophic consequences. As mentioned earlier, Joseph Kaiser discovered the effect named after him during his Ph.D. studies in the 1950s. The Kaiser effect describes the lack of AE activity until a specific previous highest load has been exceeded. It results from the changes and damage that have occur in the material during previous loading steps which do not evolve further until the previous maximum stress has been exceeded [136].

The plot in figure 37 shows both the Kaiser and Felicity effects. The sample is initially gradually loaded from 0 up to point B. During loading at point AE damage begins to evolve in the sample

and hence AE activity starts to accumulate. At point B the load is reduced up to point C. While the load is reduced no appreciable AE activity is recorded. Subsequently the sample is reloaded from point C to point B. Up to point B which is the previous maximum no further AE activity is recorded. However, as soon as the load exceeds point B appreciable damage begins to accumulate once more. As the load is increased further and more damage accumulates the sample is nearing its failure point. At the same time AE activity accumulates exponentially up to point D. At this point the sample is again unloaded down to point E. During the unloading again the recorded AE activity is minimal. However, as the sample is loaded once more, appreciable AE activity begins to accumulate at point F which is a lower load than the previous maximum in point D. This is known as the Felicity effect and it occurs when the material is closing nearer to failure and accumulated damage has reached a critical level. Subsequently, the AE activity accumulates at a dramatic rate with every small increment in load, finally reaching a maximum at the point of failure which occurs at point G. H shows the total AE activity recorded including the fracture event which takes place at the loading level indicated as point G in the plot [137].

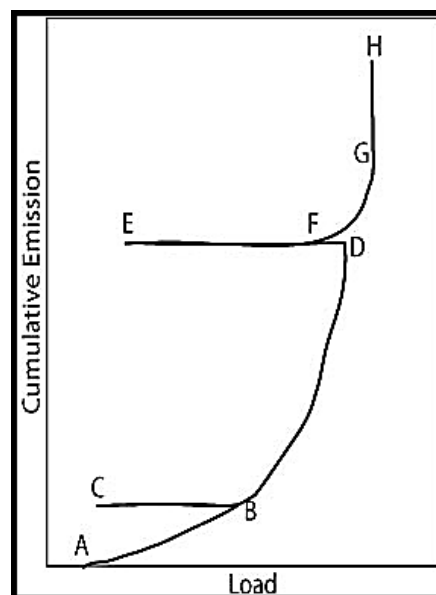


Figure 37: Kaiser and Felicity effect on AE activity.

B-D part is also called as the stable phase. If the load level D is exceeded, the material enters unstable phase. In other words, after passing level D, drastic cracks and discontinuities occur. The Felicity effect is quantified using the Felicity Ratio F/D where F is the resuming AE activity load and D is the previous maximum load.

If the Felicity Ratio is higher than 1, stable damage propagation will occur with increasing applied load. If the Felicity Ratio it is lower than 1, then the material has entered the unstable phase and failure is imminent (D-H). As mentioned earlier, macro-cracks reach critical size at this stage [138].

In brief, the Kaiser and Felicity Effects have been widely used to detect major structural defects and evaluate stable and unstable phases. Thanks to these two Effects, AE signals can be categorised depending on their significance.

3.3.3.4 Determination of the concrete quality and durability using AE testing

AE testing has been used as a tool for condition and structural health monitoring method for various types of structures such as bridges, dams, buildings, power plants, wind turbine blades, etc. It allows the timely detection of important structural problems which could result in increased collapse or failure risk. AE has been employed in a wide range of applications including the evaluation of the structural integrity of critical components, the detection and localisation of defects, detection of leaks in pressure vessels and the assessment of weld quality. Furthermore, it can be used to detect corrosion activity and creep damage in metal components in steel pipes, storage tanks and pressure vessels [139].

AE sensors are capable of detecting AE waves originating from the propagation of both micro or macro-cracks and dynamic displacements occurring inside a structural component such as column, beam, slab and bridge cable. The acquired AE signals are then statistically analysed to evaluate damage levels in a particular structure under monitoring.

The properties and characteristics of recorded AE signals provide reliable information about the structural health of an engineering component. As explained in the following chapter, significant changes in AE energy, cumulative energy, root-mean-square, amplitude, frequency and other AE signal properties contribute in the evaluation of the quality, durability and overall compressive strength of concrete structures [140].

CHAPTER 4

Experimental Results and Discussion

4.1 Summary of the chapter

This chapter will discuss the experimental work, results obtained and their analysis for different concrete samples of varying quality. The samples on which the experiments were carried out have been divided into two groups, namely experimental group 1 and 2. The following sections will detail the experimental work carried out together with the salient points arising from the results obtained together with the analysis carried out with respect to the quantitative assessment using NDT means.

4.2 Experimental group 1 concrete samples

This part of the thesis described the approach followed for the quantitatively evaluating the quality experimental group 1 concrete samples by using a combination of visual inspection, AE testing and UPV measurements. The reliability arising from the application of the selected NDT techniques for estimating concrete durability, quality and strength has been investigated and the findings are presented in this chapter. The effect of different mixture contents, such as water to cement ratio on the destructive and NDT results are analysed in detail.

Experimental group 1 consisted of 6 concrete beams and 6 cubic concrete specimens as shown in figure 42. These specimens have been produced using two different mixture contents having diverse cement types, chemical admixtures and mixing analogies. As a result, they exhibit different compressive and flexural strength levels. Two specimens were prepared using one type of mixture for testing after seven and twenty-eight days respectively.

After preparation of the specimens, visual inspection, UPV measurements and AE tests were carried out in order to evaluate the quality of the concrete samples produced as well as quantify damage propagation during mechanical testing. The changes arising in the ultrasonic wave velocity measurements were related to the strength values obtained from the mechanical tests carried out. In addition, AE signal characteristics such as energy, root-mean-square, amplitude and frequency were examined in relationship to the measured concrete strength.

Compressive and flexural strength testing were carried out on group 1 samples in order to obtain the actual strength values. NDT testing results have been correlated the destructive testing data to assess reliability. Furthermore, specific interpolations and correlations have been researched to correctly estimate concrete durability, quality and strength using UPV testing and AE results. More specifically, AE data were acquired during compressive and flexural testing. AE activity was monitored and correlated to concrete damage evolution in conjunction with the mixture content and strength exhibited. Damage quantification with increasing load has been evaluated and degradation of the structural integrity plotted against increasing load for experimental group 1 samples. Various statistical analysis methods such as cumulative energy have been considered in trying to effectively quantify damage evolution.

4.2.1 Preparation of the group 1 samples

Concrete specimens of experimental group 1 were prepared using two different mixture contents as shown in figure 38 and summarised in table 4. Maximum aggregate diameters of the first and second mixtures were 1 mm and 5 mm respectively. Also, there were two different chemical admixtures employed to decrease hardening or setting time and increase concrete strength.

The cement type of experimental group 1 samples closely resembles that of CEM 1 or portland cement. However, they also contain calcium chloride as chemical admixture. Calcium chloride has been used to reduce the setting time and increase the concrete strength. Therefore, the cement types in mixture 1 and 2 have similarities to composite cement types CEM 2 and 5 already discussed in chapter 2.



Figure 38: Mixture designs 1 and 2 in the experimental group 1.

The water content used for these mixtures was calculated according to the specified water to cement ratios. The mixture contents and other details are shown in the following table.

| Mixture | 1 | 2 |
|----------------------------------|------------------------|------------------------|
| Density without water | 2300 kg/m ³ | 2382 kg/m ³ |
| Max aggregate diameter | 1mm | 5mm |
| Water/Cement | 0.14 | 0.10 |
| Fresh concrete weight for 1 cube | 2.63 kg | 2.61kg |

Table 4: Mixture content of number 1 and 2.

These two mixtures have high compressive strengths which were estimated in the range between 90 and 120 MPa for 28 days. Their water cement ratios are so low because the increase of the water content leads to a decrease in the compressive strength of the concrete. These types of concrete have been generally used in high-end structures such as wind turbine foundations. After preparation of the fresh concrete mixtures, they were cast in cubic and beam molds. The cube dimensions were 100x100x100 mm and beam dimensions were 100x100x500mm as shown in figure 39 and 40.

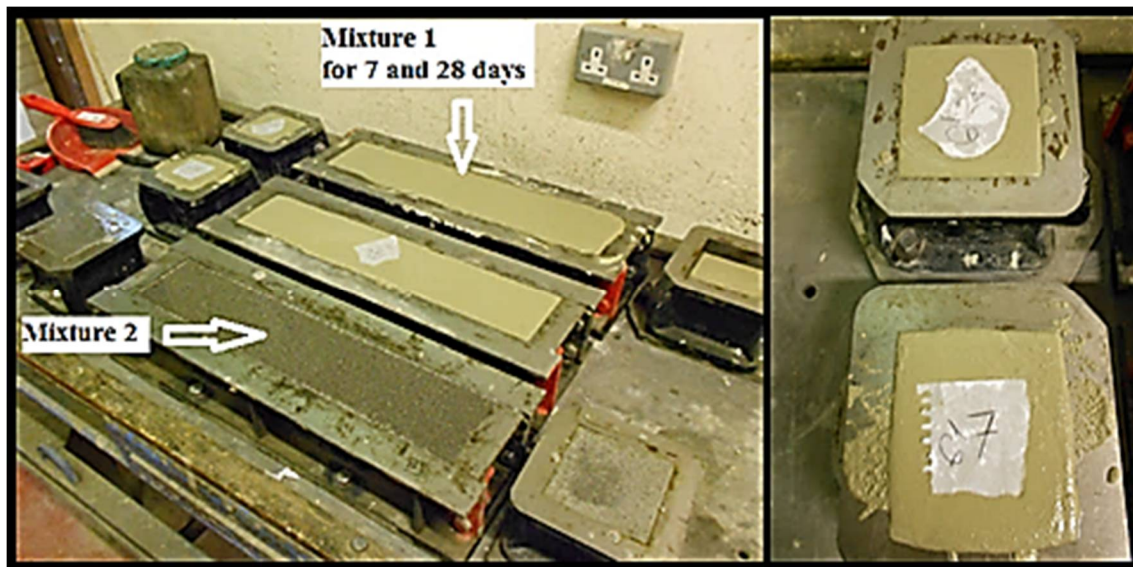


Figure 39: Casting of the fresh concrete mixture 1 and 2.

| Hardened concrete specimens in the experimental group 1 | |
|---|--------------------|
| From the mixture 1 | From the mixture 2 |
| 3 Cubes | 3 Cubes |
| 3 Beams | 3 Beams |

Figure 40: Specimen types and numbers of specimens produced in group 1.

After one day, hardened concrete specimens were remolded and put into the curing pool shown above. Curing is the procedure used for promoting the hydration of cement and adjusting temperature and moisture content into the concrete.

Therefore, concrete specimens have to be put in a curing pool according to many national and international standards such as BS1881, ASTM and Turkish Standard TSEN.

All specimens from experimental group 1 were placed in the curing pool for 7 and 28 or more than 28 days, which were specified as standard time periods to test concrete specimens. Finally, they were given individual codes to allow discrimination between them and their mixture groups as shown below in table 5. Each of the codes has been used for both beam and cube samples.

| From the Mixture 1 (maximum aggregate diameter 1mm) | Mixture 2 (maximum aggregate diameter 5mm) |
|---|--|
| Specimen 2 (S2) | S1 |
| S4 | S3 |
| S5 | S6 |

Table 5: The names of cubic and beam specimens.

4.2.2 Destructive testing for the group 1

For the destructive tests, compressive and flexural strength experiments were carried out on the specimens of experimental group 1 in order to obtain the exact strength value for each one. This was done in order to validate the relationship between the ultrasonic pulsed velocity measurements as well as damage propagation monitored using AE. Compression tests were carried out on the cubic specimens of experimental group 1 whilst flexural strength tests were applied on the beam specimen together with AE structural health monitoring.

4.2.2.1 Compressive strength testing results for group 1 samples

Compressive strength testing was carried out on the cubic specimens made using mixtures 1 and 2. Each sample was tested after 7, 28 or more than 28 days. The dimensions of the specimens were input to the test device shown below before the compressive load was applied. The compressive strength was displayed as shown in figure 41.

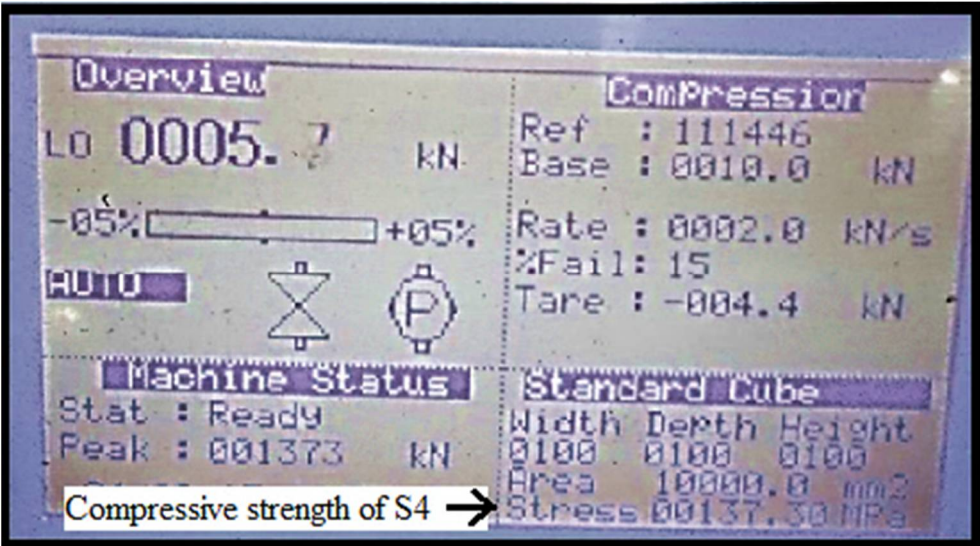


Figure 41: The compressive testing device showing the results of S4.

The test device applies compressive load until the specimens fail. Then, it records the failure loads. The results obtained are summarised in table 6.

| Results of the mixture 1 (maximum aggregate diameter 1mm) | Results of the mixture 2 (maximum aggregate diameter 5mm) |
|--|---|
| For 7 days:specimen2 (S2) Cubic: 92.40 MPa | For 7 days: S1 Cubic: 86.6 MPa |
| For 28 days: S5 122 MPa | For 28days:S3 122.1 MPa |
| More than 28 days S4 137.3 MPa | More than 28 days S6 125.0 MPa |

Table 6: Compressive strength testing results of the group 1 cubic specimens.

According to table 6, compressive strengths of the specimens are significantly different from each other, with the exception of S3 and S5. During the ultrasonic pulse velocity measurements, the velocities recorded for each specimen are related to their compressive strength results.

4.2.2.2 Flexural strength testing results for the group 1

Four-point bending tests were carried out in conjunction with AE structural health monitoring of the samples. Four R50A sensors were used to monitor the AE activity and a sampling rate of 2MS/s. The pre-amplification was set at 40dB whilst the main stage amplification was set at 6dB.that the 4-point bending setup used during testing is demonstrated in figure 42.

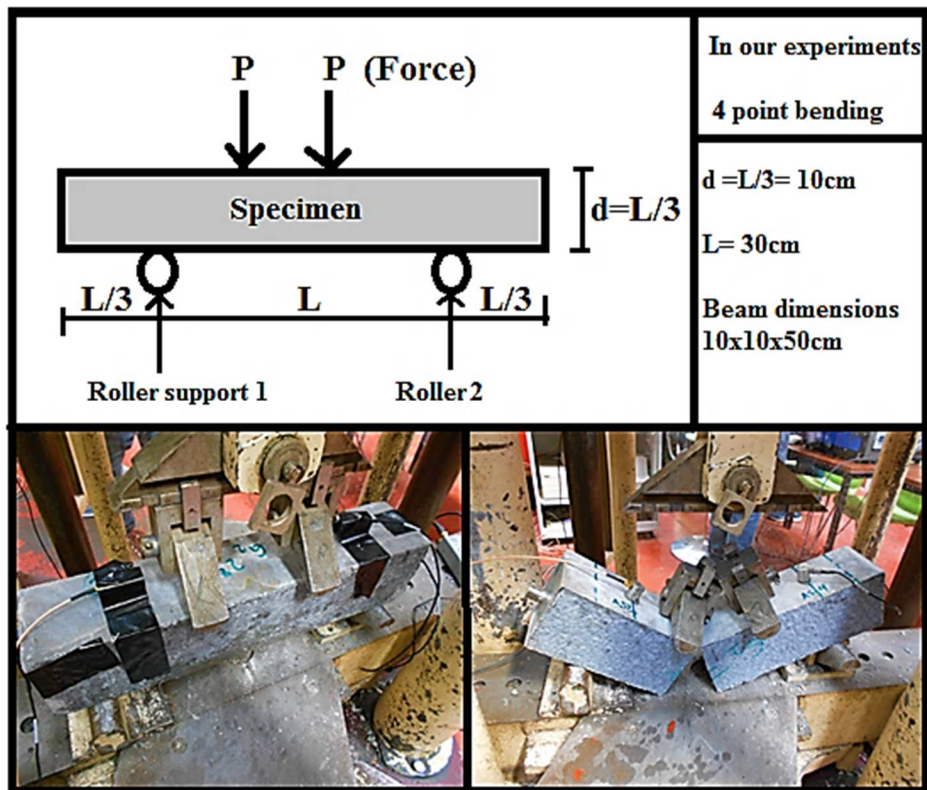


Figure 42: 4-point bending setup and AE testing from research studies.

During the bending test, 10x10x50cm concrete beam specimens were placed on two roller supports. Afterwards, force was applied with the help of the loading cell from the top at two points. The load was gradually linearly increased until the sample catastrophically failed in brittle fashion. The failure load was recorded by the test machine. Table 7 summarises the flexural strength values obtained from the flexural tests for each of the samples.

| Group 1 Beam Specimens | S1 | S2 | S3 | S4 | S5 | S6 |
|----------------------------|------|------|-------|------|-------|-------|
| Flexural failure load (kN) | 21.3 | 29.6 | 39.1 | 49 | 39.3 | 44.8 |
| Flexural strength (MPa) | 6.39 | 8.88 | 11.73 | 14.7 | 11.79 | 13.44 |

Table 7: Bending test results of beam samples in group 1.

As it is shown above, flexural testing results of the beam specimens are in good agreement to the compressive strengths values obtained from the tests on the cubic specimens the results of

which were summarised earlier in table 6. Specimen 1 has been found to have the lowest flexural strength as well as the lowest compressive strength. On the other hand sample 4 has been found to exhibit the highest flexural strength and highest compressive strength. As it can be clearly seen from the compressive and flexural results obtained, there is a significant difference between samples 1 and 4. The flexural strength of specimen 2 is remarkably lower than that of samples 4 and 6. Furthermore, there are significant similarities among the recorded flexural strength values of S3 and S5 samples. Similar characteristics were expected to be observed in the ultrasonic pulse velocity and AE testing results.

4.2.3 Non-destructive testing of group 1

For pulse velocity measurements, various types of UPV testing equipment are used by the construction industry. Here a commercial UPV testing device has been used to evaluate the ultrasonic wave velocity in the different samples produced and relate the results to the mechanical test results reported in the previous section. AE testing has been employed as an advanced condition monitoring method for the evaluation and quantification of structural damage during flexural loading up to final failure [141].

Preliminary visual inspection was employed in order to evaluate the specimens for any surface-related irregularities or defects which could affect adversely the test results obtained.

4.2.3.1 Ultrasonic pulse velocity testing for the group 1

For coupling purposes vaseline is applied to the surface of the transducer and receiver to eliminate any air pockets and decrease the acoustic mismatch at the sensor and sample surface interface. Both direct and semi-direct transmission measurements were performed as shown in figure 43.

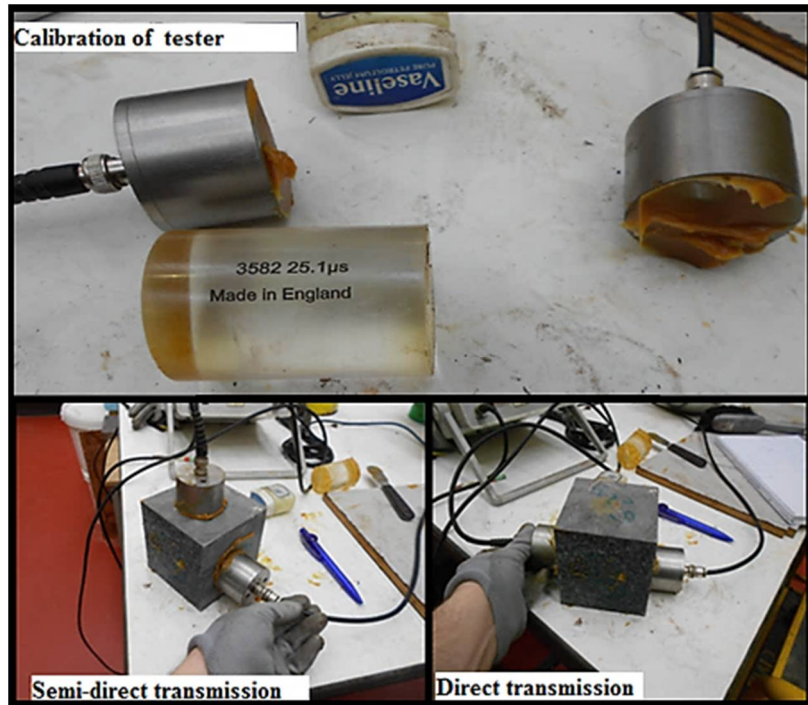


Figure 43: Calibration of the test device and application of direct, semi-direct transmission.

Before any measurements a calibration block was used to ensure consistency and accuracy of the UPV measurements carried out.

4.2.3.2 UPV testing results and discussions for the group 1

Pulse velocity results of the group 1 are presented below with their corresponding compressive and flexural strength values.

| Group 1 Specimens | | S1 | S2 | S3 | S4 | S5 | S6 |
|--------------------------|--------------------|--------|---------|---------|---------|---------|---------|
| Compressive Strength | MPa | 86.6 | 92.4 | 122.1 | 137.3 | 122.0 | 125.0 |
| Flexural Strength | MPa | 6.39 | 8.88 | 11.73 | 14.7 | 11.79 | 13.44 |
| Direct transmission | Pulse velocity m/s | 4219.4 | 3921.57 | 4309.93 | 4629.62 | 4114.82 | 4424.78 |
| | Time μ s | 23.7 | 25.5 | 23.19 | 21.6 | 24.3 | 22.6 |
| Semi-direct transmission | Time μ s | 14.5 | 15.0 | 14.2 | 13.2 | 14.8 | 13.7 |

Table 8: Direct and semi-direct transition time and velocities for the group 1 specimens.

By looking into the results shown in table 8 above, it is evident that there is a good correlation between concrete strength, quality, durability and measured ultrasonic pulsed velocity.

Generally, as the strength increases so does the measured ultrasonic pulsed velocity.

However, discrepancies can be observed for samples with similar compressive and flexural strengths but these are related to the different mixtures used.

In experimental results of the group 1, the recorded ultrasonic pulse velocity results were approximately between 3900 and 4700 m/s. According to the evaluation based on the BS1936 and BS1881, these results indicate that the quality and durability of the samples is good to excellent. In other words, the specimens do not contain any major cracks, discontinuities, deformation, large air bubbles or voids, segregation or suffered from degradation at macroscopic scale.

Apart from this, their strengths are not easy to accurately estimate just by looking at the measured ultrasonic pulse velocities because most of the results are not directly aligned with the mechanical testing strengths. For instance, the compressive strength of specimen 2 is higher than the strength of specimen 1 while their pulse velocities are indicating the opposite.

Moreover, the compressive strength of sample S3 is almost equal to that of sample S1, although the measured ultrasonic pulse velocities for each of them is different.

As discussed already, the samples tested were produced from two different mixture contents. Therefore, they have different void to volume ratios, different maximum aggregate diameters, cement and chemical admixture types. These factors can cause the ultrasonic pulse velocity differences observed in the measured values.

However, it is still possible to qualitatively evaluate the concrete strength based on the ultrasonic pulse velocities measured, if the concrete samples have similar mixture contents and have been aged for the same time. For instance, the pulse velocities of specimens 2,4 and 5 are similar to their compressive and flexural strength values. In other words, magnitudes of their velocity and strength values can be classified by following the same order.

For example, S2 which is the sample with the lowest ageing time, exhibits the lowest pulse velocity in comparison with S4 and S5, whilst also exhibiting the lowest compressive strength. In addition, S1, S3 and S6 which were produced from the same mixture content, but different ageing times exhibit similar results. Therefore, their pulse velocities and compressive strengths have also been following the same order as for the samples made with the other mixture.

S1 has the lowest compressive and flexural strength and pulse velocity overall while S6 exhibits the highest values among the mixture 2 specimens.

On the other hand, there are not simple correlations between the magnitudes of the pulse velocities and concrete strengths measured. For example, the ratio of the compressive strength of S1 and S6 is 0.69, though the ratio of their pulse velocity values is 0.95 which suggests the relationship of strength with ultrasonic pulsed velocity is non-linear. Similarly, the ratio between the compressive strength of S1 and S3 is 0.71, although their ultrasonic pulse velocity ratio is 0.91. Apart from the examples from mixture 2 samples, the correlation between the compressive strength of S2 and S4 is 0.67, while the ratio of the measured ultrasonic pulse velocity values is 0.84.

Therefore, it can be concluded that pulse velocities of the specimens from mixture 1 and 2 do not have the similar ratios when comparing their strength and ultrasonic pulse velocity values. Therefore, an interpolation has been attempted in order to reliably estimate concrete strength values based on the ultrasonic pulse velocity measurement carried out.

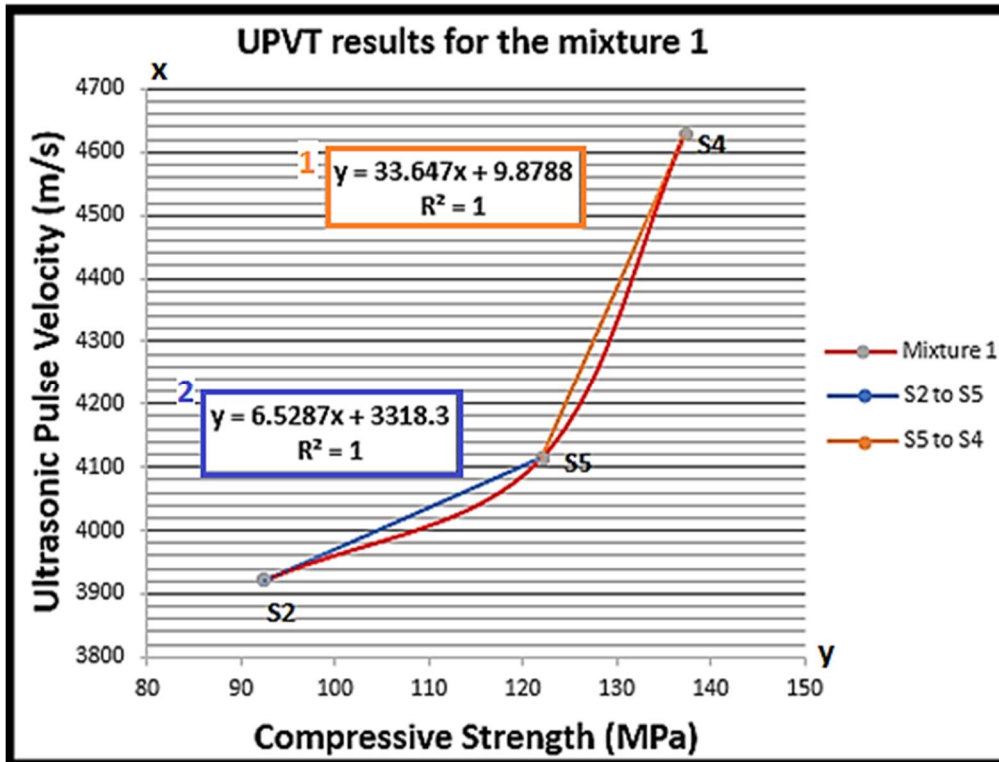


Figure 44: Correlation between UPV and the strength values from the mixture 1 samples.

The plot in figure 44, shows the ultrasonic pulsed velocity values with compressive strength for the specimens of mixture 1. The experimental data together with linear interpolations are presented in order to analyse the relationship between ultrasonic pulse velocity and compressive strength values measured.

It can be obviously seen that the ultrasonic pulse velocity rises exponentially when the compressive strength increases. However, these increments are different from each other. For instance, a drastic increment is observed from 4114 m/s to 4630 m/s when the compressive strength increases from 122 to 140 MPa. However, the ultrasonic pulse velocity exhibits only a minor increase from 3921 m/s to 4114 m/s while its compressive strength value has increased from 90 to 122 MPa respectively.

Furthermore, it can be clearly seen that the slope is clearly higher than the second one further highlighting the non-linear relationship of ultrasonic pulsed velocity with concrete strength.

Nevertheless, the pulse velocity and strength results obtained are generally in agreement in

terms of their trends. Hence, the compressive strength values are consistent with the ultrasonic pulse velocity results.

However, as mentioned previously, there is no simple relationship between ultrasonic pulse velocity and compressive strength since it is non-linear in nature. Therefore, further work is required in order to attain accurate compressive strength estimations using just ultrasonic pulsed velocity measurements. Moreover, there is a clear need for calibration samples based on the same cement mixture.

As explained earlier, apart from the strength estimations, durability and quality of the group 1 samples can be obtained from their ultrasonic pulse velocity values using empirical quality classification tables. According to the BS1881, the samples from mixture 1 are classified between the good and excellent condition.

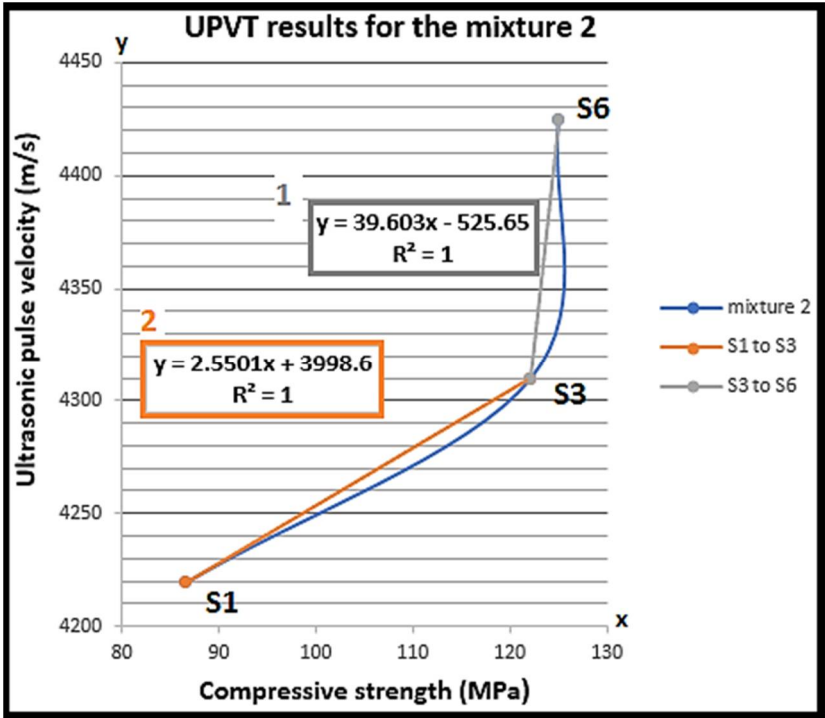


Figure 45: Correlation between UPV and the strength values for the mixture 2 samples.

The results for mixture 2 samples are summarised in figure 45. Similar to the previous figure, it is apparent from the plot in figure 45 that the pulse velocities have been risen importantly

from 4219 to 4424 m/s when the concrete strengths have climbed exponentially from 86 to 125. Additionally, slope of the first line is greater than inclination of the second plot. Significantly, it may be clearly observed that pulse velocity results of the S1 and S3 are remarkably close to each other, though their compressive strengths have been noticeably different. Moreover, the pulse velocity difference between S1 and S3 is 90.5 m/s because the compressive strength of S3 is 35.5 MPa higher than the strength of S1. However, pulse velocity of the S6 is 114.9 m/s greater than the velocity of S3, although the distinction between their compressive strengths is only 3MPa.

4.2.3.3 Acoustic emission tests for the group 1

As expailened formerly, to apply AE test, concrete specimens have to be under a specific load or load combinations because AE test can not be used without it. For this reason, flexural load has been applied to the concrete beam specimens during the AE tests. First of all, flexural strength test device and AE system components monitor and digitization unit, amplifiers and sesors are connected to each other. It is shown in figure 46 and explained in the chapter 3.

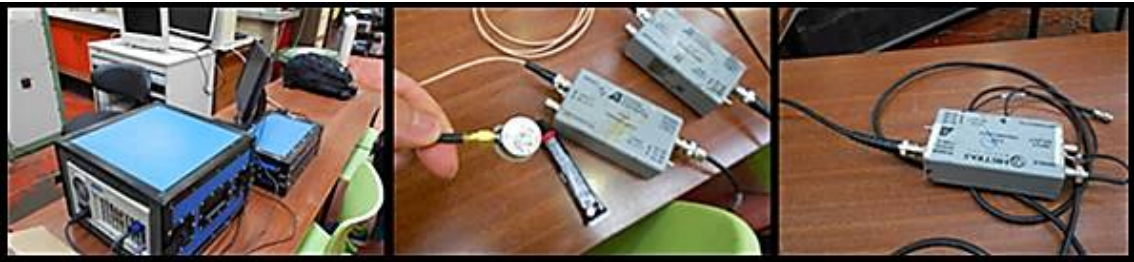


Figure 46: Connections of the sensor, amplifier, display and digitization components.

After combining of AE test components, the sensor locations are specified on the concrete samples and 4 AE sensors are placed on beam specimens of the group 1 by using a kind of glue shown in the following figure.



Figure 47: Placing of the sensors on the concrete surface by using a glue.

Afterwards, calibration process has been started by employing the pencil lead test which is applied to obtain information about sensitivity of AE device and to test its reliability. During the test, the 4 sensors have to perceive each break as AE hits shown in the next figure.

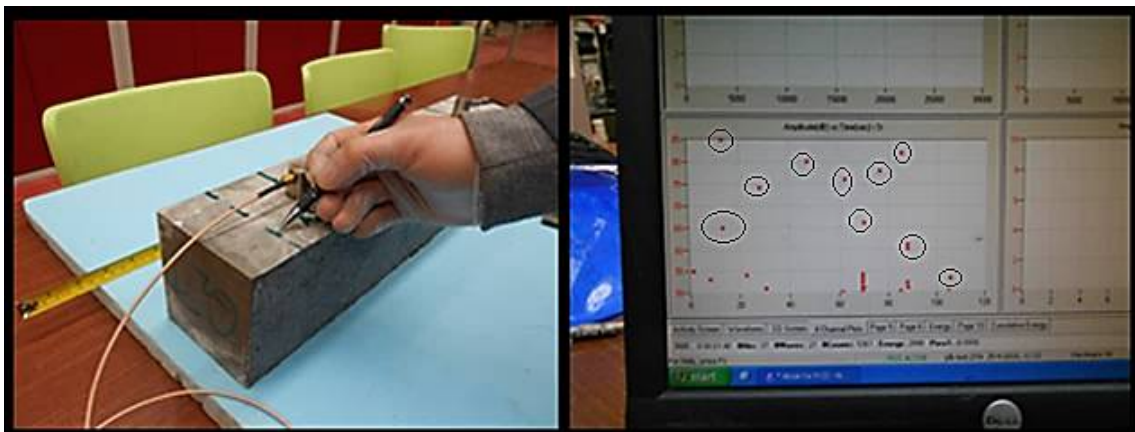


Figure 48: AE hits during the pencil lead test.

The number of hits has to be equal to the amount of pencil breaks. For instance, in our research, a mechanical pencil breaks 10 times and the display unit shows at least 10 AE hits indicated in figure 48. That means the AE system is successfully detecting AE waves traveling through the beam specimens.

After these processes, flexural strength and AE tests are simultaneously applied to beam specimens from the group 1, as it is shown in figure 49.

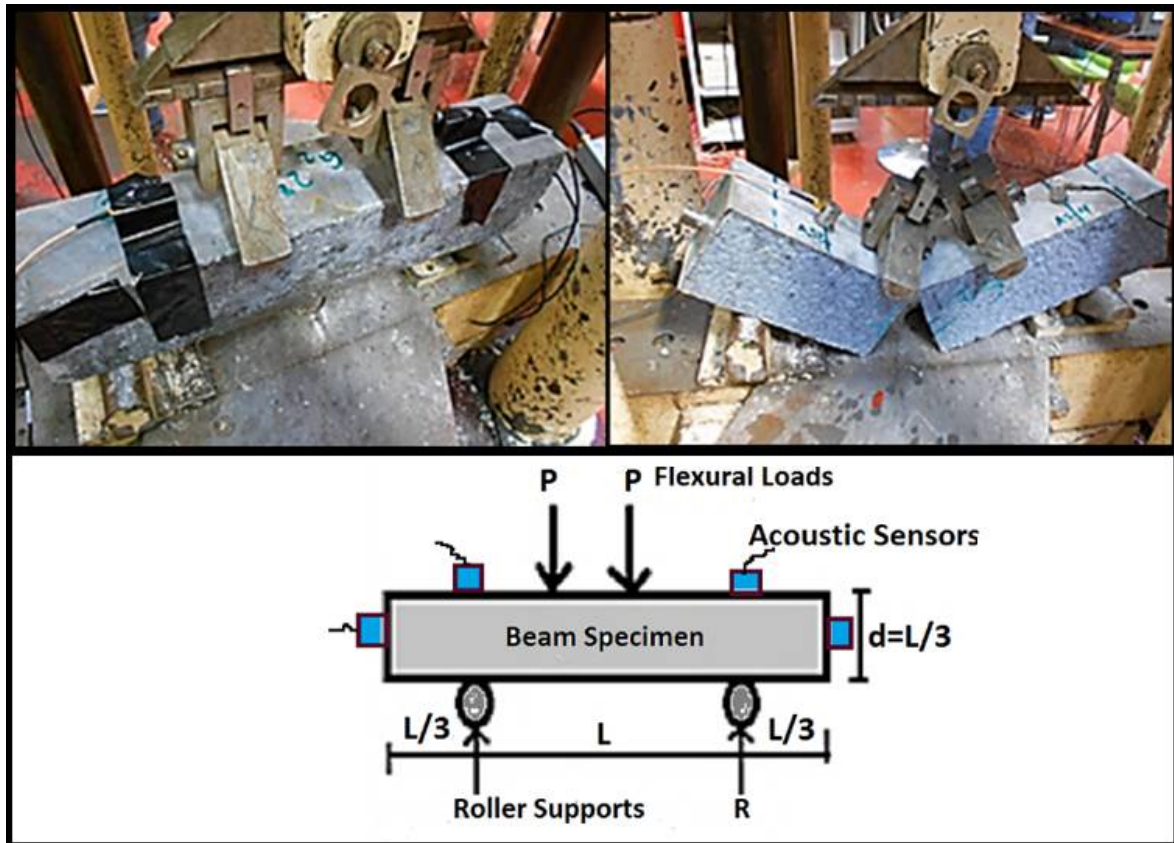


Figure 49: 4 point bending setup and AE application.

During the flexural strength test, tensile stress increases on the bottom of the beam, while compressive stress has been rising on its top. Additionally, dynamic displacements, minor and major cracks, important defects and discontinuities have occurred inside the beam structures.

Afterwards, as explained formerly, dynamic displacements, minor and major cracks may propagate the AE waves inside the sample. Then, these AE waves are detected by AE sensors and transferred to the amplifiers as electrical AE signals. Finally, they reach to digitization unit of AE to be collected and recorded, as particularly mentioned in chapter 3.

4.2.3.3.1 AE energy results and discussion for the group 1

AE results of the group 1 specimens are plotted as specific graphs which are energy, cumulative energy, root-mean-square, frequency and amplitude versus time.

The first plots of AE results are represented as energy versus time graphs for S1, S2 and S3 in figure 50. Afterwards, they have been converted to cumulative energy graphs to analyze their energy increments in detail. As mentioned in chapter 3, energy means the magnitude of acoustic emission ‘‘hit’’. Hit occurs when an AE signal exceeds the ‘‘threshold’’ value [142]. Threshold is limit value of AE to record signal waves as AE signal.

Most importantly, increment of AE energy represents increase of intensive AE activities, collapse or failure risks, dynamic displacements, major and minor cracks, defects, deformations and discontinuities [143].

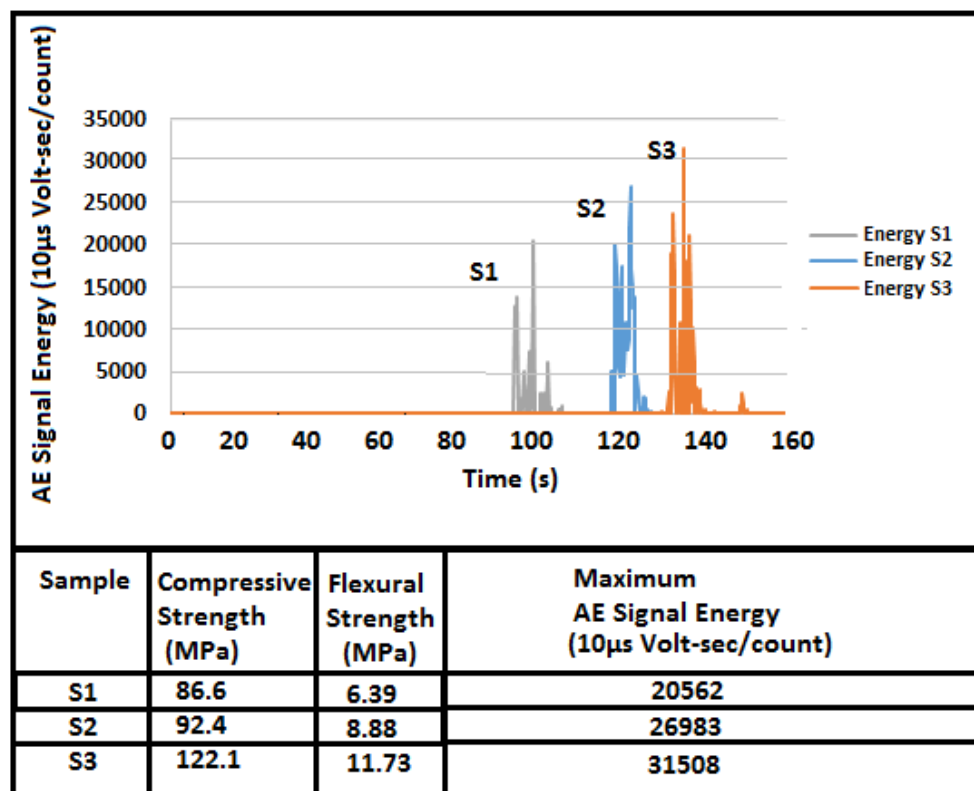


Figure 50: Plot of the AE signal energy versus time for the sample 1, 2 and 3.

It is apparent from the plot in figure 50 that the specimen 3 has the highest compressive and flexural strength if it is compared to S1 and S2. Additionally, Its AE energy reaches to the highest level before its failure. In contrast to the UPV results, AE signal values are not affected by the different mixture contents. For instance, AE signal values of the S1, S2 and S3 have been following the same order with their compressive and flexural strength values.

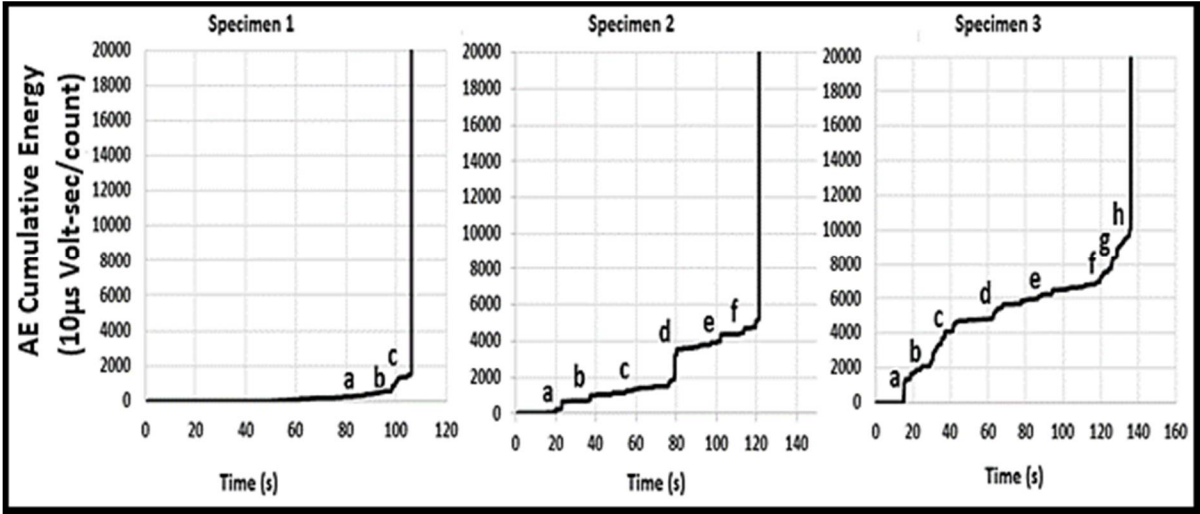


Figure 51: Plot of the AE cumulative energy versus time for S1,2,3.

The other significant plots, in figure 51, indicate the AE cumulative energy plots up to the energy value 20000 (10µs Volt-sec/count). Additionally, it shows important energy increment stages named as a, b, c, d, e, f, g and h. The cumulative energies of S1,2 and 3 increase vertically beyond f, c and h levels, because of the fracture or failure. Therefore, these stages can be named as critical energy levels

It may be clearly observed that S3 has more energy increment levels than S2 and S1. Furthermore, S2 shows rapid increase from stage c to d. This type of sharp increments represents important acoustic events such as AE wave coming from a major crack [144]. Therefore, it can be estimated that S2 experiences a great damage while its cumulative energy is rapidly climbing from c to d.

Moreover, S1 and S2 generally experience steady growths while S3 is generally indicating exponential rises in its cumulative energy graph. For instance, S1 and S2 increase gradually from a to b while S3 is showing sharp increase shown in figure 49. Furthermore, the energy plot of the S3 has the higher slope than S2 and S1.

Apart from S1,2,3, the energy results of S5 and S6 are plotted below.

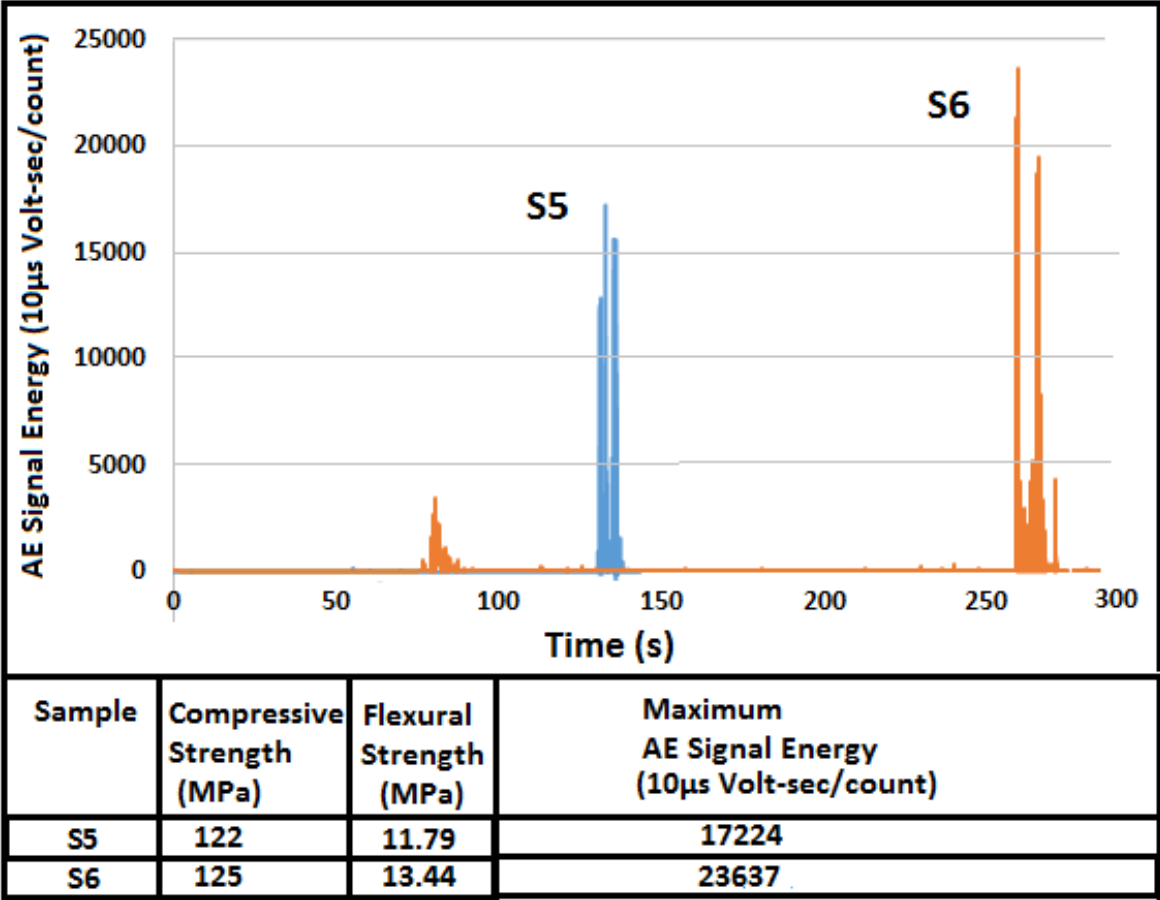


Figure 52: Plot of the AE signal energy versus time for the sample 5 and 6.

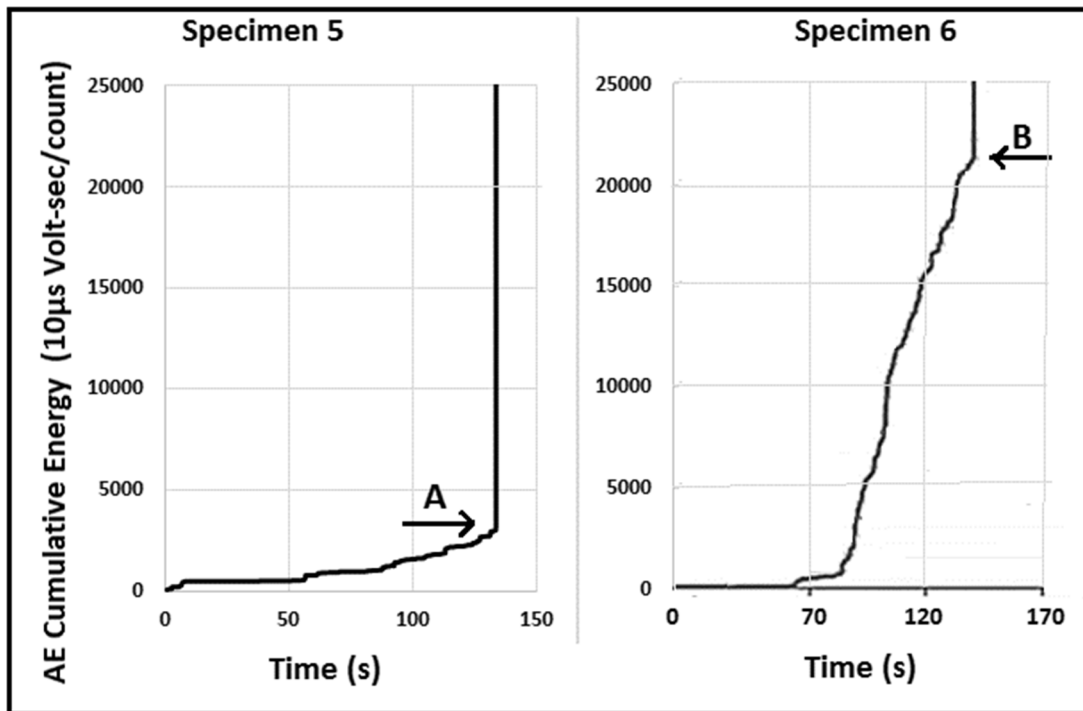


Figure 53: Plot of the AE cumulative energy versus time for S5 and 6.

In figure 52, maximum AE signal energy of the sample 6 is remarkably higher than the specimen 5. Additionally, the following figure shows the AE cumulative energy plots up to the energy value 25000 (10µs Volt-sec/count). it may be clearly seen that the cumulative energy plot of the sample 6 shows the dramatic rise from its bottom to the B which is critical level before the fracture. On the contrary, specimen 5 climbs steadily to its critical level A.

In the case presented in the previous figures, the highest amount of the acoustic activities has been observed in specimen 6 as compared with the other beam specimens of the group 1.

It has the highest cumulative energy slope than the other graphs. Moreover, two significant slopes can be observed in the cumulative acoustic energy of S6. The first slope near its bottom indicates a small amount of energy accumulation, which is related with a low amount of distortions in the specimen [145]. After an important energy level, the ratio of damage accumulation rises drastically and it means high probability to fail.

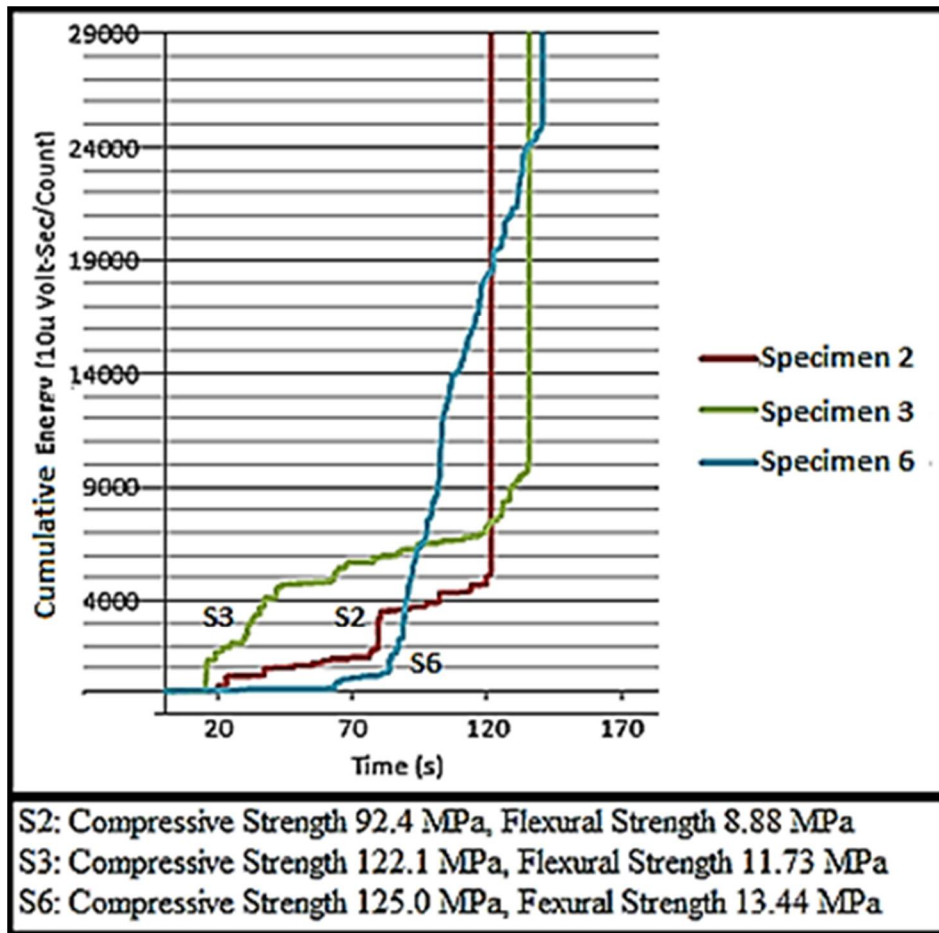


Figure 54: Cumulative energy comparison of S2,3,6.

Furthermore, as shown above, cumulative energy plot of the S6 has the greatest slope when its cumulative energy experiences sharp increments.

In the same figure, it may be clearly observed that the cumulative energies and slopes of the graphs increase as the concrete strengths are increased. For instance, sample 2 has the lowest strength values and AE cumulative energy slopes and energy levels while the sample 6 has been showing the highest strength values, cumulative energy slopes and levels.

Most importantly, these cumulative energy plots indicate a part of their final cumulative energy levels. According to the experimental results, S6 has the highest final cumulative energy value than the other samples. Generally, there are good correlations among the compressive and flexural strength values and AE energy results.

4.2.3.3.2 Quantifications of the progressive structural integrity losses for the group 1 samples.

Structural integrity is the term used for the performance analysis of a material, structure, and structural component. It represents the collapse-resisting capability of an item to hold together its components under internal and external loads such as its own weight, compression, tension, torsion, shear and bending without deforming excessively [146]. Additionally, it is so significant to resist progressive collapse in structures. Progressive collapse may be observed when a primary structural component, such as a column, beam and slab, fails [147]. Especially within the construction industry, there are some significant codes containing structural integrity term such as ASCE-7 ACI-318, BS 5950 and BS 7910.

Inside a concrete material, progressive structural integrity losses may be originated by the deformations such as major and minor cracks, dynamic displacements, defects and distortions explained in chapter 2 and 3.

To quantify the deformations and structural integrity losses inside the concrete samples, AE signal properties such as AE energy may be used. Especially, cumulative energy values may be successfully employed [148].

To prove this, some significant theories, relating the crack characteristics, may be researched to compare with the cumulative energy plots in this research study. For instance, in 1963, American scientist Paul C. Paris and Turkish scientist Fazil Erdogan published an important theory relating the stress intensity factor to crack growth rate under a fatigue stress regime. They had been tried to detect three significant crack growth phases, shown in figure 55, under an increased load cycle. Today, this theory has been known as Paris–Erdogan Law. Especially, their fatigue crack growth model, shown in figure 55, is the most popular used in materials science.

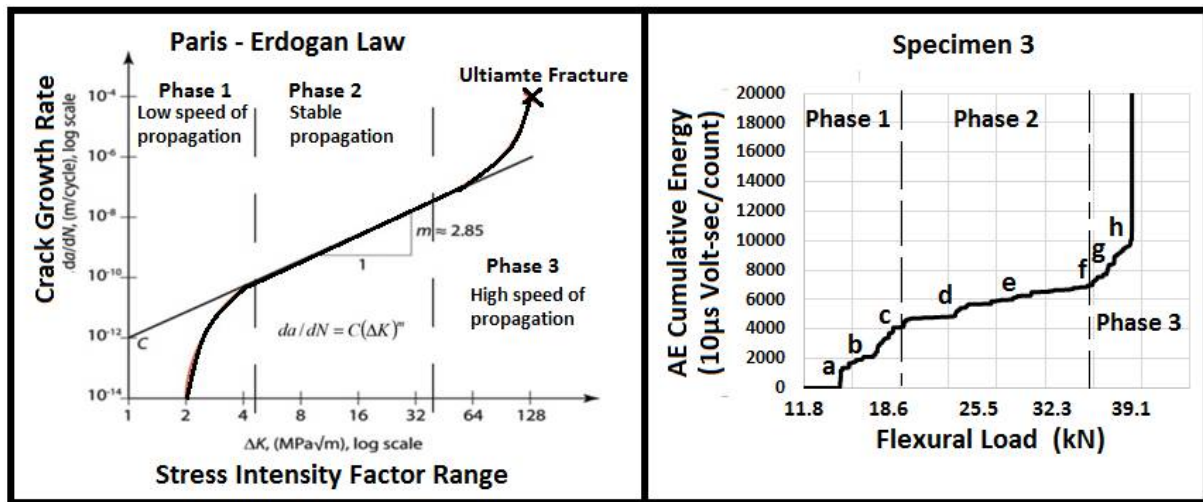


Figure 55: Paris-Erdogan crack growth model and cumulative energy plot of the S3 [149].

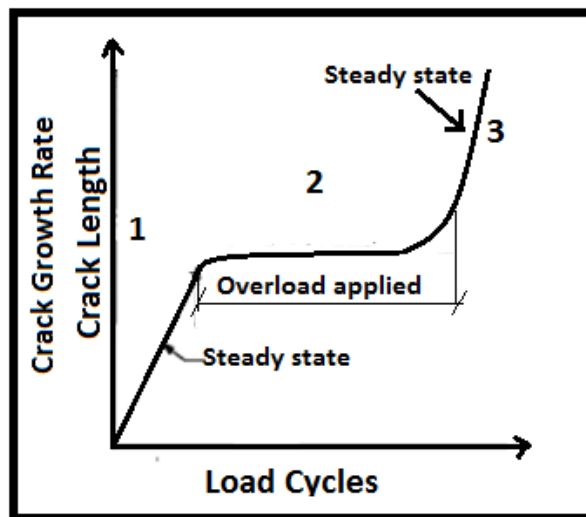


Figure 56: The fatigue crack growth model presented by J. R. Rice and D. M. Tracey [150].

Additionally, there are similar crack growth models found by different scientists. For example, J. R. Rice and D. M. Tracey research the crack length and growth rate depending on the increased load cycle. Finally, they produce an important model shown in figure 56 [149-150]. Most importantly, there are many significant similarities between the AE cumulative energy plots and the most popular crack growth models. For instance, as indicated in figure 55, the Paris-Erdogan model and cumulative energy plot of the sample 3 show 3 significant phases. Additionally, the shape of the model is so close to the plot of S3.

Therefore, it may be concluded that the AE cumulative energy values represent the crack propagations inside the concrete samples. Most significantly, they may give information about the structural integrity losses inside the specimens.

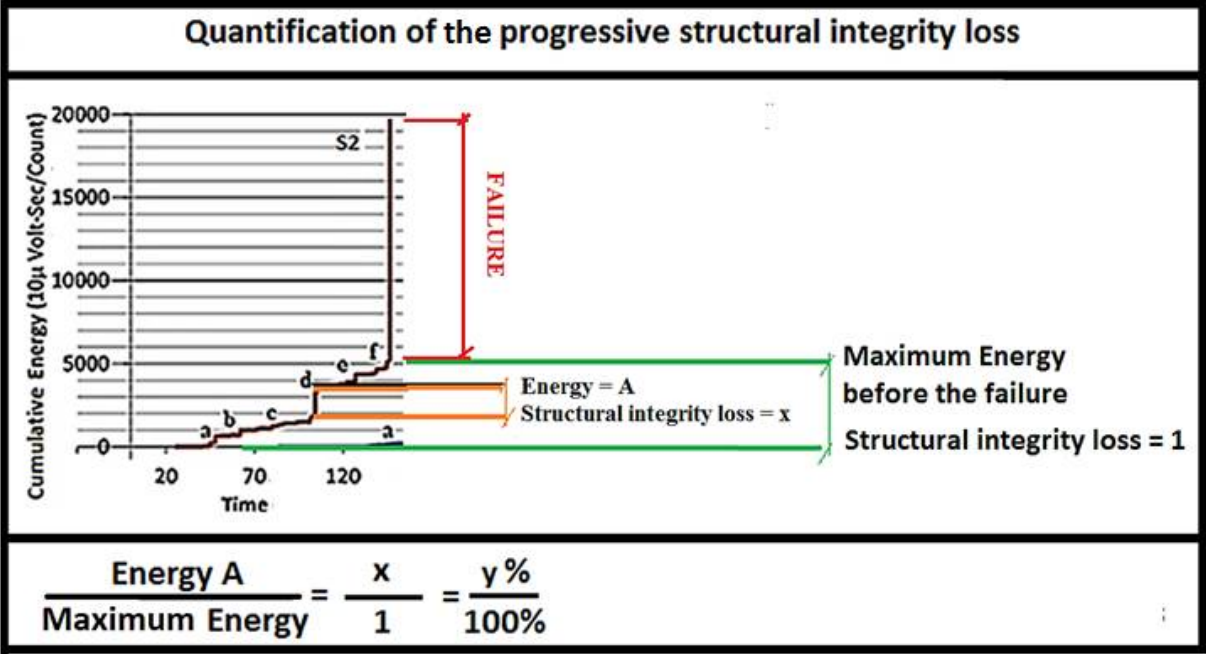


Figure 57: An example of the quantification of the progressive structural integrity loss.

To investigate the damage quantification process, figure 56 has been presented. As mentioned formerly, cumulative energy plot of the sample 2 indicates a significant energy increment from level c to d. To quantify the damage between these levels, structural integrity loss may be detected by using some statistical approaches.

First of all, the magnitude of the energy increment A may be easily found by looking energy values on the vertical axis. Additionally, energy level f, representing the maximum energy before the failure, may be properly obtained from the same axis. Afterwards, a statistical proportion may be found between cumulative energy increment A and structural integrity loss x, as shown in figure 57. Additionally, the result may be obtained as a structural integrity number and percentage.

Finally, by detecting the integrity loss, damage and dynamic displacements inside the concrete specimen may be quantified. As given in the following figures, this approach has been applied to each of the group 1 samples.

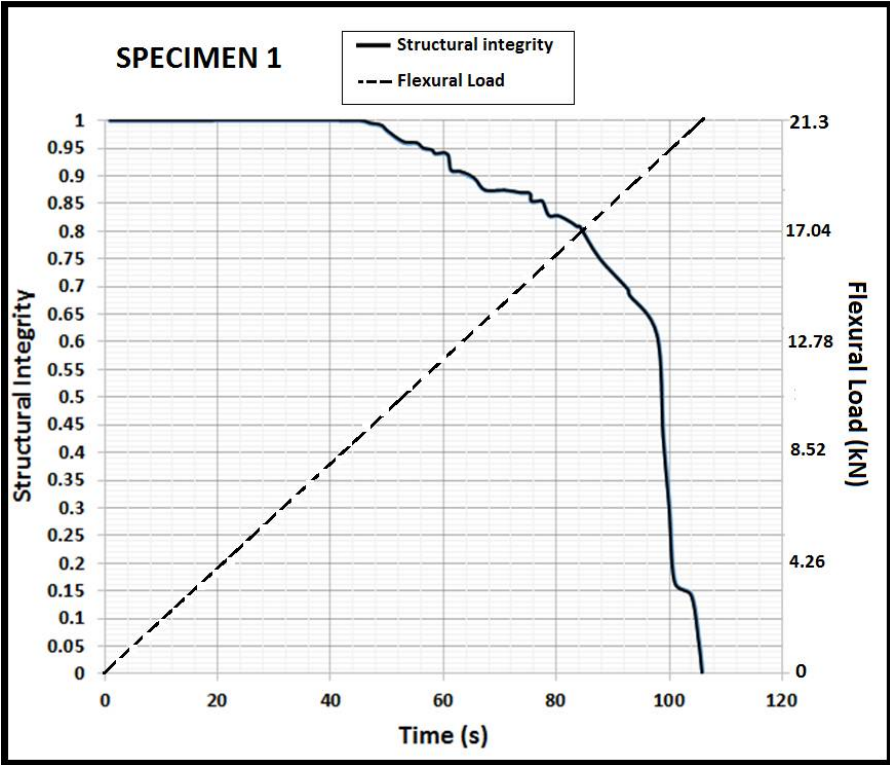


Figure 58: Quantification of the progressive structural integrity loss for the sample 1.

It is apparent from the plot in figure 58 that structural integrity of the specimen 1 is almost constant for the first 40 seconds. It means that there is no significant deformations inside the sample at the beginning of the flexural strength and acoustic emission tests. Between 40 and 60 seconds, it may be observed that almost 6% percentage of the total structural integrity has been lost. Furthermore, from 60 to 80 seconds, approximately 10 % of the structural integrity has been vanished. Most importantly, structural integrity number has plunged from 0.82 to 0.35 in between 80 and 100 seconds. It represents almost 50 % reduction of the total structural integrity. After 19 kN flexural load, slope of the plot has drastically risen because the sample is close to its failure . Finally, it has completely lost its structural integrity.

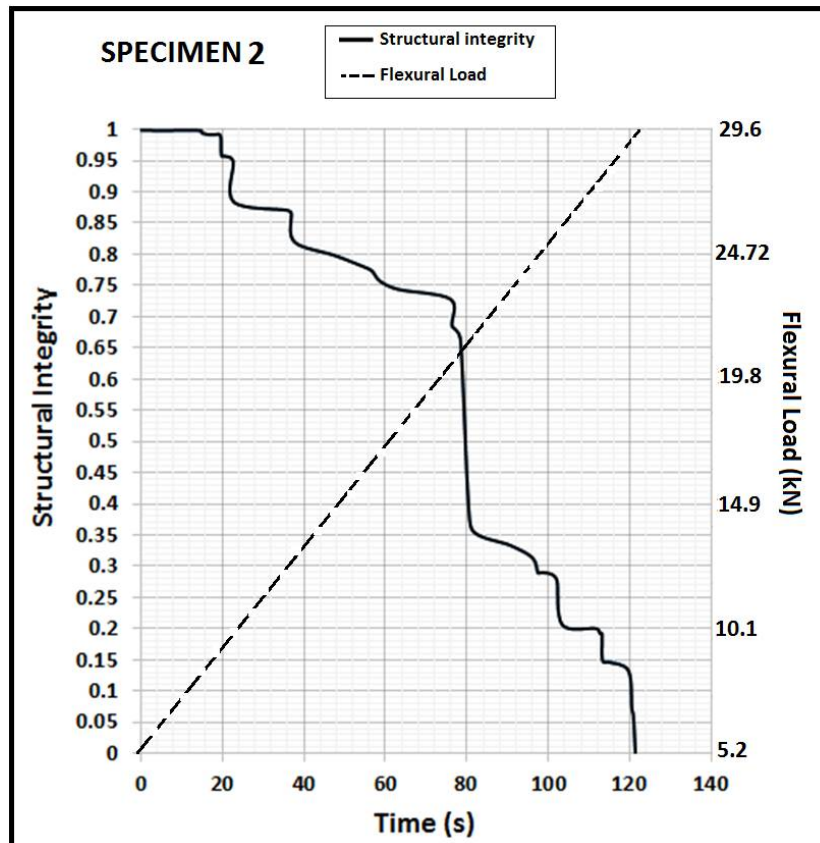


Figure 59: Quantification of the progressive structural integrity loss for the sample 2.

The other significant plot is represented in the figure 59 showing the progressive structural integrity loss for the sample 2. It may be clearly seen that there is no significant change on the integrity value for the first 20 seconds. However, at 20th second, a drastic decrease has been observed from structural integrity number 1 to 0.85 approximately. It represents almost 20% structural integrity loss of the whole structure. Then, the plot moves horizontally. This movement represents small changes on its structural integrity values. However, the graph indicates vertical drop before the 40th second.

Between 40th and 75th second, structural integrity decreases gradually. However, near the 80th second, a huge plunge has been detected on the structural integrity value from almost 0.72 to 0.35. This vertical movement represents almost 40% structural integrity loss. It is experienced under 20 kN flexural load approximately. At the end, the sample fails, after a gradual decrease from 0.35 to 0.15.

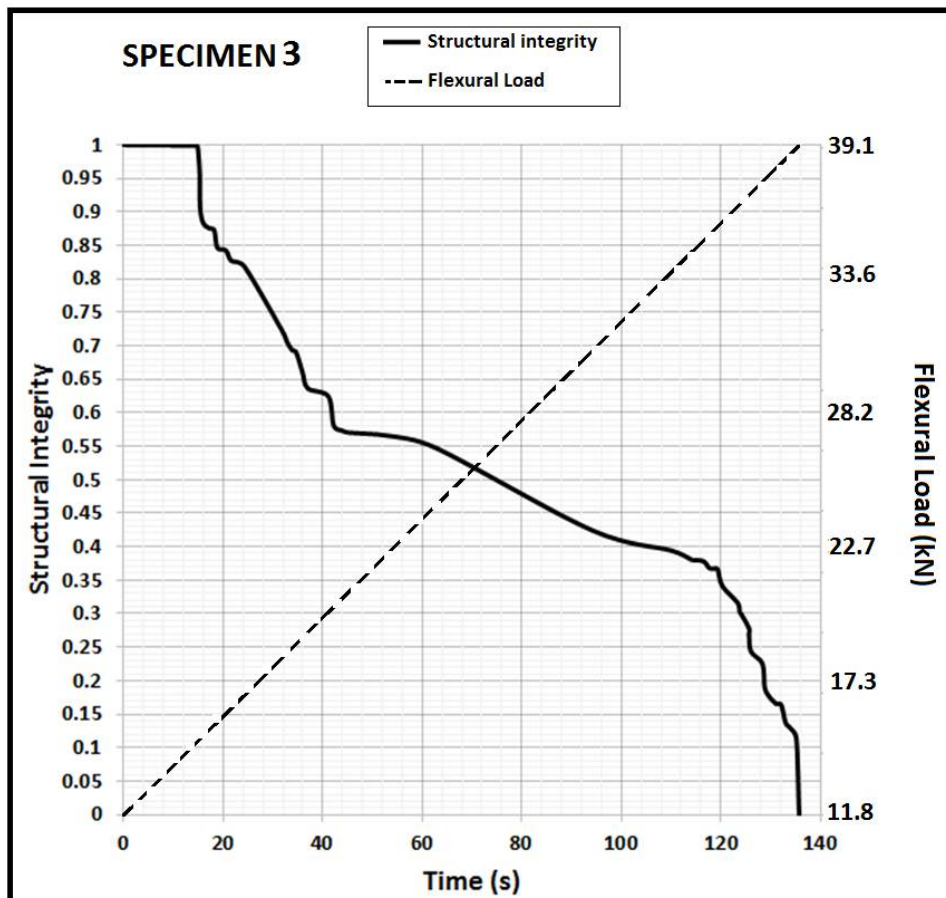


Figure 60: Quantification of the progressive structural integrity loss for the sample 3.

Furthermore, figure 60 shows structural integrity versus time plot for the specimen 3. It may be apparently observed that there is no significant damage in the sample for the first 17 seconds. Then, a significant drop occurs in structural integrity value from 1 to 0.85. During this drop, applied flexural load have been reaching almost 17 kN. Between 20th and 40th seconds, deformations go on. However, from approximately 41th to 60th seconds, there is no important change on the integrity value close to 0.55. Then, the integrity value gradually decreases to the 0.35 with in almost 60 seconds. After crossing the 34 kN flexural load, the integrity value drastically drops. In other words, the concrete beam S3 fails.

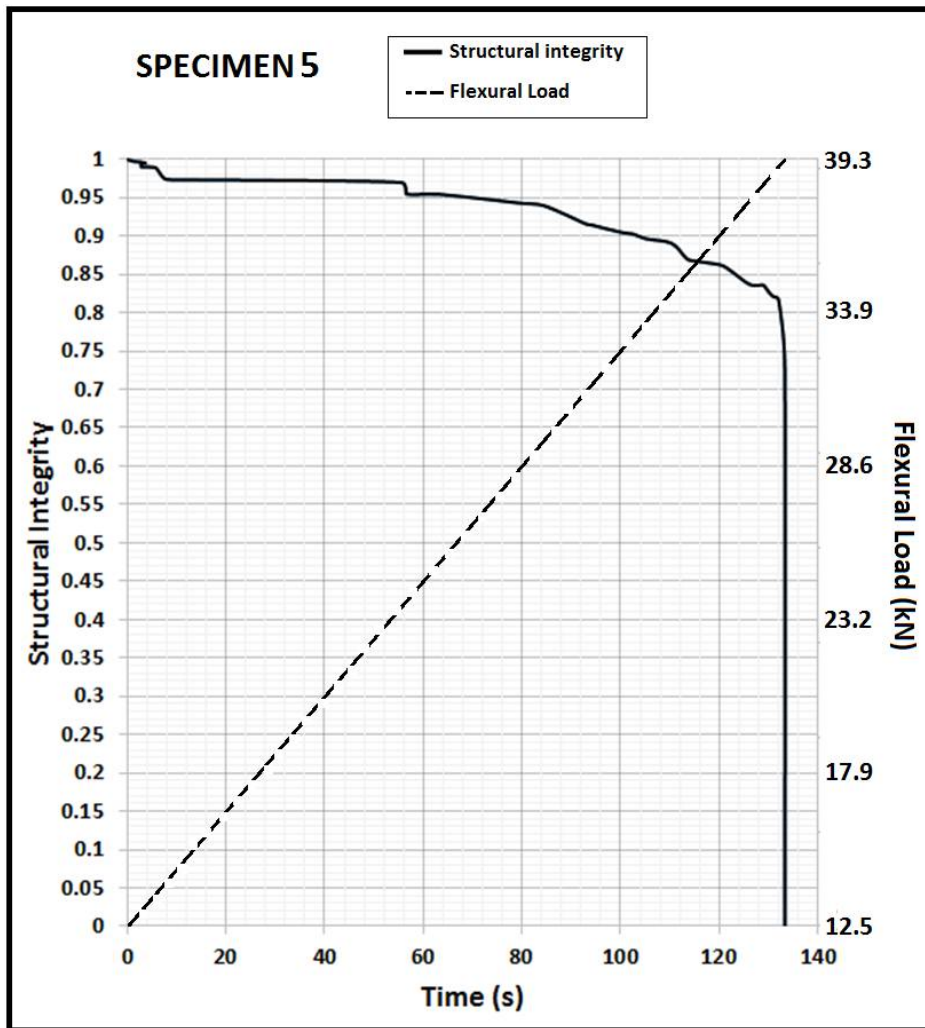


Figure 61: Quantification of the progressive structural integrity loss for the specimen 5.

Figure 61 indicates the structural integrity and applied flexural load plots for the sample 5. First of all, it indicates a slight decrease in its integrity number from 1 to 0.95 for the first 80 seconds approximately. Additionally, under an increasing flexural load from 12.5 kN to 31 kN, the sample try to resist the failure, though it loses almost 5% of its structural integrity. Afterwards, the reduction of the structural integrity value has exponentially risen. Most importantly, the sample has suddenly lost almost %85 of its total structural integrity value when the applied flexural load reaches to 39.3 kN.

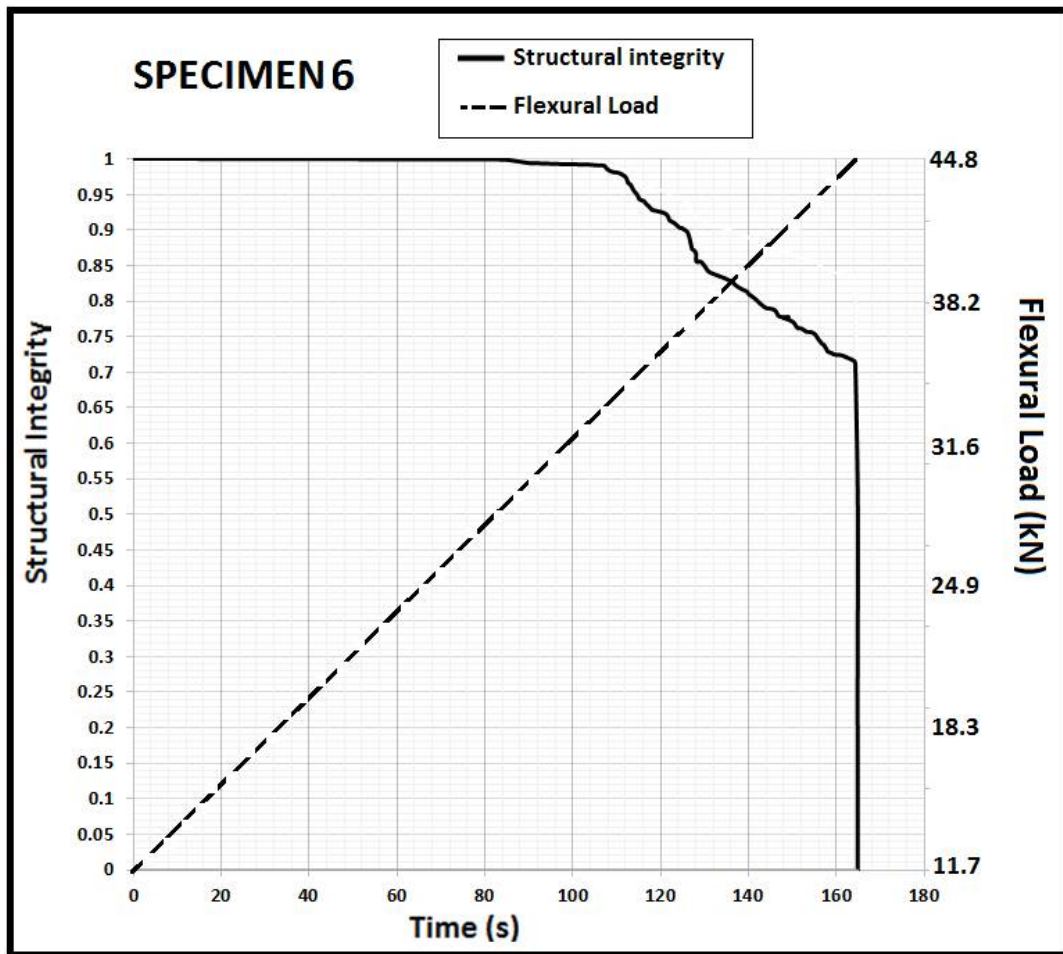


Figure 62: Quantification of the progressive structural integrity loss for the specimen 6.

As plotted in figure 62, similar to the S5, sample 6 does not experience significant change on its structural integrity value for the 110 seconds approximately. It has been trying to resist the increased flexural load. However, after crossing almost 35 kN applied flexural load, structural integrity of the sample decreases by approximately 30 %. Afterwards, similar to the sample 5, huge amount of the structural integrity value, which is almost 0.72, has been lost during the failure.

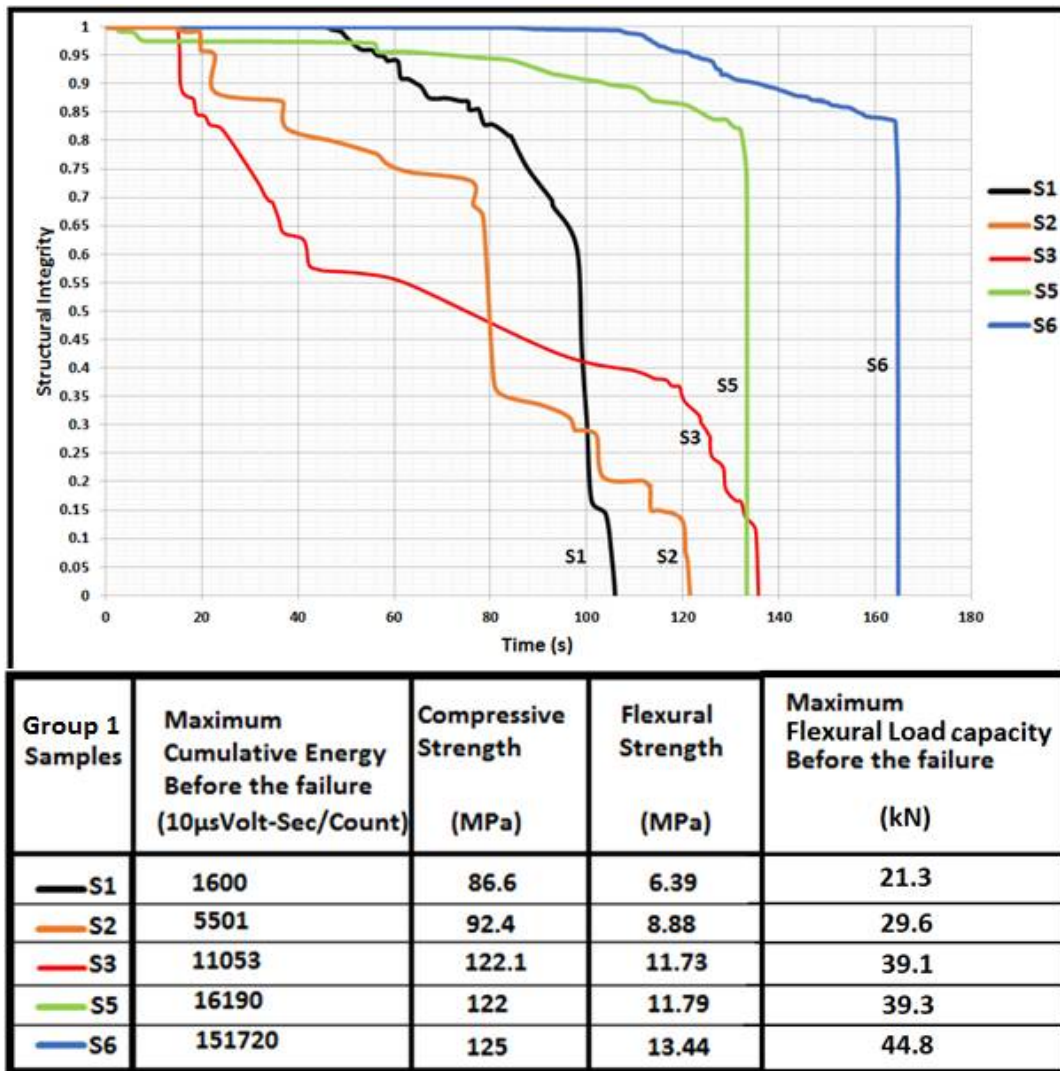


Figure 63: Comparison of the progressive structural integrity losses for the group 1 samples.

Although the structural integrity values are unique or individual, the structural integrity plots of the samples have been jointly presented to compare their structural integrity and maximum cumulative energy values with their compressive and flexural strengths.

It may be clearly observed in figure 63 that the structural integrity plots indicate horizontal movement when the compressive and flexural strength values have been rising. However, the samples, having higher strength values, have been suddenly losing a big part of their structural integrity values. Therefore, it may be concluded that the concrete samples indicate more brittle behavior, though their compressive strength and flexural strength values have been risen.

Furthermore, as mentioned formerly, the sample 3 and 5 come from different mixture contents, though they have close flexural and compressive strengths. Most importantly, the characteristics, in their structural integrity plots, are significantly different from each other, though their failure time is so close. Therefore, it may be concluded that the behavior of the concretes under a load may be different from each other, though the concretes have the same compressive and flexural strength values. For instance, specimen 3 and 5 have separate concrete mixture content, porosity, aggregate size, cement and chemical admixture type and water to cement ratio as mentioned earlier. Therefore, their crack propogations, crack growth rates and structural integrity losses may be various, although they have the same strength values.

4.2.3.3.3 AE RMS results and discussions for the group 1

Addition to the energy plots, root-mean-square graphs of the group 1 are produced. RMS can be explained as the square root of the function representing a continuous waveform or a set of values [151]. Continuous and burst type of AE waveforms are mentioned in chapter 4. RMS is generally preferred to use continuous waveforms.

Furthermore, RMS voltage has been usually calculated to obtain suitable measurement of a variable current or voltage. It has been generally named as the effective voltage which is always between average and peak voltage [152]. Finally, it can be calculated by using the formula given below [153].

$$\text{RMS value} = \frac{\text{Peak value}}{\sqrt{2}} = 0.707 \times \text{Peak value} = 1.11 \times \text{Average value}$$

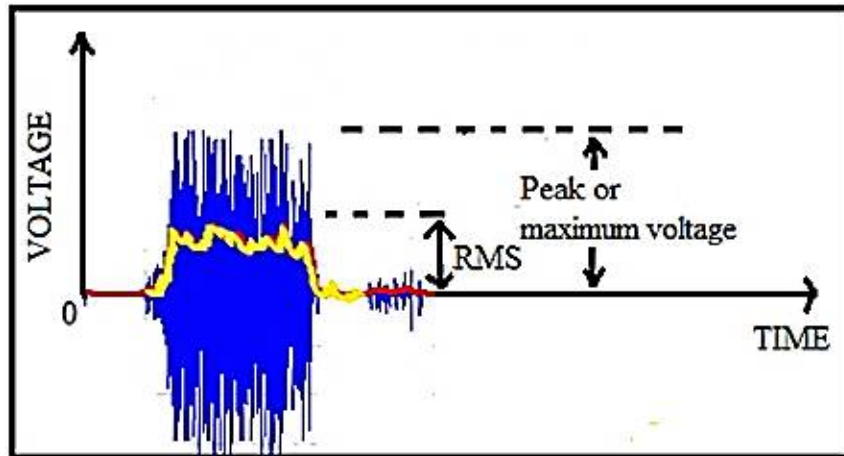


Figure 64: An example plot of RMS voltage (yellow) and raw signal (blue).

As it is shown above, plot of a raw signal can be difficult to express the magnitude of a variable voltage [153]. However, RMS plot properly shows great voltage variations affecting the average voltage of a raw signal. Therefore, RMS plots of the group 1 specimens are produced and represented in the following figures.

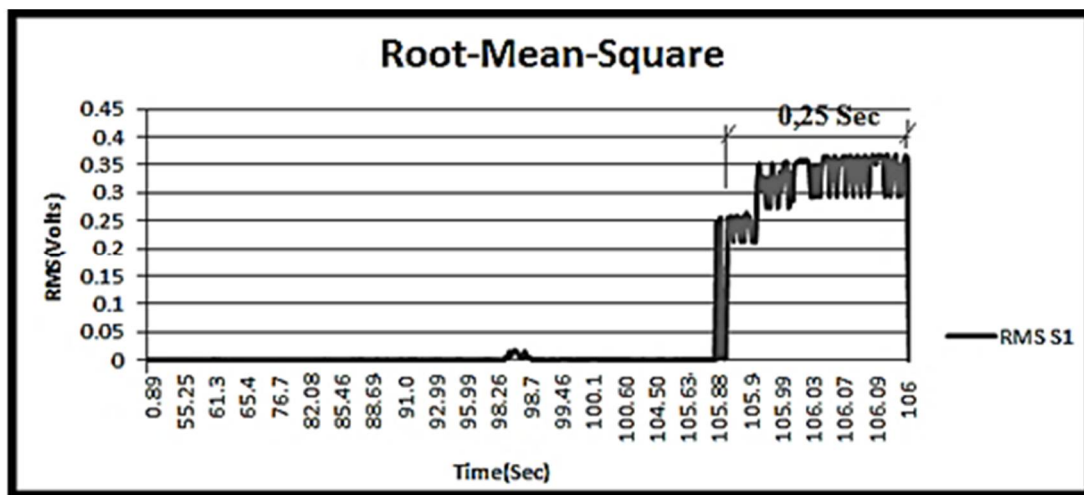


Figure 65: RMS Voltage plot of the sample 1

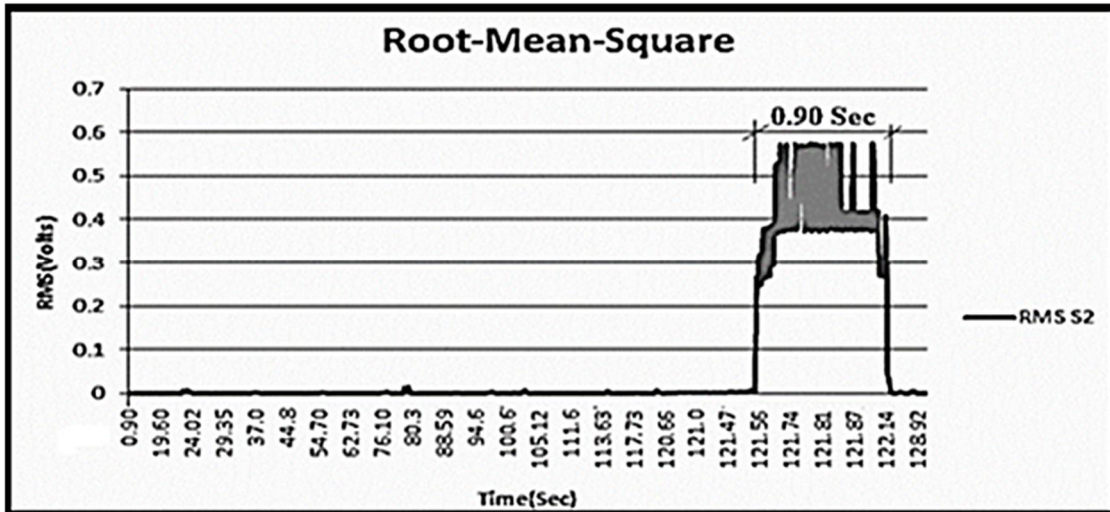


Figure 66: RMS Voltage plot of the specimen 2

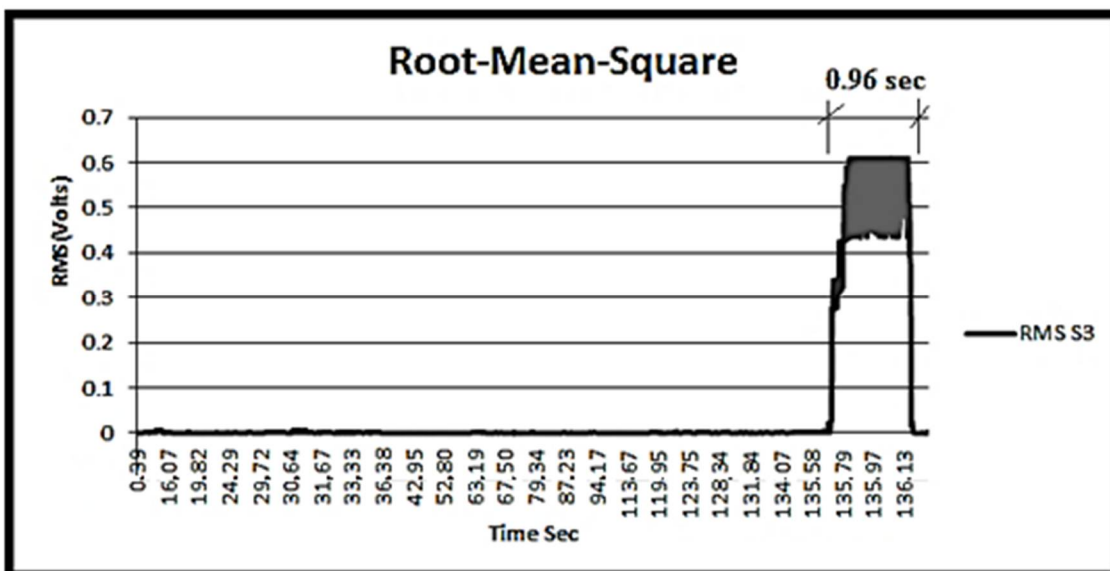


Figure 67: RMS voltage plot of the sample 3.

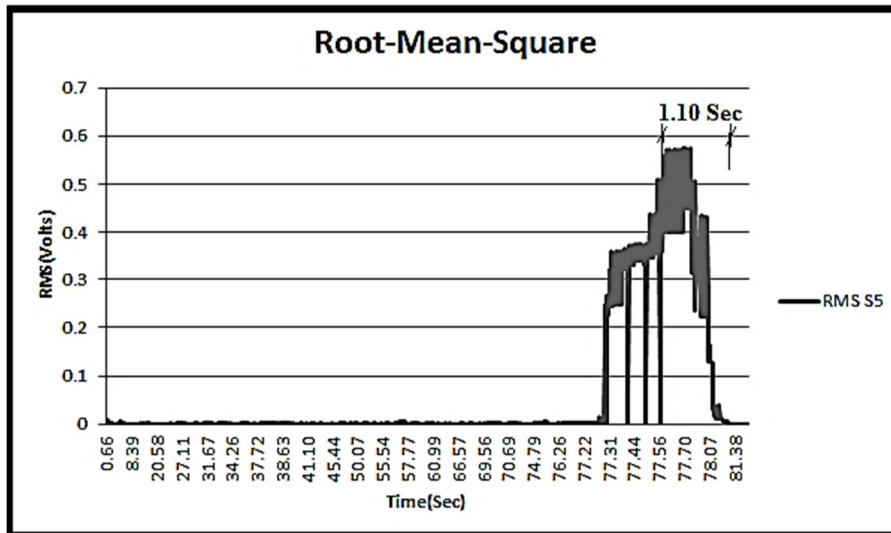


Figure 68: RMS voltage plot of the sample 5.

In these figures, significant information about dynamic displacements and deformations such as major and minor cracks can be obtained from the shape of RMS plots [154]. Most importantly, as shown in the figures, time gap and voltage level of the horizontal wave forms can give reliable information about damages inside of a test sample [155]. For instance, their sudden increments represent AE signals coming from major cracks. Additionally, the horizontal wave forms mean continuous destructive damages [156].

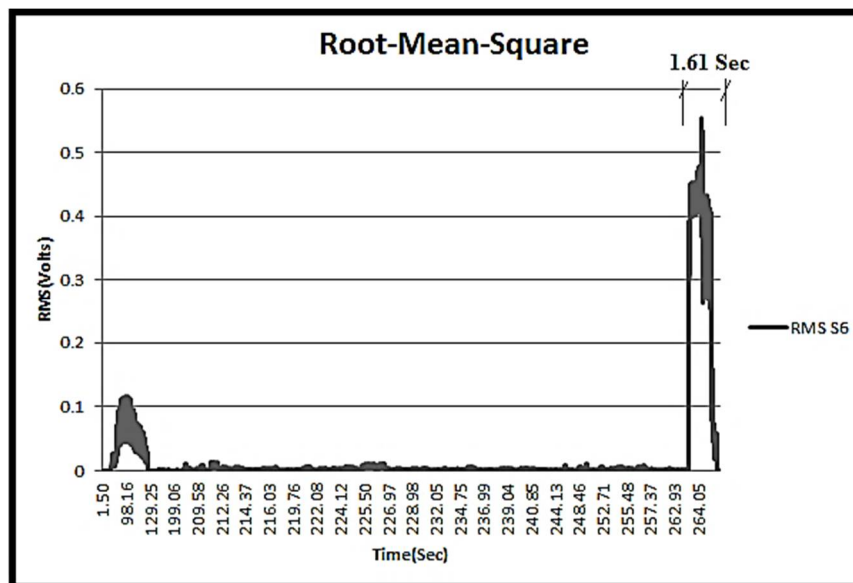


Figure 69: RMS voltage plot of the specimen 6.

Furthermore, it may be clearly observed that RMS plots of the group 1 show great increments. Afterwards, they generally indicate horizontal wave forms or RMS cycles from the beginning to the end of these increments. To obtain information about destructive damages, maximum duration between sharp increase and decrease is detected for each RMS plots.

Most importantly, as shown in figure 69 and 65, S6 having 125 MPa compressive strength experiences the highest duration among the other samples, while S1, having 86.6 MPa compressive strength, is indicating the smallest duration. Furthermore, it is apparent from the plots that S1 has the lowest maximum RMS voltage level, which is 0.367 volts, among the group 1 samples. Additionally, the voltages of S2, 3, 5 and 6 are 0.573, 0.610, 0.543 and 0.555 volts respectively. They represent destructive impacts of cracks and distortions inside the samples.

4.2.3.3.4 AE Amplitude results and discussions for the group 1

Addition to the RMS, AE signal amplitudes of the group 1 specimens are reflected as graphs in the following figures.

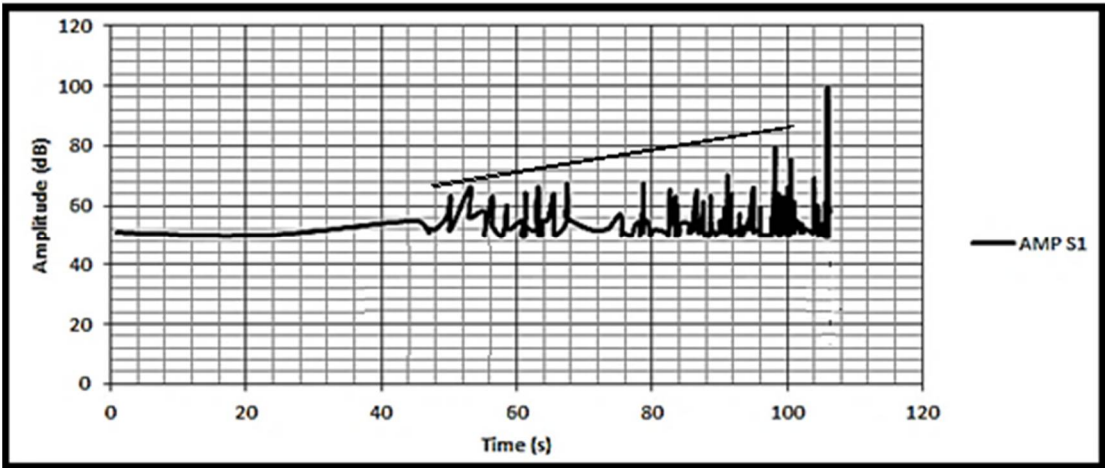


Figure 70: AE amplitude plot of the specimen 1.

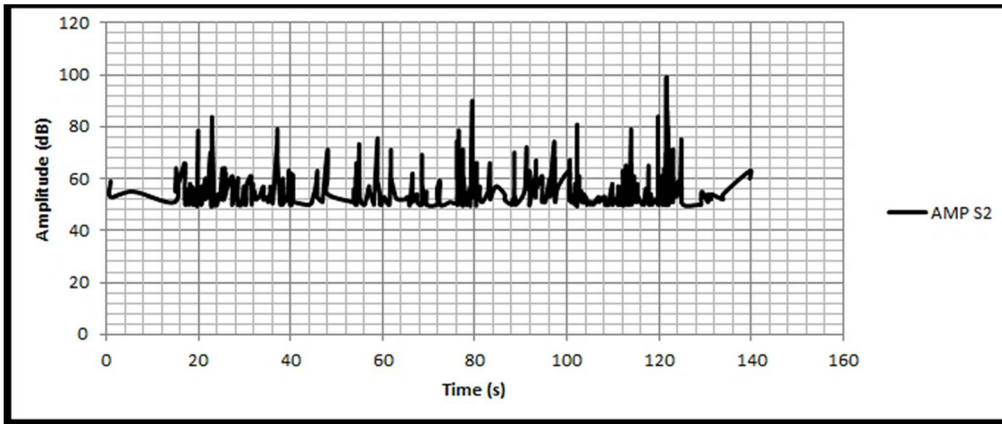


Figure 71: AE amplitude plot of the sample2.

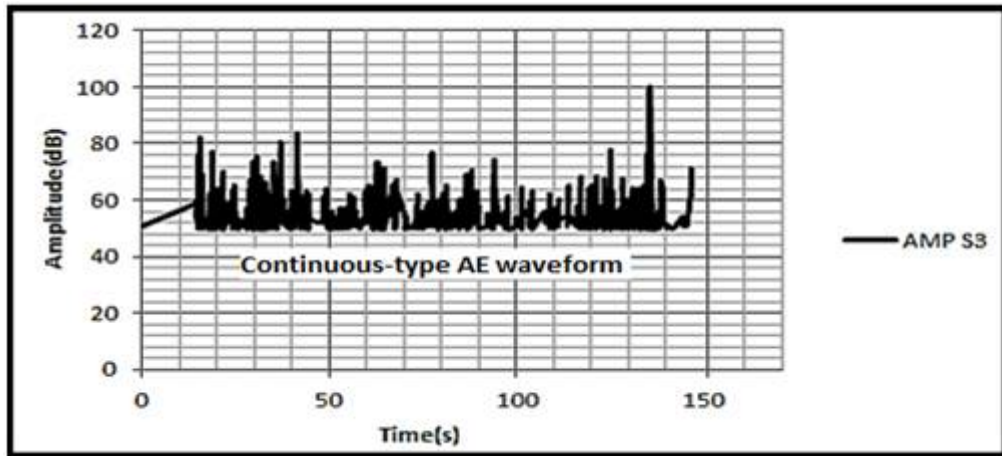


Figure 72: AE amplitude plot of the sample3.

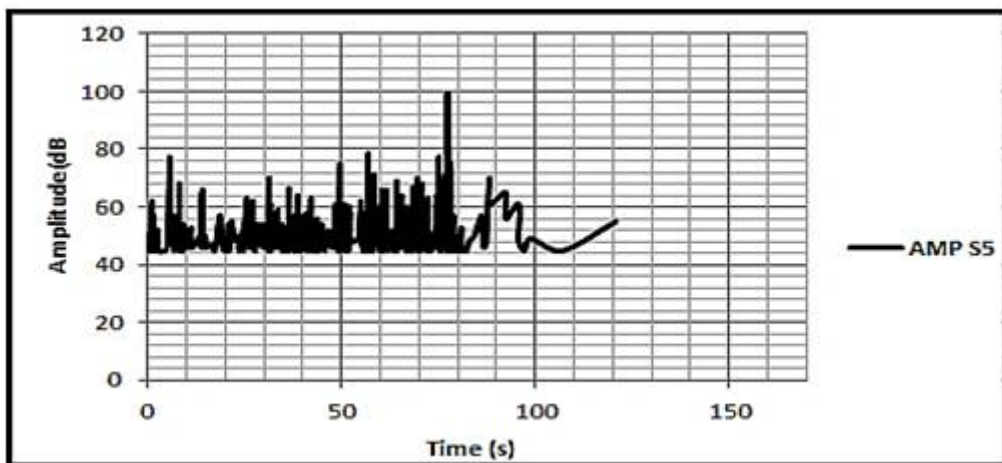


Figure 73: AE amplitude plot of the sample 5.

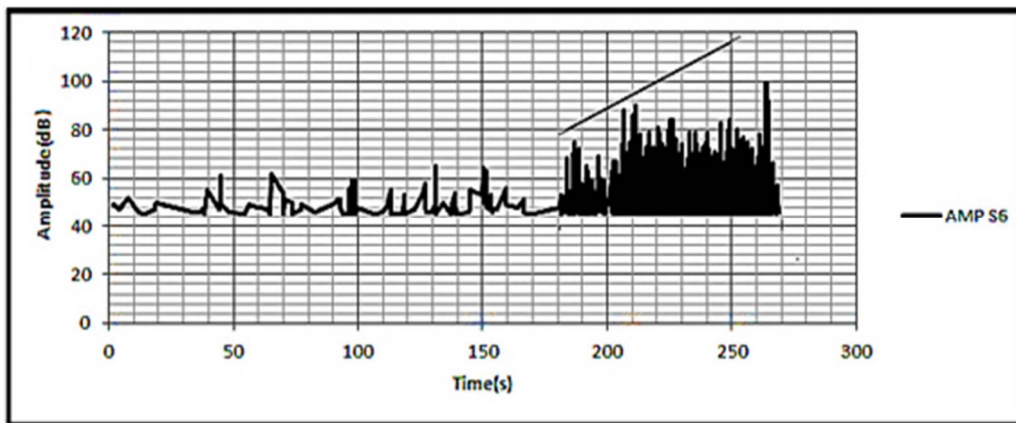


Figure 74: AE amplitude plots of the specimen 6.

The figures from 70 to 74 have been plotted to demonstrate amplitude values of the group 1 samples. It is apparent from these figures that the plots are close to continuous type of AE waveforms because group 1 specimens have high flexural strength values. However, they frequently consist burst type of AE signals in their continuous forms, because of the brittle behavior of the concrete material.

Additionally, it may be obviously observed that intensity of the AE signals has been significantly risen, when the compressive and flexural strengths have remarkably increased. For instance, acoustic signal intensities detected from S1 have been considerably lower than the signal intensities of the other samples.

Furthermore, it can be commonly observed that the rise time and duration of the AE waves generally decrease while the flexural strengths of the samples are increasing. For instance, the amplitude of S5 has increased exponentially while the plot of S1 is climbing slightly. Meaning of the rise time and duration have been mentioned in chapter 3. Additionally, they have been shown below.

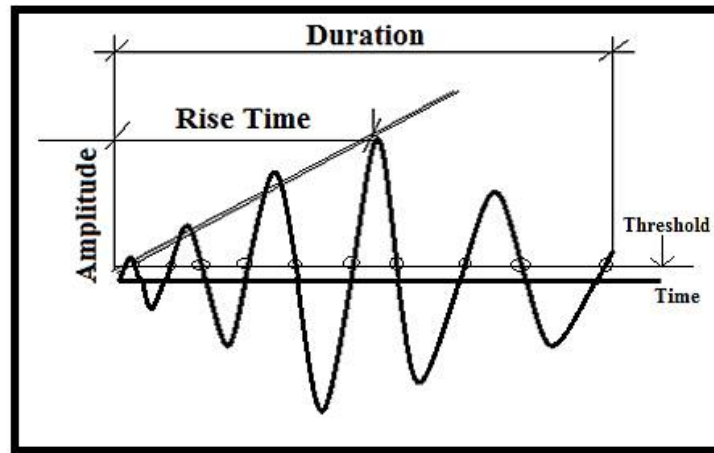


Figure 75: Rise time and duration for a typical waveform [157].

Most importantly, decrease of the rise time means the sharp increases in AE signal amplitudes. These sudden increments represent dynamic displacements and deformations such as major cracks inside the group 1 samples. At the end, AE amplitudes of the specimens reach to the highest levels because of their failures [157].

4.2.3.3.5 AE Average frequency results and discussions for the group 1

Addition to the AE signal amplitude, average frequency values of the AE signals, obtained from the group 1 specimens, have been presented in the following figures.

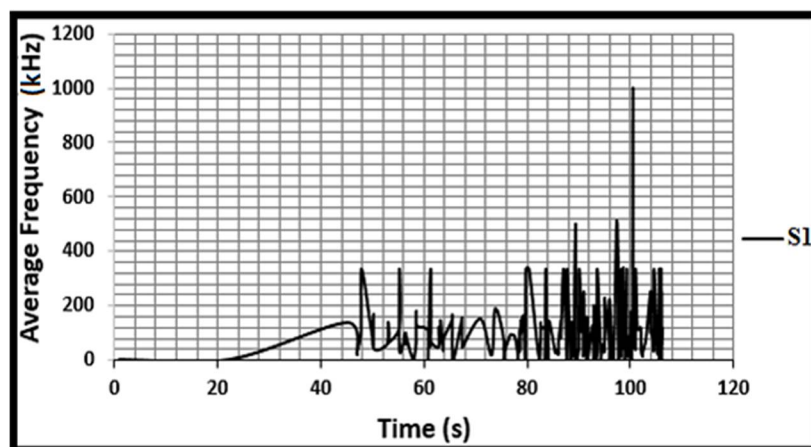


Figure 76: Average frequency values of the AE signals detected from the sample S1.

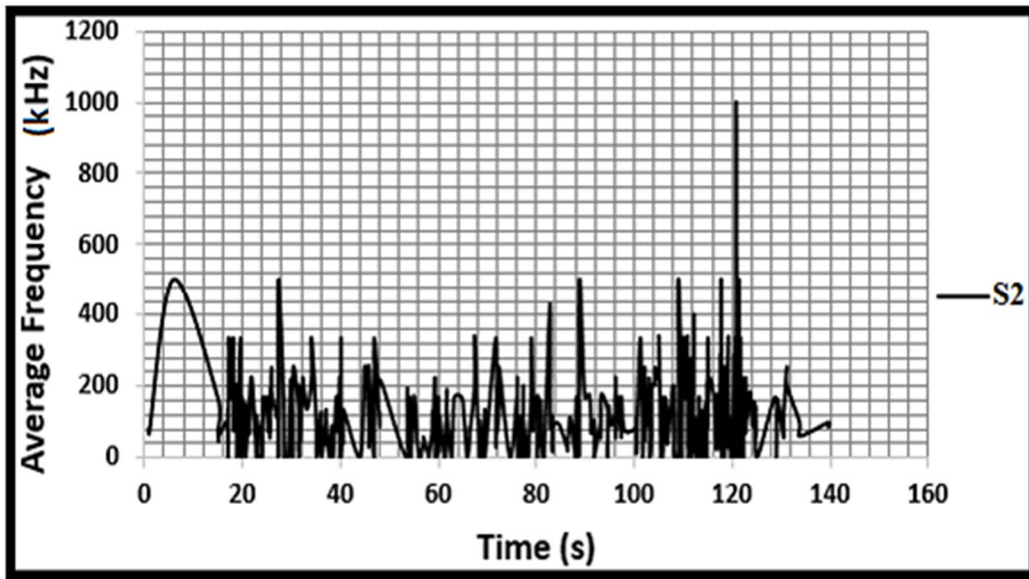


Figure 77: Average frequency values of the AE signals detected from the specimen S2.

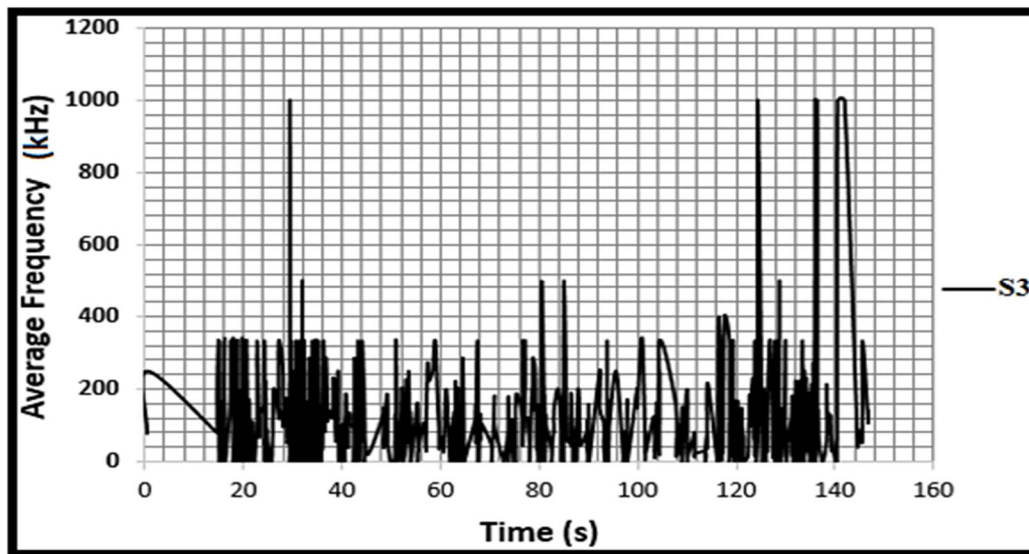


Figure 78: Average frequency values of the AE signals detected from the sample S3.

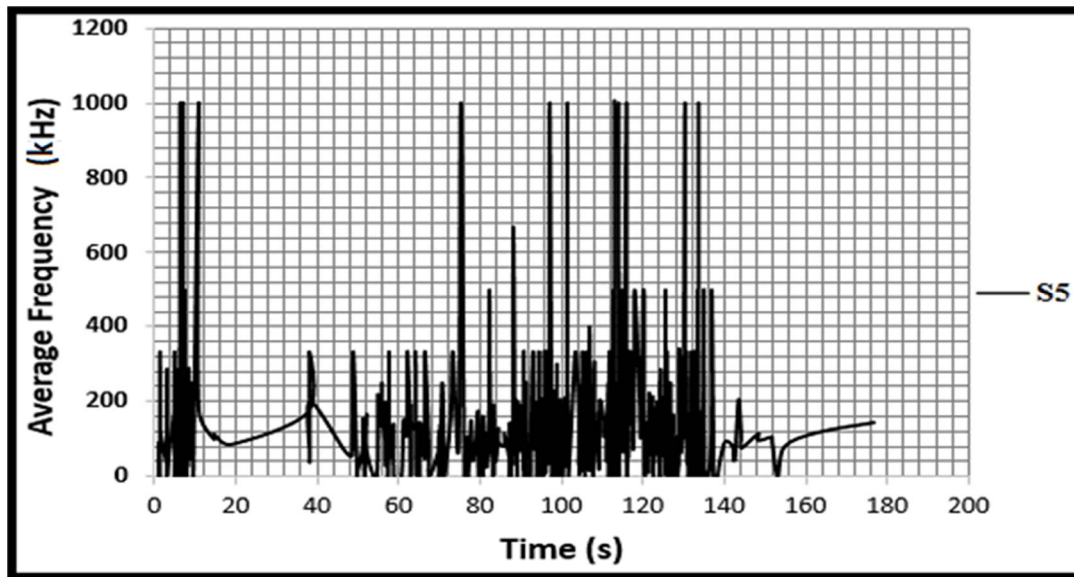


Figure 79: Average frequency values of the AE signals detected from the sample S5.

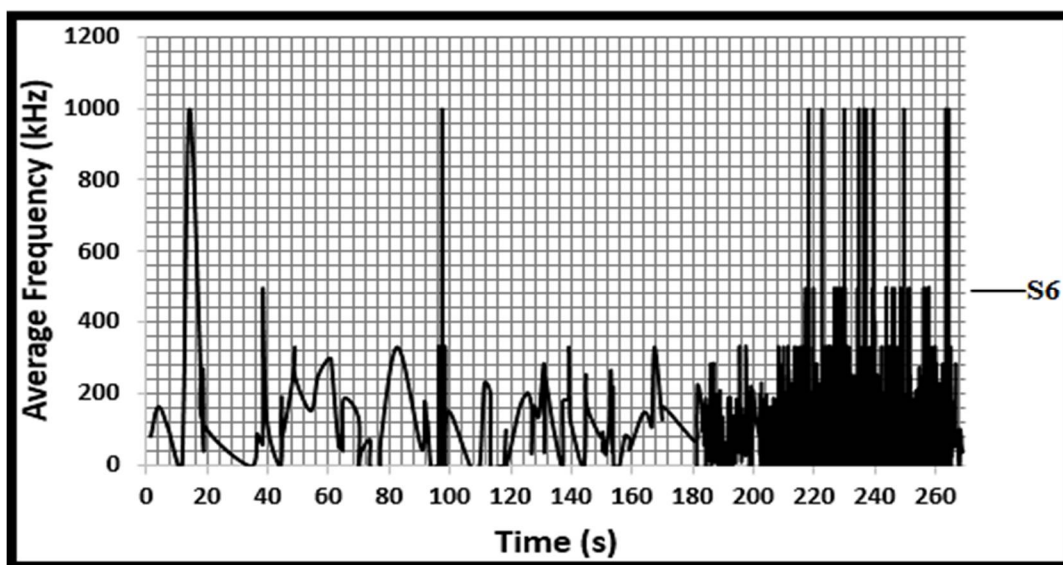


Figure 80: Average frequencies of the AE signals detected from the specimen S6.

| Group 1 Beam Specimens | S1 | S2 | S3 | S4 | S5 | S6 |
|----------------------------|------|------|-------|------|-------|-------|
| Flexural failure load (kN) | 21.3 | 29.6 | 39.1 | 49 | 39.3 | 44.8 |
| Flexural strength (MPa) | 6.39 | 8.88 | 11.73 | 14.7 | 11.79 | 13.44 |

Table 7: Bending test results of the beam samples from group 1.

It is apparent from the table 7 and figures from 76 to 80 that the average frequency levels have been remarkably rising when compressive and flexural strengths of the samples have been increasing. Additionally, the figures have illustrated that intensity of the frequency waves have risen, as the applied flexural loads have been increased.

Furthermore, volatility of the frequency fluctuation has been growing when the specimens have closed to their failures. In other words, as major cracks and dynamic displacements increase, the average frequencies have dramatically risen. Therefore, it is thought that high frequencies have occurred during crack growth.

4.3 Experimental group 2

The second experimental group includes 1 beam and 4 cubic concrete samples. They base on 4 diverse mixture contents consisting of 4 different water cement ratios.

In this part of the research study, the main objective is to observe water effects on ultrasonic pulse velocity and acoustic emission test results. For this purpose, UPVT versus compressive strength and w/c ratio graphs have been plotted and analysed statistically. Additionally, linear functions of the plots are calculated to obtain reliable correlations among pulse velocity, compressive strength and water cement ratios. Characteristics of the test results have been observed when the water amount has been elevated.

Furthermore, acoustic emission test is applied on 1 beam specimen to investigate AE energy, AMP, RMS and frequency results. The AE values of the beam specimen has been compared to the specimen 3 from the research group 1. Finally, by using AE testing technique, progressive structural integrity losses has been detected inside the beam sample.

4.3.1 Preparation of the group 2 specimens

For the group 2 samples, 4 main concrete mixture contents have been designed by only changing their water amounts. Amount of the cement and aggregate has been kept constant, though water cement ratios have been increased from 0.54 to 0.90 indicated below.

| For 1 Cube 10x10x10cm | Water/Cement | Cement(kg) | Water(lt) | Aggregate(kg) | Max Diameter Aggregate(mm) |
|--------------------------|--------------|------------|-----------|---------------|-------------------------------|
| Mixture 3 | 0.54 | 0.352 | 0.190 | 1.82 | 10 |
| Mixture 4 | 0.69 | same | 0.243 | same | same |
| Mixture 5 | 0.80 | same | 0.281 | same | same |
| Mixture 6 | 0.90 | same | 0.316 | same | same |



Table 9: Mixture contents of the group 2 specimens

As shown in the table 9, maximum diameter of the aggregates have been measured as 10 mm for the each mixture design. Additionally, same type and amount of the cement which is portland CEM 1, mentioned in chapter 2, have been used for all mixture designs in the research group 2.

4.3.2 Destructive tests for the group 2

Similar to the research group 1, flexural and compressive strength testing approaches have been applied to the group 2 specimens. These destructive techniques have been applied to the cubic and beam samples under laboratory conditions to detect remarkable similarities between destructive and non-destructive test results. Compressive test has been preferred to apply on the cubic specimens while flexural strength test is being used for the beam specimens to create dynamic displacements during acoustic emission test

4.3.2.1 Compressive and flexural strength test results for the group 2

As mentioned previously, compressive strength test has been applied on the group 2 cubic samples having different w/c ratios. In chapter 3, the test procedure has been explained in great detail. Significantly, the test results have been indicated below.

| Cubic Specimens 10x10x10cm | Water/Cement | Compressive Strength(MPa) |
|-------------------------------|--------------|---------------------------|
| Mixture 3 | 0.54 | 38.29 |
| Mixture 4 | 0.69 | 27.6 |
| Mixture 5 | 0.80 | 9.74 |
| Mixture 6 | 0.90 | 4 |

Table 10: Compressive strength test results of the group 2 cubic specimens.

According to the table shown above, compressive strengths of the specimens have been plunged from 38.29 to 4 MPa, when the water to cement ratios have been elevated from 0.54 to 0.90. It can be clearly seen that the water content has negatively affected concrete strength.

Most importantly, non-destructive testing values should indicate similar characteristics to destructive results. Therefore, it is necessary to observe these similar drastic changes and negative influences in ultrasonic pulse velocity and acoustic emission test results.

Furthermore, flexural strength test has been only applied on the beam specimen produced from mixture 3 because a big part of the group 2 specimens has low compressive strengths. For instance, M5 and M6 have 9.74 and 4 MPa strength, respectively. It can be clearly evaluated that they are too brittle to be applied bending test. Therefore, the test has not been applied on all group 2 specimens. The test procedure has been fully explained in chapter 3 and previous section. For the beam sample M3, magnitudes of the flexural strength and flexural load capacity have been measured as 3.98 MPa and 13.26 kN respectively. Additionally, cubic sample M3 indicates 38.29 MPa compressive strength value. Flexural strength testing for the specimen M3 has been shown in the following figure.

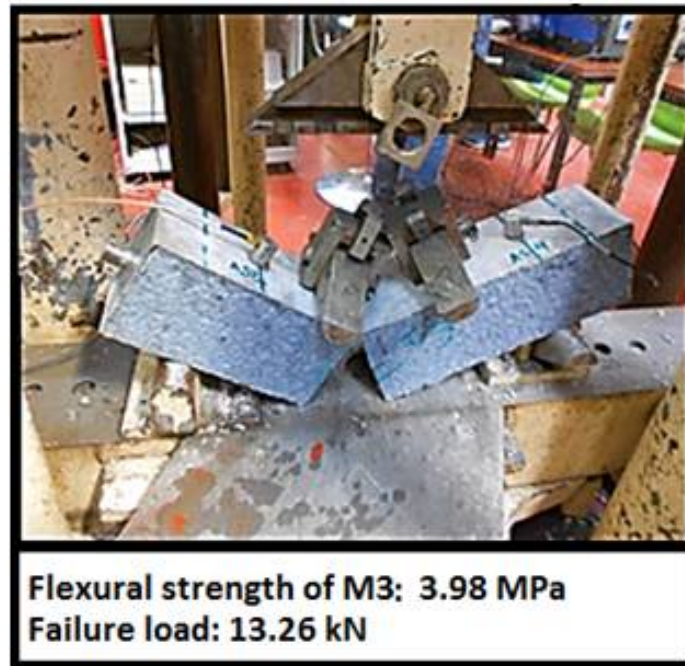


Figure 81: 4 points-bending setup, flexural strength and failure load for the specimen M3.

4.3.3 Non-destructive testing for the group 2

As it is explained previously, acoustic emission, ultrasonic pulse velocity and visual inspection tests have been preferred to use in the research group 2 because they have generally represented the sound and geometry-based NDT methods. They have been particularly explained in the chapter 4 and previous section.

4.3.3.1 UPV test results and discussion for the group 2

In this group, ultrasonic pulse velocity test has been preferred to observe the similarities and differences between destructive and non-destructive testing tests. Furthermore, water content of the group 2 mixtures has been gradually increased to investigate the influence of the elevated water to cement ratios on UPVT values. Pulse velocities of the group 2 samples have been compared with their compressive strength values to detect similarities and differences between destructive and non-destructive values.

Fundamentally, the test procedure has been described in the chapter 3 and former section. A part of the UPV applications for the group 2 samples have been shown in figure 82.

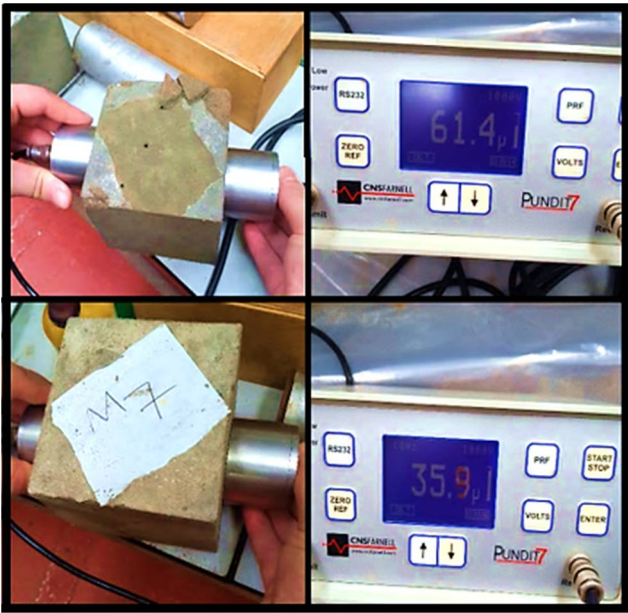


Figure 82: UPV tests for 2 cubes from group 2 samples.

Also, table 11 shows the compressive strength and pulse velocity testing results fo the group 2 cubic samples depending on the elevated water cement ratios.

| Cubic Specimens 10x10x10cm | Water/Cement | Compressive Strength[MPa] | Pulse | |
|----------------------------|--------------|---------------------------|----------------|----------|
| | | | (m/s) Velocity | Time(μs) |
| Mixture 3 | 0.54 | 38.29 | 3846.24 | 26 |
| Mixture 4 | 0.69 | 27.6 | 3472.3 | 28.8 |
| Mixture 5 | 0.80 | 9.74 | 2785.1 | 35.9 |
| Mixture 6 | 0.90 | 4 | 1628.7 | 61.4 |

Table 11: Compressive strength and UPV test results of the group 2 cubes.

From the table above, it can be clearly seen that the water to cement ratios have exerted the most significant influence on the UPVT results and concrete strengths. For example, pulse velocity and compressive strength values have drastically decreased, while water to cement ratios have been rising from 0.54 to 0.90.

Significantly, the pulse velocity and compressive strength values have been following same order. For example, M6 has the smallest compressive strength, when it shows the lowest pulse velocity. Additionally, specimen M3 has shown the highest compressive strength and pulse velocity value.

On the other hand, there is no a simple correlation among the water to cement ratios, pulse velocity and concrete strength values. For instance, relationship between the compressive strengths of M3 and M4 is 1.38, while their pulse velocity ratio is 1.11. Correspondingly, ratio of the M5 and M6 strengths is 2.44, although their pulse velocity ratio is 1.71. Addition to these examples, compressive strength of M4 to the M5 strength is 2.83 while the ratio of their pulse velocities is 1.25. Therefore, as shown in the following figures, some linear interpolations have been created to estimate concrete strengths and water to cement ratios by looking their pulse velocity values.

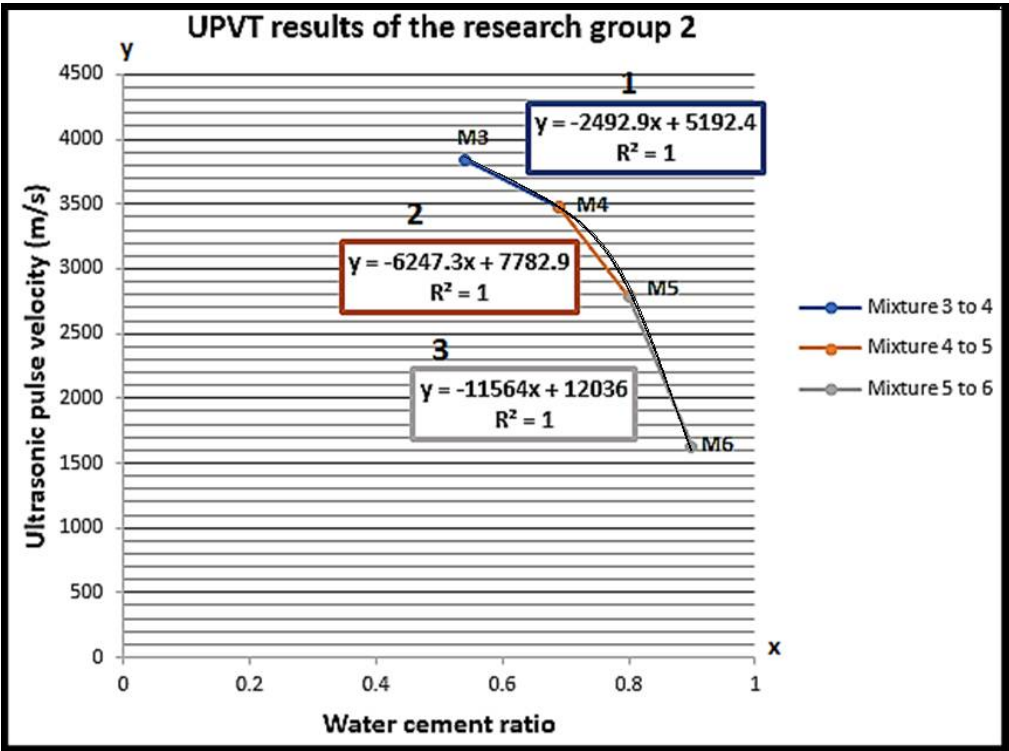


Figure 83: Linear interpolations of the UPV and w/c values for the group 2 samples.

The first plot has been created to review how diverse degrees of the water to cement ratios affect the pulse velocity in concrete. Additionally, it has been conducted on the samples having elevated water contents. The water effect to the UPVT value is properly illustrated in figure 83. It can be clearly seen that the pulse velocities have dramatically decreased, while the water to cement ratios have been rising. Furthermore, the concretes having w/c ratios from 0.54 to 0.69 indicates UPV values of between 3846.24 and 3472.3 m/s. Additionally, pulse velocity results decrease from 3472.4 to 2785.1 m/s when the water to cement ratios increase from 0.69 to 0.80. Moreover, pulse velocities fall in the range of 2785.1 and 1628.7 m/s while w/c ratios are in the range of 0.80 and 0.90.

As it is mentioned previously, the results have been interpolated linearly. 3 main interpolations have been calculated to reliably estimate w/c and pulse velocity. For instance, w/c ratios of the concretes having pulse velocities between 3886 and 3472 m/s can be believably estimated by using the linear equation between M3 and M4.

Similarly, the pulse velocities between 3472 and 2785 m/s can give reliable information about the w/c ratios between 0.69 and 0.80 if the second equation have been used. Finally, the third linear equation in figure 83 represents the UPV and w/c ratio values between M5 and M6.

Importantly, it can be obviously observed that slopes of the 3 linear plots have risen exponentially when w/c ratios have increased importantly. Especially, slope of the third linear plot between M5 and M6 is the highest if it is compared with the other linear plots.

Addition to figure 83, compressive strength versus pulse velocity plot has been produced to observe water effect on the experimental results of the group 2 samples.

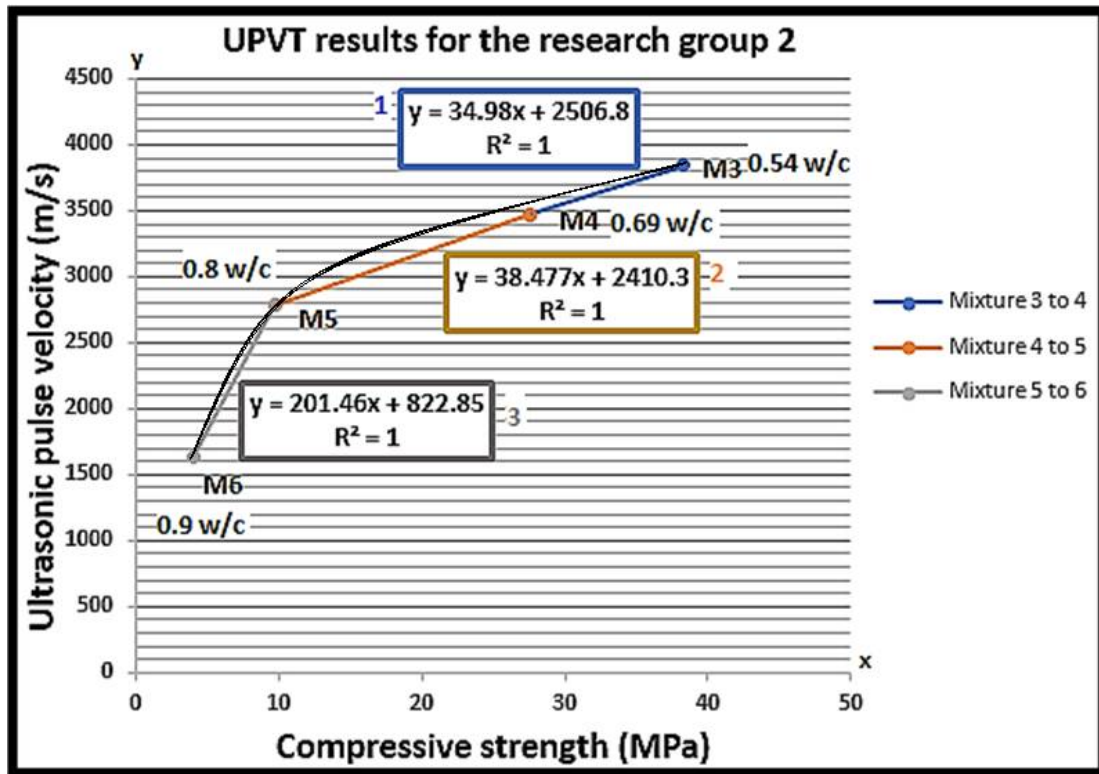


Figure 84: Linear interpolations of the UPV and strength values for the group 2.

In figure 84, the experimental studies and their statistical functions have been presented to address the water effects on the ultrasonic pulse velocities and concrete strengths for the cubic specimens.

For the 4 w/c ratios, the relationship between UPV and compressive strength have been indicated as 3 linear line and their equations in the same figure. It can be obviously observed that the pulse velocities and the compressive strengths have decrease importantly when the water to cement ratios have been increased.

Furthermore, it can be clearly seen that slopes of the first and second plot are close to each other. However, the pulse velocities and compressive strengths have experienced a dramatic plunge while w/c ratios have been rising from 0.8 to 0.9. These imply that, the UPV and compressive strength changing rates of high and low w/c ratio concrete are importantly different from each other.

Fundamentally, pulse velocity and compressive strength of the concrete having low water/cement ratio are greater than strength of the concrete containing high w/c ratio. In other words, decrease of the w/c ratio causes dense structure in hardened concrete. Therefore, the concrete strength and pulse velocity have been rising while w/c ratio has been falling. Additionally, low w/c ratio induces reduction of porosity and void ratio inside the hardened concrete. After the hardening process, water evaporates and the void ratio increases in the concrete structures mentioned in chapter 2.

Furthermore, velocity of the pulse travelling through a water is lower than pulse velocity inside a concrete material. Therefore, water contents of the group 2 concrete samples have affected the pulse velocities negatively.

4.3.3.2 Acoustic emission test for the group 2

For the experimental group 2, acoustic emission test has been applied to the sample M3 to investigate characteristics in its test results. Especially, it is aimed to observe relationships between various flexural, compressive strengths and AE signal properties.

For this purpose, acoustic emission signal properties of the group 1 samples have been compared with results of the specimen M3. Particularly, energy, cumulative energy, root-mean-square, frequency and amplitude plots of the sample M3 have been compared with the group 1 samples. Additionally, progressive structural integrity losses in the sample M3 have been tried to quantify by using its AE cumulative energy values.

As it is mentioned previously, AE test method has not based on concrete geometry such as aggregate size, void ratio. It has been affected by dynamic displacements and crack sounds inside a concrete test sample. These factors have mainly depended on the material strength, durability and quality.

As mentioned earlier, AE test can not be used without a specific load. Therefore, flexural load has been applied to the concrete beam specimen during the AE tests. Application of the AE test to the beam specimen M3 has been shown in figure 85.



Figure 85: 4 points-bending setup and AE test for the beam sample M3.

4.3.3.2.1 AE energy results and discussion for the group 2

AE signal properties of the sample M3 have been plotted as AE signal energy, cumulative energy, root-mean-square, amplitude and frequency versus time graphs.

In figure 86, AE energy values of the sample M3 have been shown by comparing to the sample 3 from the group 1. In the following figure, the energy values have been converted to the cumulative energy graphs to analyze energy changes in detail.

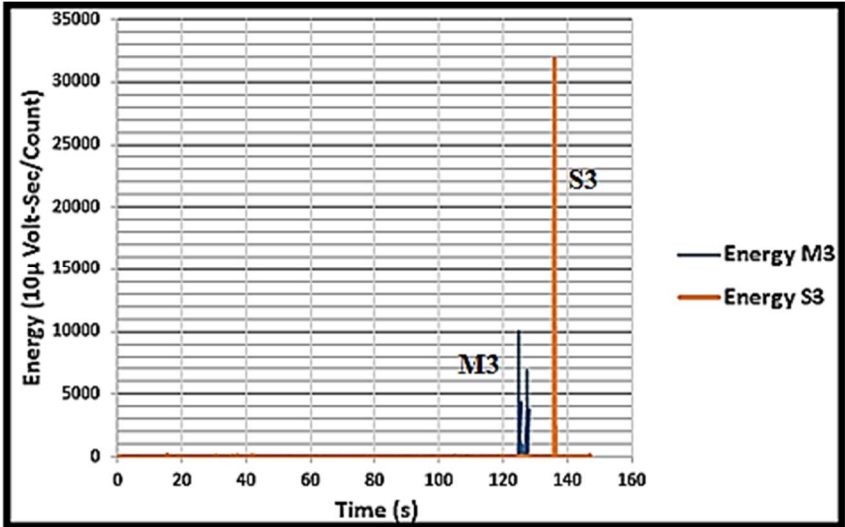


Figure 86: AE signal energy plots for the M3 and S3.

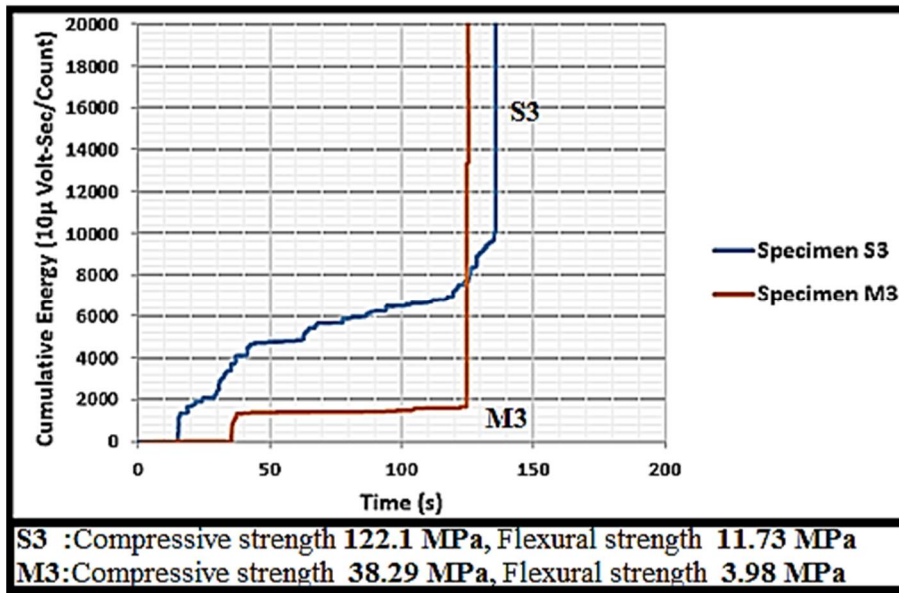


Figure 87: AE signal cumulative energy graphs for M3 and S3.

It is apparent from the previous figures that the specimen 3 from group 1 has the greatest compressive and flexural strength if it is compared to the M3 from group 2. Strength values of the S3 have been nearly three times as big as the results of M3. Similarly, energy versus time plots have indicated significant energy differences between S3 and M3. Therefore, it can be clearly concluded that the energy results of M3 and S3 have been remarkably consistent with their strength values.

Furthermore, the other important figure is cumulative energy versus time plot. it may be evidently observed that S3 has more energy increment levels than M3. As it is mentioned previously, energy increments have represented minor and major cracks, dynamic displacements and distortions inside the test samples. Most importantly, sudden vertical increments have indicated quite drastic damages inside the concrete samples.

Moreover, S3 has indicated rapid growth from start to the end of its cumulative energy plot. However, cumulative energy of M3 has gradually risen after a sudden increment seen in figure 65. Additionally, cumulative energy plot of S3 has greater slope than the M3 graph. Finally, they have shown vertical burst effect because of the fracture.

4.3.3.2.2 Quantification of the progressive structural integrity losses for the group 2 sample.

As explained in section 4.1.3.2.2, it may be concluded that the AE cumulative energy values represent the crack propagations inside the concrete samples. Most significantly, they may give information about the structural integrity losses inside the concrete samples.

For this reason, as shown in the following figure, a significant plot has been created to detect the progressive structural integrity losses inside the sample M3.

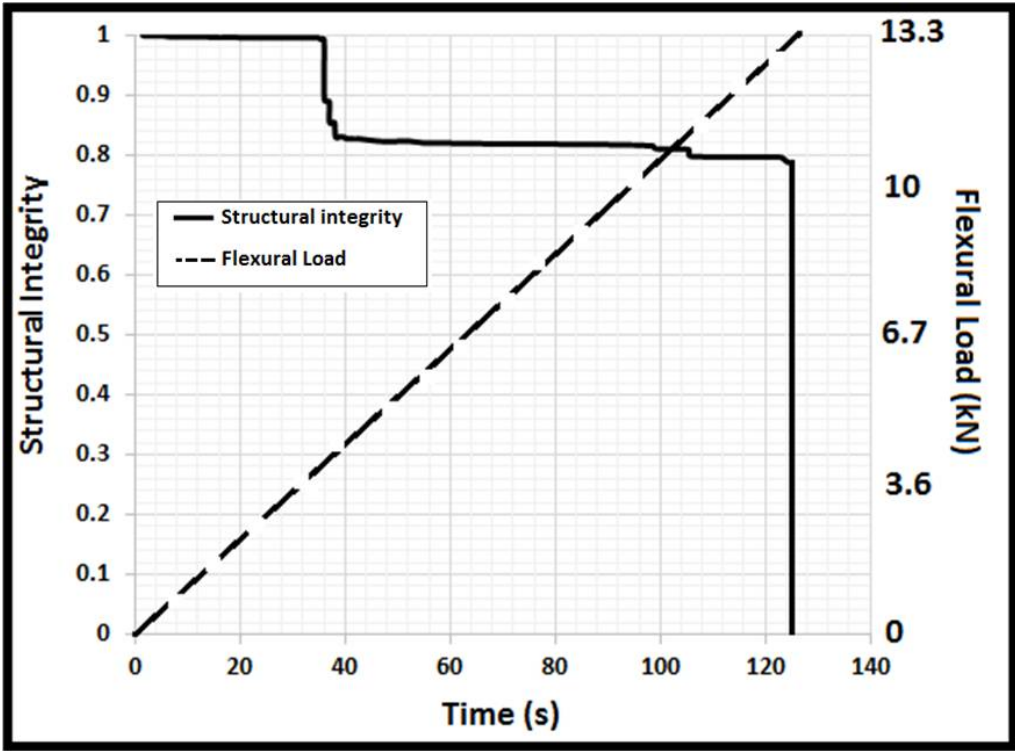


Figure 88: Quantification of the progressive structural integrity loss for the sample M3.

It may be easily observed in figure 88 that the structural integrity plot of the M3 shows horizontal movement for the first 38 seconds approximately. Afterwards, the sample has been suddenly losing a significant part of its structural integrity value. However, it indicates the horizontal movement after that drastic drop. By observing these significant movements, it may be concluded that the sample has been trying to resist increased flexural load, though it has lost almost 20 % of its structural integrity.

At the end, huge amount of the structural integrity value, which is almost 0.8, has been lost, because of the failure. Although, there is no significant change in the integrity value, before the failure.

4.3.3.2.3 AE RMS results and discussions for the group 2

Apart from the energy plots, root-mean-square graph of the sample M3 has been created. As it is mentioned in previous section, RMS may be defined as the square root of the function indicating a continuous waveform or a set of values [158]. Continuous and burst type of AE waveforms has been particularly explained in chapter 3. Fundamentally, RMS has been preferred to use for continuous type of the AE waveforms. Additionally, RMS voltage has been commonly calculated to obtain proper measurement of a variable current or voltage. It has been usually named as the effective voltage which is always between average and peak voltage. Its model figure and empirical formula have been given in the section 4.2.3.3.3.

As it is mentioned previously, plot of a raw signal can be complicated to explain the magnitude of a fluctuating voltage. However, RMS plots can properly indicate great voltage variations influencing the average voltage of a raw signal. Therefore, RMS plots of the M3 has been produced. Additionally, it is compared to the plot of the S3 from group 1, as shown in the following figures.

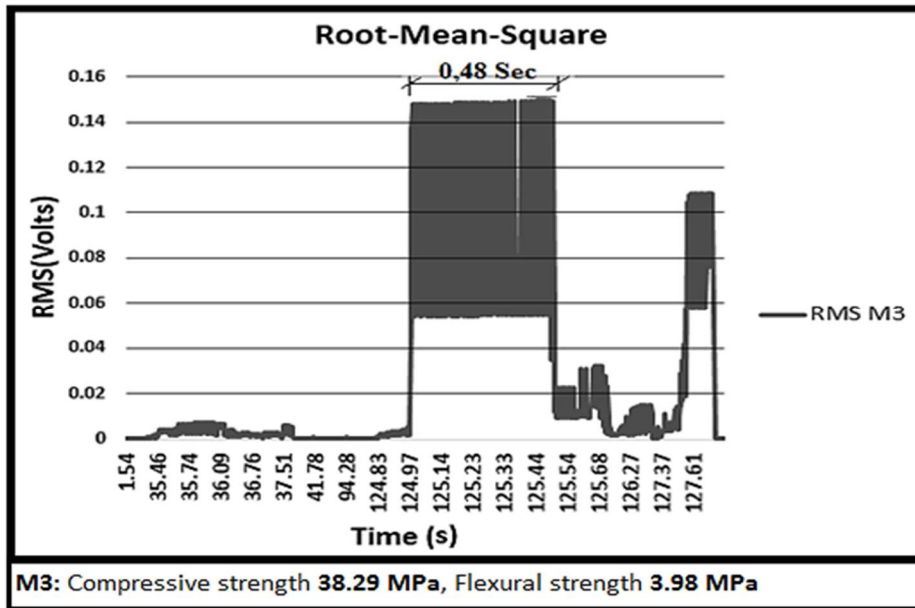


Figure 89: RMS voltage plot for the specimen M3 from group 2.

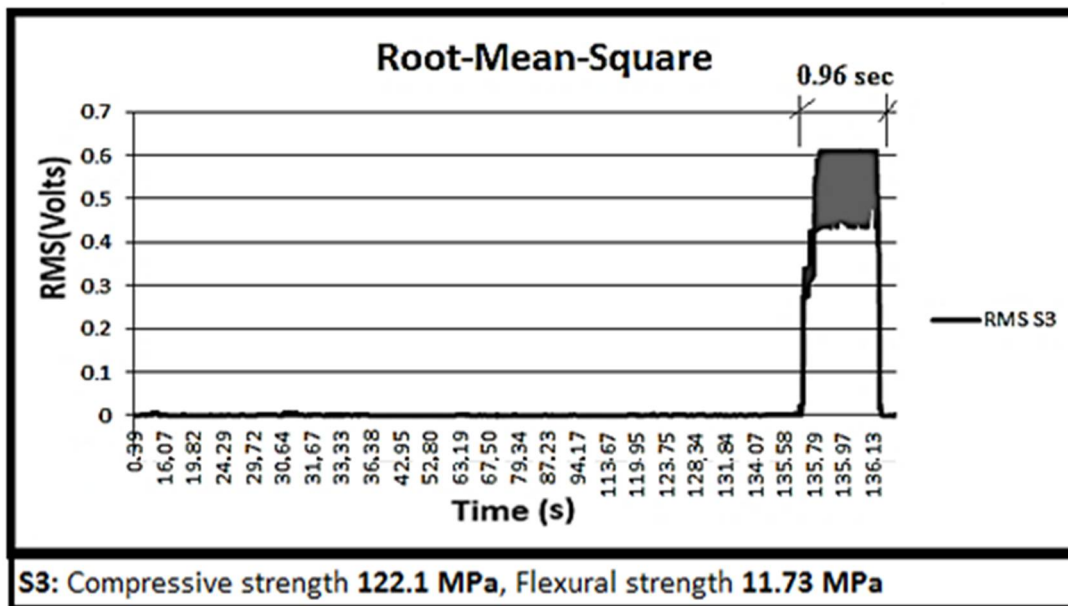


Figure 90: RMS voltage plot for the specimen S3 from group 1.

In figure 89, M3, having 3.98 MPa flexural and 38.29 MPa compressive strength, has indicated lower RMS voltage levels than the results of S3, possessing 11.73 MPa flexural and 122.1 MPa compressive strength. For instance, maximum RMS voltage of the S3 has been tested as 0.61 Volt while M3 has been showing 0.15 Volt.

Additionally, it may be easily observed that voltage values of the RMS plots have shown sharp increments. Afterwards, horizontal wave forms or RMS cycles have been detected from the beginning to the end of these increases. As it is mentioned formerly, duration of these type of RMS wave forms may be so important to detect a destructive damage, crack growth, major crack inside a test sample. Therefore, maximum durations between sharp increases and decreases have been shown in these figures. It may be clearly seen that the duration of M3 has been measured as 0.48 second when 0.96 second has been experienced from S3.

4.3.3.2.4 AE Amplitude results and discussions for the group 2

Addition to the RMS, AE signal amplitudes of the specimen M3 and S3 have been given as AMP plots in the following figures.

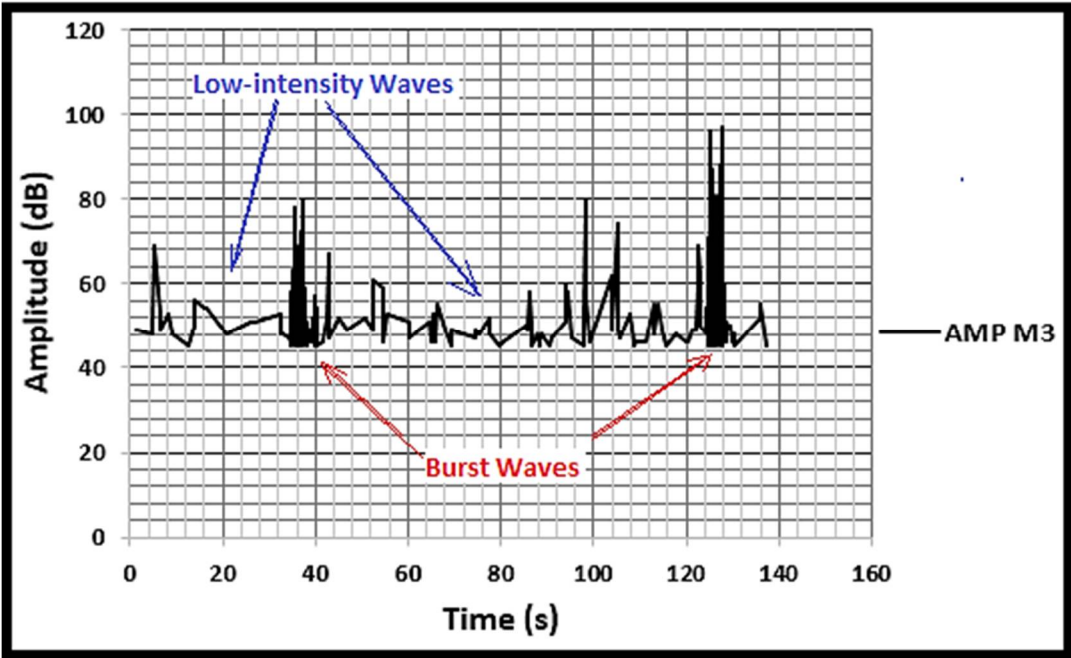


Figure 91: AE amplitude plot of the sample M3 from the group 2.

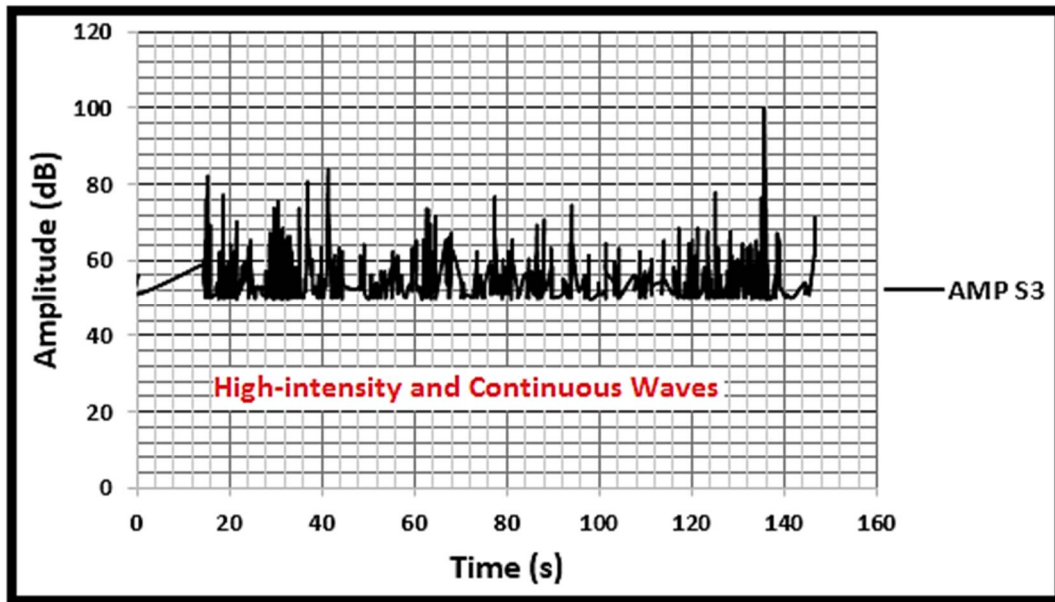


Figure 92: AE amplitude plot of the specimen 3 from the group 1.

It is apparent from the figure 91 that M3 has the AE signal waves having low-intensities. Furthermore, specimen M3 has the quite low flexural strength. In other words, it may be called as the brittle material. Therefore, its wave form has indicated sudden increments. It has burst type of the waves shown in the figure. As it is explained previously, burst type of the waves may mean the significant deformations such as a major crack and crack growth inside a test sample. Finally, plot of the specimen has indicated the strongest burst signals before its fracture. However, specimen S3 from the group 1 has the higher flexural and compressive strength than M3. Importantly, it has continuous type of the AE waveforms shown in figure 92. Also, it has intensely consisted burst type of AE signals in its continuous form because burst waves have been commonly sourced by brittle materials mentioned in chapter 4. At the end, the highest burst signals have been observed before its failure.

4.3.3.2.5 AE Average frequency results and discussions for the group 2

Apart from the signal amplitudes, average frequencies of the AE signals, obtained from the sample M3 and S3, have been shown below.

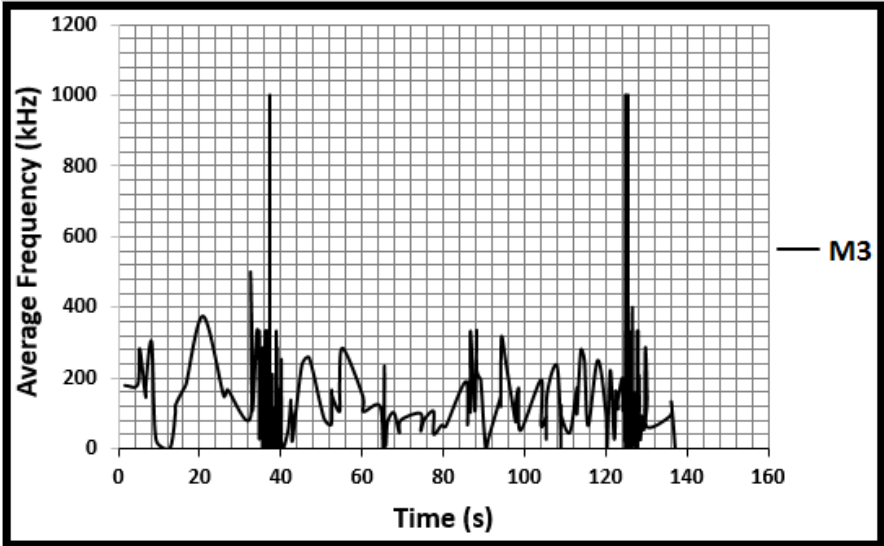


Figure 93: Average frequency plot of the AE signals detected from the specimen M3.

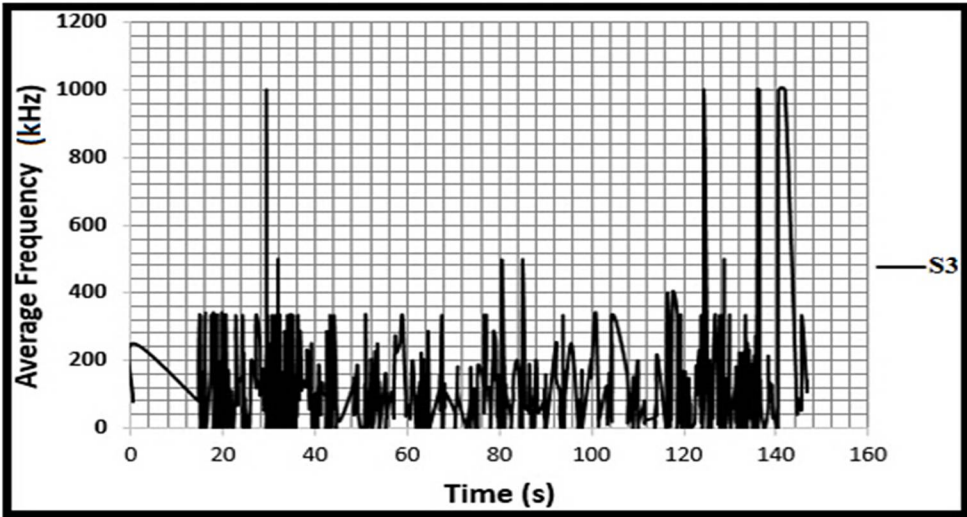


Figure 94: Average frequency plot of the AE signals detected from the sample S3.

It may be clearly observed that the average frequency levels have been significantly growing when compressive and flexural strengths of the samples have been rising. In figure 93, the sample M3 has indicated lower average frequency levels than the sample S3 in figure 94.

Furthermore, intensity of the frequency fluctuations has increased when the samples have closed to their failures. In other words, as the drastic damages such as a major crack increase inside the test samples, their average frequencies have exponentially increased. Therefore, it is deduced that quite high frequencies have been detected during growth of the major cracks inside the samples.

4.2.3.4 Visual inspection test for the group 2 samples

As it is mentioned in chapter 3, visual inspection test is the oldest and the most common non-destructive test methods for concrete structures. Especially, it has been frequently used to detect surface cracks [159-161]. Afterwards, these cracks have been classified depending on their shapes and positions on the concrete surfaces.

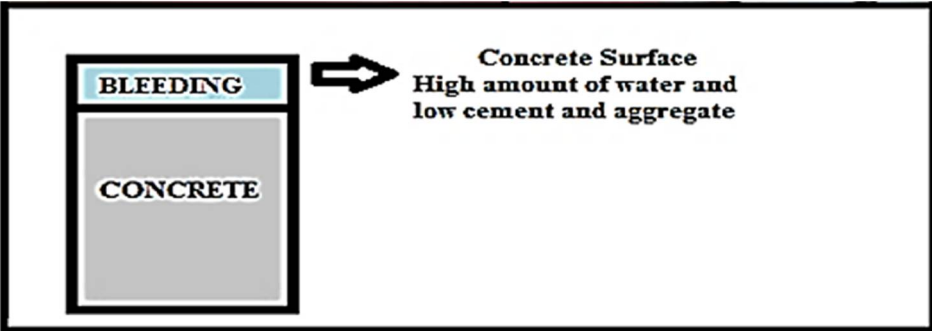


Figure 95: Bleeding cracks on the concrete surface.

In figure 95, bleeding crack type and its main cause have been represented. As it is explained formerly, bleeding is an important problem for hardened and fresh concrete. It occurs, when high amount of the water moves to the upward or surface of the concrete. Most importantly, the heavier particles such as coarse aggregates move to the downward or bottom of the concrete. Therefore, on the surface, excess water and low amount of aggregate may be detected.

As mentioned formerly, in the research group 2, water to cement ratios of the group 2 samples have been increased from 0.54 to 0.90. Therefore, water contents of the specimens have excessively risen. Because of the excess water content in the sample M6, bleeding cracks, shown in the following figure, have been detected during visual inspection tests.

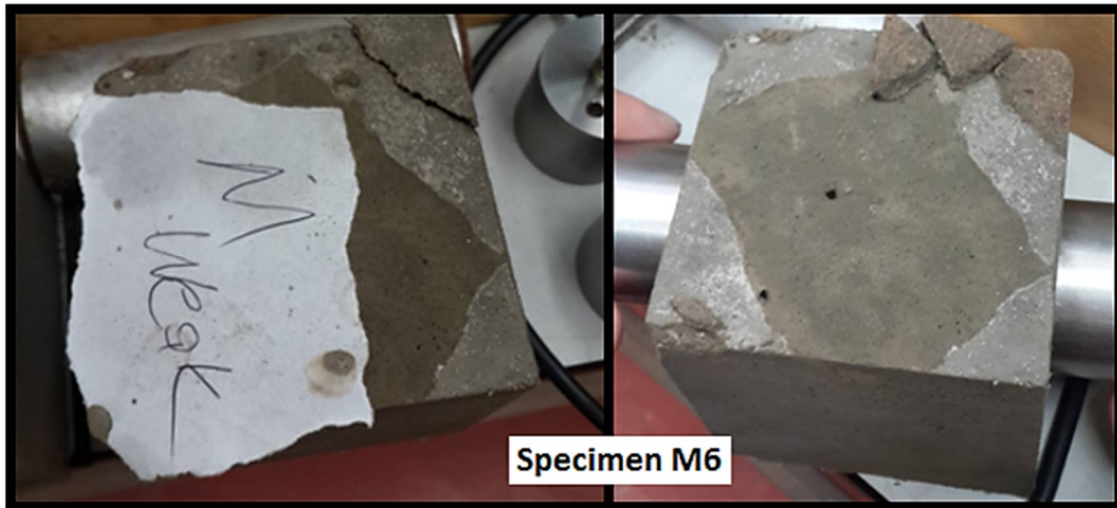


Figure 96: Bleeding cracks on surface of the sample M6.

It may be clearly seen that there are small particules on the surface of M6 though it has been consisting 10 mm aggregates in its mixture content. As mentioned earlier, coarse components of the sample have moved to the downward. Afterwards, excess water has moved upward. Finally, it has caused a drastic reduction of the concrete strength on the sample surface. Therefore, major bleeding cracks have been observed. They have affected the concrete strength, durability and quality negatively.

CHAPTER 5

Conclusions

In this research study, visual inspection, acoustic emission and ultrasonic pulse velocity testing have been employed to quantitatively evaluate the quality, strength and durability of concrete beam and cubic specimens produced using a variety of mixtures. Destructive evaluation has also been carried out in the form of compressive and flexural strength testing in order to validate the results obtained with the NDT techniques employed. The results for both destructive and NDT methods have been thoroughly discussed and analysed. The various experimental setups employed have been described in adequate detail to ensure repeatability of the experiments should that be needed.

During the four-point flexural testing, AE testing was used in order to monitor damage propagation sustained by the samples with increasing load. Various features of interest have been considered in order to determine damage accumulation and reduction in the structural integrity of each sample including AE signal energy, average frequency, root-mean-square, signal amplitude and cumulative AE energy. The experimental results arising from the flexural tests have been compared with the recorded AE activity to evaluate the relationship between concrete strength, quality and durability with damage propagation, structural integrity degradation and AE activity. Different mixtures have been employed representing a wide range of possible concrete qualities and strengths to evaluate their effect in the consistency of the results arising from the NDT methods used. The use of cumulative AE energy has been employed as the prime means of quantifying the progressive loss of structural integrity for group 1 and 2 beam samples during flexural testing.

Ultrasonic pulse velocity measurements have been applied on the cubic samples made with varying mixture contents. Water to cement ratio in cubic samples of experimental group 2 has been increased considerably in order to evaluate the effect of water and voids on ultrasonic pulse velocity measured values. The results of ultrasonic pulse velocity measurements have been validated using compressive strength tests. The experimental results from arising from the different tests have been compared and discussed quantitatively in depth. The surface quality of the samples tested was evaluated prior to any tests using visual inspection as described in the relevant inspection standards for concrete structures.

From these experimental results discussed in the present thesis, the following conclusions have been drawn.

5.1 Conclusions from the acoustic emission testing

- In contrast to the ultrasonic pulse velocity results, AE signal energy values are not significantly affected by the different mixture contents. The final cumulative AE energy values follow the same order as the compressive and flexural strength values, despite the samples having different mixture contents. In other words, the sample having the highest compressive and flexural strength values show the greatest final AE cumulative energy value.
- In general, the comparison between the destructive testing values and AE signal properties such as AE signal energy, cumulative AE energy, average frequency, root-mean-square, signal amplitude indicates that reasonable relationships can be established for the quantitative assessment of the quality, durability and strength of concrete structures. The trend of cumulative AE energy plot increases with increasing concrete compressive and flexural strength.
- The critical level of sustained damage can be established based on the cumulative AE energy trend and the structural integrity reduction can be reliably extrapolated. As mentioned previously, AE activity drastically increases when failure is imminent.

- The AE activity characteristics related to amplitude, frequency and root-mean-square, during the loading process depend on level of damage as well as concrete microstructure which is a function of the mixture content.

5.2 Conclusions from the ultrasonic pulse velocity and visual inspection testing

- Compressive strength values of a concrete samples, having totally different mixture contents, are not easy to accurately relate to ultrasonic pulse velocity measurements. However, from the results obtained the strength can be closely estimated by looking at the ultrasonic pulse velocity when concrete samples of similar mixture content and close ageing times are assessed. Velocity and strength values can be classified correctly although the relationship between the two parameters appears to be non-linear.

- Visual inspection can provide significant information with respect to the magnitude and root cause of the damage.

- In this research study, the samples are produced from two different mixture contents. Therefore, they have different void ratios, maximum aggregate diameters, cement and chemical admixtures. These factors cause the pulse velocity differences. Nevertheless, quality of the samples may be generally categorized by using the standard classification tables such as BS 1881-203:1986.

- The water to cement ratios have exerted the most significant influence on the UPVT results and concrete strengths. Pulse velocity and compressive strength values have drastically decreased, with increasing water to cement ratios.

The present research study has shown that the UPV values can be used to estimate concrete strength accurately if the samples have been produced from similar mixtures. AE can be used to effectively evaluate damage propagation and determine the degradation of the structural integrity of concrete elements in service. Moreover, it is possible to identify the points of critical damage accumulation at which collapse of a concrete structure becomes likely as cracks become unstable.

CHAPTER 6

Future Work

- A specific interpolation between voltage and duration value of the root-mean-square can be produced to quantify the damage inside the concrete. Especially by using maximum voltage level and its duration, a specific function giving information about amount of the deformation may be found. Similar to the AE cumulative energy, progressive structural integrity may be obtained from the RMS parameters.
- During the 4 point-bending and acoustic emission testing, the beam samples having reinforced steel rebars should also be considered. Significant changes on AE signal arising with increasing crack lengths can be compared in order to investigate the capability of the technique for damage quantification. In addition, alternative concrete mixture contents can be employed in order to assess in more depth the effect of concrete microstructural characteristics to AE activity and damage propagation behaviour.
- In addition, monitoring damage propagation with high-speed cameras so cracking evolution can be directly related with AE activity would be particularly beneficial in understanding how damage propagates until it reaches a critical level and failure becomes imminent.

CHAPTER 7

References

1. Why concrete cracks geological factors in concrete failure, *Journal of The Proceedings of the Geologists' Association*, France, 2005.
2. A. Masi, D. Nigro, M. Vona: Effect of core drilling and subsequent restoration on RC column strength, Department of Structures, Geotechnics and Engineering Geology, University of Basilicata, Italy.
3. Calavera I., Aparicio G., Delibes A., Gonzalez C.: Effects of cores from coring test and bore filling on column behaviour, Quality control of concrete structures, Stockholm, 1979.
4. Ponzo F.C., R. Ditommaso, G. Auletta: Structural Health Monitoring of Reinforced Concrete Structures using Nonlinear Interferometric Analysis, University of Basilicata, Italy.
5. Francisco R. Candel: Methods and equipment for non-destructive testing of reinforced concrete in harbour docks, MSc Thesis, Chalmers University of Technology Goteborg, Sweden 2010.
6. Kevin C. Arne: Crack depth measurement in reinforced concrete using ultrasonic techniques, Georgia Institute of Technology, Atlanta, Georgia, April 7, 2014.
7. S. Ashok Kumar and M. Santhanam: Detection of Concrete Damage Using Ultrasonic Pulse Velocity Method, Department of Civil Engineering, Chennai-600 036, IIT Madras.
8. Kemal Gokkaya: Geographic analysis of earthquake damage in Turkey between 1900 and 2012, *Geomatics, Natural Hazards and Risk, Volume 7, 2016 - Issue 6*, Published Online, 25 Apr 2016.
9. Bungey, J.H.: Recent developments in Civil Engineering NDT in the UK. *Insight - Journal of British Institute of NDT*, 45, No: 12, UK, Dec. 2003
10. Breyse D. and Abraham O.: Nondestructive assessment of damaged reinforced concrete structures: From needs to answers. *A National State of the Art. Proc. NDT-CE*, Berlin, 2003.
11. ASTM C876: Half-cell potentials of uncoated reinforcing steel in concrete. *American Society for Testing and Materials*, Philadelphia.
12. Building Research Establishment: Carbonation of concrete and its effects on durability, Digest 405, 1995.
13. ASTM C803: Penetration resistance of hardened concrete. *American Society for Testing and Materials*, Philadelphia.
14. Kear P. and Leeming M: Radiographic inspection of post-tensioned concrete bridges, *Insight - Journal of British Institute of NDT*, 36, No. 7, July 1994.
15. Redmer B., Likhatchev A., Weise F. and Ewert U.: Location of reinforcement in structures by different methods of gamma radiography, Berlin, 2003.
16. Yi Ching Lin, Chao-Peng Lai and Tsung Yen.: Prediction of ultrasonic pulse velocity (UPV) in concrete, *ACI Materials Journal*, 100, No. 1, Jan.–Feb. 2003.

17. Prine David W.: Acoustic emission monitoring of in-service bridges, *Senior Engineer Research Report UKTRP-87-22*, August 1987
18. Hinsley J.F.: Non-Destructive Testing, *MacDonald and Evans Ltd.* London, 1959.
19. Flaherty I.J.: History of magnetic particle testing, *Materials Evaluation*, 1990.
20. Bainton K.F.: Characterizing defects by determining magnetic leakage field, *NDT International*, 1979.
21. BS EN 571-1: Non-destructive testing, Penetrant testing, Part 1, *General principles British Standard*, 1997.
22. Doris Simonis: An Encyclopedia of People Who Changed the World Scientists, Mathematicians, and Inventors.
23. Manbachi A. and Cobbold R.S.C.: Development and application of piezoelectric materials for ultrasound generation and detection, *Ultrasound. 19 (4)*, 2011.
24. Joseph Woo: A short History of the development of Ultrasound in Obstetrics and Gynecology, part 1, 1998.
25. Hornibrook, F.B.: Application of sonic method to freezing and thawing studies of concrete, *ASTM Bulletin, 101*, 1939.
25. Thomson, W. T.: Measuring changes in physical properties of concrete by the dynamic method, *ASTM Proceedings, vol. 40*, 1940.
26. Jones, R. (1948). The application of ultrasonic to the testing of concrete, *Research*, London, England.
27. Milton Nunez: On subneolithic pottery and its adoption in Late Mesolithic Finland, *Fennoscandia archeological VII*, 1990.
28. Haq Syed Nomanul: Names, Natures and Things: The Alchemist Jabir Ibn Hayyan and His Kitab Al-Ahjar (Book of Stones), 28 February 1995.
29. Mix Paul E.: Introduction to nondestructive testing: a training guide, *WileyInterscience*, 2005.
30. Liptai R. G., Harris D. O. and Tatro C. A.: An introduction to acoustic emission, *Acoustic Emission*, 1972.
31. Kelly's Directories Ltd.: Metallurgical abstracts (general and non-ferrous), Part 11, Volume 4, London, November 1937.
32. T. F. Drouillard: Acoustic Emission, a Bibliography with Abstracts, New York, Washington-London, 1979.
33. BINDT publishes: Insight - Non-Destructive Testing and Condition Monitoring, www.bindt.org.
34. British Standard 1881, part 201-210:1986,
35. The American Society for Non-destructive Testing, Inc. (ASTN).
36. ASTM International ASRM e114: 2007.
37. The American Society of Mechanical Engineers (ASME).

38. International Organization for Standardization (ISO) iso 9712, iso/iec 17024.
39. European Committee for Standardization (CEN) EN 4179.
40. Arshad A. Khan, William D. Cook, and Denis Mitchell: Tensile Strength of Low, Medium, and High-Strength Concretes at Early Ages, *Materials Journal volume 93 issue 5*, 1996.
41. Roar Myrdal: Accelerating admixtures for concrete, 2007.
42. Rixom R and Mailvaganam N, Chemical Admixtures for Concrete, Chapter 6, London, 1999.
43. Yalley P. P. and Sam A.: Effect of Sand Fines and Water/Cement Ratio on Concrete Properties, 2018.
44. Johannes Weber, Anthony Baragona, Farkas Pintérb, Christophe Gosselin: Hydraulicity in ancient mortars: its origin and alteration phenomena under the microscope, Netherland, 2015.
45. ACI Committee: Use of Raw or Processed Natural Pozzolans in Concrete, *American Concrete Institute, ACI 232.1R-00*, Michigan, 2000.
46. Roy Junior Leonard: The pozzolanic activity of certain fly ashes and soil minerals, Iowa State College, 1958.
47. Lea FM.: The Chemistry of Cement and Concrete. 3rd Edition, Edward Arnold Publishers Ltd, London England, 1970.
48. Ozguner AM.: Prospection of Portland cement raw material: A case study in the Marmara region of Turkey, *Journal of African Earth*.
49. Konstantinos G. Kolovos, Glikeria Kakal: Factors affecting the reactivity of the CaO-SiO₂-Al₂O₃-Fe₂O₃ system, *Key Engineering Materials*, October 2001.
50. Lopez-Sanchez, Fernandez-Gomez JA, Moragues-Terrades A: Comparison on the durability of different portland cements after five years exposure to sulfate and to sea water attack, Spain 2011.
51. Carette G., and Malhotra V.: Mechanical Properties, Durability, and Drying Shrinkage of Portland Cement Concrete Incorporating Silica Fume, *Cement, Concrete, and Aggregates, American Society for Testing and Materials*, West Conshohocken, USA 1983.
52. D. W. Lewis: Research on Concrete Aggregates, *Purdue University*, 1962.
53. ACI Committee 221, Guide for Use of Normal Weight Aggregates in Concrete, *ACI 221R-96, American Concrete Institute*, Farmington Hills, Michigan, 1996.
54. ACI Committee 221, Guide to Alkali Aggregate Reactions, *ACI 221.1-98, American Concrete Institute*, Michigan, 1998.
55. Berube, M. A.; Fournier, B. and Durant, B., Vezina D, Fournier B.: Alkali-Aggregate Reaction in Concrete, *11th International Conference*, Canada, June 2000.
56. Vladimir G. Haach, Graca Vasconcelos, Paulo B. Lourenco: Influence of aggregates grading and water/cement ratio in workability and hardened properties of mortars, *Volume 25, Issue 6*, June 2011.

57. Andrew Chiu, Ian Robinson: Hydration of Tricalcium Silicate (C3S), University College London, 2016.
58. M. Kassir, K. Bandyopadhyay, S. Bush, B. Mather, P. Shewmon, M. Streicher, B. Thompson, D. van Rooyen, J. Weeks: Aging mechanisms for concrete components of high-level waste storage tanks, BNL-61651.
59. Christopher Carde, Raoul Francois: Effect of the leaching of calcium hydroxide from cement paste on mechanical and physical properties, *Cement and Concrete Research Volume 27, Issue 4*, April 1997.
60. Peter Taylor, Paul Tennis, Karthik Obla, Prashant Ram, Thomas Van Dam, Heather Dylla: Durability of concrete, second edition, *TRB Durability of Concrete Committee, Transportation Research Board Number E-C171*, September 2013.
61. Jamshid M. Armaghani, Torbjorn J. Larsen, and David C. Romano: Aspects of concrete strength and durability.
62. Turng-fang F. Lee, Menashi D. Cohen: Significance of transition zones on physical and mechanical properties of portland cement mortar, strength and durability of concrete: effects of cement paste-aggregate interfaces, Purdue University, India, 1998.
63. H.Cai, X.Liu: Cement and Concrete Research, Freeze-thaw durability of concrete: ice formation process in pores, *Volume 28, Issue 9*, September 1998.
64. Berke N. S., M. C. Hicks, R. J. Hoops, and P. J. Tourney.: Use of laboratory techniques to evaluate long-term durability of steel reinforced concrete exposed to chloride ingress, *American Concrete Institute, SP 145-16*, 1994.
65. LiuBaoju, XieYoujun, ZhouShiqiong, LiJian: Some factors affecting early compressive strength of steam-curing concrete with ultrafine fly ash, *Cement and Concrete Research Volume 31, Issue 10*, October 2001.
66. Rozalija Kozul, David Darwin: Effects of aggregate type, size, and content on concrete strength and fracture energy, *University of Kansas Center for Research, Inc. Lawrence, Kansas*, June 1997.
67. Neville A. M.: Properties of Concrete, Fourth Edition, New York, 1996.
68. Mather B., Home W. G.: Amount of water required for complete hydration of portland cement, *American Concrete Institute (ACI) Concrete International Volume: 24 Issue number: 6*, 2002
69. I. Lyse: Effect of type of cement on strength and durability of concrete, *Proc. ACI, Vol. 31, Reprint No. 36(35-7)*.
70. Naaman A. E., Wongtanakitcharoen T. and Hauser G.: Influence of different fibers on plastic shrinkage cracking of concrete, *ACI Materials Journal Vol 102, No. 1*, January–February 2005.
71. Grant T. Halvorsen: Troubleshooting concrete cracking during construction, concrete construction, 1993.
72. Ranchhod Mata, Jayeshkumar Pitroda, J. J. Bhavsar: Mechanical compaction of concrete: A governing factor for durability and serviceability of the concrete, India, 2014.

73. Mustafa Tuncan, Omer A, Kambiz R, Bekir K, Ahmet Tuncan and Kadir K.: Effect of Compaction on Assessed Concrete Strength, 2007.
74. Non-Structural Cracks in Concrete - *Concrete Society Technical Report 22*, 1992.
75. Gabriel A., Khoury, Yngve Anderberg: Concrete spalling review, Swedish National Road Administration, 2000.
76. Bud Early: Repair of concrete structures under construction, 2008.
77. Frank Collins, G. J. Sanjayan: Microcracking and strength development of alkali activated slag concrete, *Cement and Concrete Composites Volume 23, Issues 4–5*, August–October 2001.
78. William D. Callister, Jr.: *Materials Science and Engineering*, Hoken: John Wiley and Sons, Inc., 2003.
79. Boussahoua Youcefa, Kenai S. and Ali-Benyahia K.: Prediction of concrete strength by non-destructive testing in old structures: Effect of core number on the reliability of prediction, 2017.
80. J. M. Hodgkinson: Mechanical Testing of Advanced Fibre Composites, *Woodhead Publishing, Ltd.*, Cambridge, 2000.
81. Davis, Joseph R.: Tensile testing, 2nd Edition, *ASTM International*, 2004.
82. T. S. Thandavamoorthy: Determination of concrete compressive strength: A novel approach, *Pelagia Research Library Advances in Applied Science Research*, 6(10), 2015,
83. P. W. Keen: Some tests on the durability of concrete mixes of similar compressive strength, *Magazine of Concrete Research*, ISSN 0024-9831 | E-ISSN 1751-763 volume 13, issue 37, 1961.
84. Concrete Bridge Development Group: Guide to testing and monitoring the durability of concrete structures. *Tech Guide 2*, *Concrete Society*, Crowthorne, 2002.
85. Guidance on radar testing of concrete, *Technical Report, 48*, *Concrete Society*, Crowthorne, 1997.
86. Frigerio, T., Mariscotti, M.A.J., Ruffolo, M. and Thieberger, P.: Development and application of computed tomography in the inspection of reinforced concrete, *Insight – Journal British. Institute NDT*, 46, No. 12, Dec. 2004.
87. Higgins, D.D.: Diagnosing the causes of defects or deterioration in concrete structures, *Current Practice Sheet 69*, *Concrete*, 15, No. 10, Oct. 1981.
88. Zhou Jing-cheng, LI Xing-fu: On causes, prevention and repairing measures of concrete cracks, *International Journal of Engineering Research and Applications* ISSN: 2248-9622, Vol. 5, Issue 5, Part 6, 2015.
89. Michael D. Kotsovos, Demetrios M. Kotsovos: Cracking of reinforced beam/column joints: Implications for practical structural analysis and design.
90. Arvind Rajabather: Investigation of cracks in buildings, *St. Peter College of Engineering and Technology*, 2016.

91. Janaka Pushpakumara, Sudhira De Silva, Subashi De Silva: Visual inspection and non-destructive tests-based rating method for concrete bridges, *International Journal Structural Engineering*, Vol. 8, No. 1, 2017.
92. S. P. Shah and Chandra S.: Mechanical behavior of concrete examined by ultrasonic measurement, *Journal of Materials, JMLSA*, Vol. 5, No.3, September 1970.
93. John H. Bungey, Stephen G. Millard, Michael G Gratham: Testing of concrete in structures, 4th Edition, page 54, London 1982 and 2006.
94. BS 1881-203, ASTM C597.
95. John H. Bungey, Stephen G. Millard, Michael G Gratham: Testing of concrete in structures, 4th Edition, page 56, London 1982 and 2006.
96. Bungey, J.H. The validity of ultrasonic pulse velocity testing of in-place concrete for strength, *NDT International, IPC Press*, Dec. 1980.
97. John H. Bungey, Stephen G. Millard, Michael G Gratham: Testing of concrete in structures, 1st Edition, London 1982 and 4th Edition 2006.
98. Malhotra V.M.: Testing hardened concrete: Non-destructive methods, *Monograph 9, American Concrete Institute*, Detroit, 1976.
99. BS 4408: part 5: Non-destructive Methods of Test for Concrete-Measurement of the Ultrasonic Pulses Velocity in Concrete, *British Standard Institution*, London, 1970.
100. Jones, R. and I. Factory: Testing of concrete by the ultrasonic pulse method, *Materials and Structures, Volume. 2, No: 10*, July-August, 1969.
101. Bungey J.H.: The Testing of Concrete in Structures, *Surrey University Press*, 1982.
102. Hakan Guneyli, Suleyman Karahan, Aslihan Guneyli, Nil Yapici: Water content and temperature effect on ultrasonic pulse velocity of concrete, *Russian Journal of Nondestructive Testing 53(2)*, 2017.
103. Hirata, T. and Uomoto, T.: Detection of ultrasonic pulse echo through steel bar in concrete crack depth measurement, *Proc. NDT-CE T. Uomoto, Elsevier*, 2000.
104. Hashimoto, S., Hashimoto, C., Watanabe, T. and Mizuguchi, H.: Study on evaluation of settlement cracks occurring on the concrete surface above steel bars of reinforced concrete slab by NDT, *Proceedings of Structural Faults and Repair, Engineering Technics Press*, Edinburgh, 2003.
105. BS 1881: Part 203
106. Swamy, R.N. and Al-Hamed, A.H.: The use of pulse velocity measurements to estimate strength of air-dried cubes and hence in-situation strength of concrete, *SP publication 82-13, American Concrete Institute*, Detroit, 1984.
107. Jones, R. and Facaoaru, I.: Recommendations for testing concrete by the ultrasonic pulse method, *Materials and Structures*, 2, No. 10, 1969.
108. Fuminori Tomosawa and Takafumi Noguchi: Relationship between compressive strength and modulus of elasticity of high-strength concrete, Tokyo, 1993.

- 109.** David Roylance: Stress-strain curves, *Massachusetts Institute of Technology* Cambridge, 2001.
- 110.** H. J. F. Diogenes, L. C. Cossolino: Determination of modulus of elasticity of concrete from the acoustic response, *Volume 4, Number 5*, December, 2011.
- 111.** Bungey J.H. and Madandoust R.: Strength variations in lightweight concrete beams pages, *Cement and Concrete Composites*, 16, 1994.
- 112.** Bungey J.H.: The validity of ultrasonic pulse velocity testing in-place concrete for strength, *N.D. T. International IPC Press*, December 1980.
- 113.** Bungey, J.H.: The influence of reinforcement on pulse velocity testing, *SP publication 82-12, American Concrete Institute*, Detroit, 1984.
- 114.** Kroggel O.: Ultrasonic examination of crack structures in concrete slabs, *Proc. Structural Faults and Repairs 93, Engineering Technics Press*, Edinburgh, 3, 1993.
- 115.** ACI Materials Journal: *Volume 95, American Concrete Institute*, 1998.
- 116.** Bungey, J.H. and Madandoust, R.: Evaluation of non-destructive strength testing of lightweight concrete, *Proc. ICE, Structures and Buildings*, 104, Aug. 1994.
- 117.** T. H. Panzera, André Luis Christoforo, Fabio Paiva Cota, Chris R Bowen: Ultrasonic pulse velocity evaluation of cementitious materials, *Advances in Composite Materials - Analysis of Natural and Man-Made Materials*, 2011.
- 118.** R. Jones: The ultrasonic testing of concrete, *Ultrasonics 1*, 1963.
- 119.** Tanvir Ahmed: Influence of types of chemical admixture and their dosages on properties of ready-mix concrete, 2016.
- 120.** Yiching Lin, Chao-Peng Lai and Tsong Yen.: Prediction of ultrasonic pulse velocity (UPV) in concrete, *ACI Materials Journal*, 100, No. 1, Jan.–Feb. 2003.
- 121.** Kaplan M.F.: The effect of age and water to cement ratio upon the relation between ultrasonic pulse velocity and compressive strength of concrete, *Magazine Concrete Research*, 11(32), 1959.
- 122.** RILEM Recommendation NDT 1: Testing of concrete by the ultrasonic pulse method, Paris, December, 1972.
- 123.** Jones, R.: Testing of concrete by an ultrasonic pulse technique, *RILEM Int. Sym. On Non-destructive Testing of Materials and Structures, Vol. 1, Paper No. A-17*, Paris January 1954, 137. *RILEM Bull.*, 19 Part 2, Paris November 1954.
- 124.** Popovics, S., Rose, J.L., and Popovics, I.S.: The behavior of ultrasonic pulses in concrete, *Cement Concrete Research*, 20, 259, 1990.
- 125.** John H. Bungey, Stephen G. Millard, Michael G Gratham: Testing of concrete in structures, 4th edition, page 66, London 1982-2006.
- 126.** Tarun Gehlot, S.S. Sankhla, S.S. Gehlot, Akash Gupta: Study of concrete quality assessment of structural elements using ultrasonic pulse velocity test, *Journal of Mechanical and Civil Engineering Volume 13, issue 5*.

- 127.** Fethi Soltani, Marc Goueygou, Zoubeir Lafhaj, Bogdan Piwakowski: Relationship between ultrasonic rayleigh wave propagation and capillary porosity in cement paste with variable water content, *NDT and E International Volume 54*, March 2013.
- 128.** - BS EN 12504-2 Testing concrete in structures: Non-destructive testing: Determination of rebound number, *British Standards Institution*, London,
- 129.** Leslie J. R. and Cheesman W. J.: An ultrasonic method of studying deterioration and cracking in concrete structures, *Journal of American Concrete Institute, Vol. 21, No. 1*, 1949.
- 130.** Sotirios J. Vahaviolos: *Acoustic Emission: Standards and Technology Update. STP-1353, ASTM International, ISBN 978-0-8031-2498-1*, Philadelphia, 1999.
- 131.** Alan G. Beattie: Acoustic emission non-destructive testing of structures using source location techniques, *Sandia Report sand2013-7779*, 2013.
- 132.** Alan G. Beattie: Acoustic emission, principles and instrumentation, *JAE 2: 96*, 1983.
- 133.** Breckenridge F.R.: Acoustic emission transducer calibration by means of the seismic pulse, *JAE 1: 87*, 1982.
- 134.** Jun Zhou: A study of acoustic emission technique for concrete damage detection, page 14, *Michigan Technological University*, 2011.
- 135.** Jun Zhou: A study of acoustic emission technique for concrete damage detection, page 15, *Michigan Technological University*, 2011.
- 136.** T. F. Drouillard: Acoustic emission, a bibliography with abstracts, ISBN 0-306-65179-3, New York-Washington-London, 1979.
- 137.** H. Borchers and J. Kaiser: *Zeitschrift für Metallkunde (International Journal of Materials)*, 1958.
- 138.** Grosse M. Ohtsu, Acoustic emission testing, 2008
- 139.** J.F Labuz, S.T. Dai: Identifying failure through locations of acoustic emission, *Transportation Research Record, 1526*, 1996.
- 140.** Ohtsu M., H. Watanabe: Quantitative damage estimation of concrete by acoustic emission, *Construction and Building Materials*.
- 141.** Non-destructive testing (NDT) – Guidance document: An introduction to NDT common methods, *document: AA050, issue 2*, 2015
- 142.** A.K. Rao: Acoustic Emission and Signal Analysis, Volume 40, No:1, *Department of Aerospace Engineering, Indian Institute of Science*, 1990.
- 143.** Berkovits A, D. Fang: Study of fatigue crack characteristics by acoustic emission, *Engineering Fracture Mechanics*, 1995.
- 144.** Labuz J, S. Cattaneo: Acoustic emission at failure in quasi-brittle materials, *Construction and Building materials*, 2001.

- 145.** Fady F. Barsoum, Jamil Suleman, Andrej Korcak and Eric V. K. Hill: Acoustic emission monitoring and fatigue life prediction in axially loaded notched steel specimens.
- 146.** Kanji Ono: Structural integrity evaluation using acoustic emission, University of California, Los Angeles, California 90095-1595.
- 147.** J. O Ehiorobo, O. C. Izinyon and R. O. Ogirigbo: Measurement and documentation for structural, integrity assessment of an in-service school, Benin City, West Africa.
- 148.** Paul Ziehl and Adrian Pollock: Acoustic Emission for Civil Structures, *University of South Carolina and Mistras Group, USA.*
- 149.** N. Pugnoa, M. Ciavarellab, P. Cornettia, A. Carpinteria: A generalized Paris-Erdogan law for fatigue crack growth, Italy, 2006.
- 150.** J. R. Rice and D. M. Tracey: Computational fracture mechanics, in numerical and computer methods in structural mechanics, *Academic Press, New York, 1973.*
- 151.** Nastase, Adrian S.: How to derive the RMS value of pulse and square waveforms, www.MasteringElectronicsDesign.com. represented in 21 January 2015.
- 152.** Chris C. Bissell and David A. Chapman: Digital signal transmission, 2nd Edition, *Cambridge University Press, 1992.*
- 153.** John Bird: Engineering Mathematics, 5th Edition, published by Elsevier Ltd, 2007.
- 154.** Mitakovi D, Grabec I and Sedmak S: Simulation of AE signals and signal analysis systems, ultrasonics, September 1985.
- 155.** Chen CH: Signal Processing in non-destructive evaluation of materials in signal processing, Marcel Dekker Inc., 1988.
- 156.** T. Kamada, M. Iwanami, S. Nagataki: Acoustic emission discrimination of crack types in reinforced concrete beams, *Fracture Mechanics of Concrete Structures Proceedings Framcos-3, Germany, Japan.*
- 157.** Soulioti D., N. M. Barkoula: Acoustic emission behavior of steel fibre reinforced concrete under bending, *Construction Building Materials.*
- 158.** A Dictionary of Physics 6th Edition, *Oxford University Press, ISBN 9780199233991, 2009.*
- 159.** Pollock, D.J. Kay, E.A. and Fookes, P.G.: Crack mapping for Investigation of concrete, *Middle East Concrete, 15, No: 5, May, 1981.*
- 160.** Non-Structural cracks in concrete, *Technical Report No: 22 3rd Edition, Concrete Society, London, 1992.*
- 161.** Smith, J.R.: Assessment of Concrete Building, *Concrete International, 13, No. 12, December 1991.*

Per Ardua Ad Alta...

Through efforts to high achievements...